SIMPLIFIED FUZZY LOGIC CONTROLLER BASED VECTOR CONTROL OF AN INTERIOR PERMANENT MAGNET MOTOR

CASEY BENJAMIN BUTT

Your file Votre référence
ISBN: 0-612-93014-9
Our file Notre référence
ISBN: 0-612-93014-9

Simplified Fuzzy Logic Controller Based Vector Control of an Interior Permanent Magnet Motor

by

Casey Benjamin Butt

A thesis submitted to the school of graduate studies
in partial fulfillment of the requirements for the degree of
Master of Engineering

Faculty of Engineering and Applied Science
Memorial University of Newfoundland

July 2003

St. John's Newfoundland Canada

Abstract

In recent years, the interior permanent magnet synchronous motor (IPMSM) has become increasingly popular for use in high performance drive (HPD) applications due to desirable features such as high torque to current ratio, high power to weight ratio, high efficiency, low noise and robust operation. As a consequence, the control of the IPMSM for use in high precision industrial drives has received heightened attention. This proposed research is directed to develop and implement a complete and practical vector control scheme for the IPMSM to be used in such applications.

This thesis presents the control of the IPMSM at rated speed and below, in the constant torque mode, by use of the maximum torque per ampere (MTPA) mode of operation utilizing an innovative Taylor series approximated approach. Coupled with this method is the development of a simplified fuzzy logic controller (FLC) based speed controller that maintains high performance standards while reducing complexity and computational burden. The performance of this proposed technique is evaluated by simulation as well as by experimental results. A comparison is made, in simulation, between a more conventional FLC based control technique with $i_d = 0$ and the proposed simplified FLC with MTPA approach.

The complete vector control scheme is implemented in real-time using a digital signal processor (DSP) controller board in a laboratory 1 hp interior permanent magnet synchronous motor.

Acknowledgements

I would like to express my sincere gratitude and appreciation to my supervisor Professor M. A. Rahman for his guidance, encouragement, advice and tutelage throughout the preparation of this thesis. His influence has helped me learn the practicalities of modern research and scientific writing.

I would like to sincerely thank the School of Graduate Studies, the Faculty of Engineering and Applied Science and Dr. Rahman for their financial support, without which the pursuit of this research would not have been possible. In addition, I would like to acknowledge Mr. Richard Newman for his expertise and assistance with the implementation of the lab equipment.

Finally, I would like to thank my wife Kimberley, my parents Mr. Benjamin Butt and Mrs. Mary Butt, and my wife's family for their support and encouragement, without which it would not have been possible for me to complete this study.

Contents

List of Figures

List of Symbols

v_a, v_b, and v_c	a, b and c phase voltages, respectively
i_a, i_b, and i_c	actual a, b and c phase currents, respectively
i_a^*, i_b^*, and i_c^*	command a, b and c phase currents, respectively
v_d	d-axis voltage
v_q	q-axis voltage
i_d	d-axis current
i_q	q-axis current
r_s	stator resistance per phase
L_d	d-axis inductance
L_q	q-axis inductance
L_l	leakage inductance
L_{md}	d-axis magnetizing inductance
L_{mq}	q-axis magnetizing inductance
ω_s	stator angular frequency
ω_r	actual rotor speed
ω_r^*	motor command speed
$\Delta\omega_r$	error between actual and command speeds ($\omega_r^* - \omega_r$)
$\Delta\omega_m$	normalized error between actual and command speeds
Δe	change in speed error

θ_r	rotor position
$\theta_r(0)$	initial rotor position
p	differential operator (d/dt)
P	number of pole pairs
T_e	developed electromagnetic torque
T_{en}^*	normalized command electromagnetic torque
T_L	load torque
J_m	rotor inertia constant
B_m	friction damping coefficient
Ψ_m	magnetic flux linkage
V_B	dc bus voltage of inverter

Chapter 1

Introduction

1.1 General Introduction to Motor Drives

Operating motors must work within specified speed and torque limits. Sudden disturbances and changes in loading and motor parameters, however, can cause the operating speed and torque output of the motor to change. It is the duty of the controlling drive system to automatically take measures to accurately and promptly restore the desired operating speed. This is the essence of motor control. There are, however, other considerations when assessing the desirability of a motor drive scheme. Cost, maintenance requirements and space requirements are fundamental concerns intrinsic in evaluating the practicality of any system.

Conventional direct current (DC), along with alternating current (AC) induction and synchronous electric machines, have traditionally been the three cornerstones serving daily needs from small household appliances to vast industrial plants. Recent years, however, have seen significant technological changes in motor drive systems, leading to increased application demands of electric motors.

Likewise, researchers have been continuing their efforts to develop new machines. The brushless DC (BLDC) machine, the switched reluctance machine (SRM), the permanent magnet hysteresis machine and the permanent magnet synchronous machine have all been developed or further developed [1-6]. Along with these advancements has come the need for sophisticated control schemes to maximize the performance and minimize the operating costs of these motors.

1.1.1 General Review of Electric Motor Drives

DC motors have been used extensively for variable speed and high performance drive systems. This is primarily because of the decoupled nature of the field and armature magnetomotive force (MMF) in the dc motor, leading to relatively simple schemes for controlling the motor's torque and speed. In addition, DC motors are known to produce excellent performances under both transient and steady state conditions.

However, the DC motor has some disadvantages. Frequent maintenance is required because of wearing between the commutators and brushes of the rotor assembly, with high associated costs. The DC motor has a limited range of speed operation and a poor capacity for overload, and brush sparking limits the power rating of the motor [73]. These drawbacks have prompted researchers to develop AC motors such as the induction and synchronous motor for use in high performance variable speed drives (where maintenance free operation and overload capacity are priorities). AC motors are suitable for constant speed operation, but due to recent technological advances, such as improved power electronic devices and microprocessors, and the continuing development of closed loop vector control techniques,

they can also have high performance applications for variable speed drives as well [7].

Of the AC motors, induction motors have traditionally been considered the workhorses of industry because of their low cost, reliability, ruggedness, reasonable efficiency and simplicity of construction. However, the induction motor has limitations. Induction motors must always operate at lagging power factors because the rotor field voltage must be induced by the stator's voltage; they lose efficiency because of slip power losses; and they must always run at speeds lower than synchronous, thus making the control of these motors very complex. The real-time implementation of these drives requires accurate modeling and estimation of motor parameters and complex control circuitry. All this has led researchers to investigate synchronous motors for use in high performance variable speed drives.

Synchronous motors run at synchronous speed (therefore, experiencing no slip power losses) and field current can be controlled from the rotor side, so their control is less complex than that of induction motors (though still more complex than that of DC motors). These attributes have made the wire-wound rotor synchronous motor a popular choice for high power AC drive systems. On the downside, however, the use of rotor windings on conventional synchronous motors requires extra power supply and maintenance-requiring slip rings and brush gears on the rotor side to supply the dc field excitation. The traditional rotor winding set-up, therefore, increases costs and reduces efficiency. This has prompted researchers to develop different types of synchronous motors with the intent of eliminating slip rings and brush gear-related losses. One such motor is the permanent magnet (PM) synchronous motor.

PM motors have desirable features such as a high torque to current ratio, a high power to weight ratio, high efficiency, low noise and good overload capacity. Unlike in the wire-wound synchronous motor, the excitation field is provided by permanent magnets, so there is no need for any extra power supply or field windings. This not only reduces the initial cost of the PM synchronous motor but also eliminates the power loss due to those windings and the costs necessary to maintain them.

1.2 Permanent Magnet Synchronous Motors

1.2.1 General Introduction

A PM synchronous motor consists of a stator with three phase windings and a rotor fitted with permanent magnets, in place of field windings, to provide the field flux. This design means, as indicated above, that the PM synchronous motor is not subject to the limitations of wound rotor motors (dc, ac induction and synchronous, etc.). The absence of rotor windings also means the absence of an external excitation supply for the rotor field and the elimination of slip rings. The elimination of the field windings reduces the cost of the motor as well as eliminates the power losses associated with such windings. In addition, permanent magnet rotors allow for more compact motor design for given output capacities.

As compared to the induction motor, the PM synchronous motor experiences no slip. Therefore, there are no slip dependent rotor losses, giving the PM synchronous motor a higher torque to inertia ratio and power density. For similar output ratings, the PM synchronous motor is smaller and lighter than the induction

motor, making it preferable in high performance applications where size and weight are of concern.

1.2.2 Classification of PM synchronous motors

Although the focus in this thesis has been, and will continue to be, on PM synchronous ac motors, permanent magnets have also been used to produce dc motors. PM dc motors are separately excited dc motors with permanent magnets as the excitation source. In industry, they are widely used as control motors. PM ac motors are, operationally, synchronous motors. Therefore, from this point in this thesis forward, permanent magnet ac synchronous motors will be referred to simply as PM motors.

PM motors are categorized broadly, based on the orientation of the permanent magnet magnetic fields. There are two such fundamental classifications: (a) radially oriented type, in which the rotor magnets are oriented such that the direction of magnetization is radial from the rotor, and (b) circumferential type, in which the rotor magnets are oriented such that the direction of magnetization is circumferential around the rotor.

In radially oriented machines the air gap flux density above the permanent magnets is approximately the same as the magnetic flux density. This means that for practical radially oriented motors to be made newly developed high-energy magnetic materials such as neodymium-boron-iron (Nd-B-Fe) and samarium-cobalt (Sm-Co) must be used. The use of low residual flux density magnetic materials such as ferrite magnets produces machines with very low air gap flux densities and, therefore, low output capacities. In this manner, radially oriented permanent mag-

net motor development has been directly dependent on recent advances in high-energy permanent magnet material technology.

Circumferentially oriented permanent magnet motors have a direction of magnetization that is circumferential in the rotor. They also typically have large numbers of poles. This design allows for reasonable output ratings to be produced utilizing traditional low residual flux density magnetic materials.

Based on the location of the permanent magnets in the rotor itself, there are three configurations of permanent magnet motors: (a) surface mounted type, where the magnets are mounted on the surface of the rotor; (b) inset type, where the magnets are fully or partially inset into the rotor core and (c) interior type, where the permanent magnets are buried within the rotor core [8]. It should be noted that surface mounted PM motors, by design, must be of the radially oriented type, whereas inset and interior type PM motors can have magnetization orientations either radial or circumferential in nature.

PM classification based on control strategy produces two more classifications of PM motors [74]: (a) the brushless dc (BLDC) motor, which is an electronically commutated rectangular wave fed three phase synchronous motor with surface mounted permanent magnets; and (b) the conventional PM synchronous motor (PMSM), which is a sinusoidal wave fed PM motor. Surface mounted type PM motors, suitable for use as BLDC motors, have large air gaps and, therefore, have weakened armature reaction effects. This restricts this type of motor to low speed and constant torque operations. These motors are commonly used as precision control motors and hard disk drive motors in computers. Inset and interior type PM motors have smaller, more uniform air gaps, allowing for operation at higher speeds in the constant power region. Interior type PM motors, in particular,

have significant motor torque contributed by the reluctance component due to the large difference between the direct and quadrature reactances, as well as the permanent magnet field component. This makes the interior PM motor ideal for use at high speeds utilizing the flux weakening method of control, as well as low speed, constant torque operations. In addition, this type of PM motor is the most economical to manufacture. These motors are commonly controlled with sinusoidal induced EMF, making them fall into the second PM classification based on control method, conventional PMSM.

Depending on the rotor cage winding, the PM motor may be further classified as: (a) cage type or (b) cageless, based on whether the rotor is fitted with a cage winding or not. In the case of the cage type motor, the cage winding provides the starting torque and hence this type of motor can be line started with rated supply voltage and frequency. Cageless motors have no cage windings and, therefore, control strategies using variable stator frequencies must be used to start the motor from standstill and accelerate it smoothly up to synchronous speed.

One further classification of the PMSM is based on whether or not the motor is equipped with a rotor position sensor. PMSMs without a rotor position sensor are classified, logically, as "sensorless". And PMSMs equipped with a rotor position sensor are known as "with sensor".

1.3 PMSM Drives

1.3.1 Vector Control Schemes

As with other types of synchronous motors, early controllers for the PMSM were based on the primitive open-loop volt/hertz (v/f) control method. Open-loop systems, obviously, are incapable of responding intelligently to dynamic changes in operating parameters. Due to this limitation, closed-loop schemes with torque and angle control have been used where better drive performance is required [75]. These scalar control techniques, however, have shortcomings due to the nonlinearity of the motor model and inherent coupling between direct and quadrature axis quantities. This leads to slow responsiveness, which is unacceptable for high performance drive applications. To solve this problem, vector, or field oriented, control techniques have been accepted almost universally for control of ac drives. The vector control technique, employing a current controlled voltage source inverter (VSI), provides a method of variable speed control for the PMSM that has fast responsiveness and follows command speeds accurately and precisely.

In the vector control technique for PMSM drives, the phase angle and the magnitude of the phase currents are controlled to provide high precision control of the motor. This is an evolution of control techniques developed in the 1970s by Blasche [7] and Hasse [9] for ac drives. At that time, however, implementation of these schemes was difficult due to technological limitations. Today, with very large scale integrated (VLSI) technologies, as well as advancing power electronic and microprocessor technologies, the practical implementation of the vector control scheme is no longer a problem.

The operating principle of vector control is based on elimination of the coupling between the direct (d) and quadrature (q) axes. This can be achieved by coordinate transformation, producing control very similar in nature to that of a separately excited dc motor. However, unlike dc machine control, in an ac machine both the magnitude and phase angle of the stator current need to be controlled. This is achieved by employing a time-varying vector that corresponds to a sinusoidal flux wave moving in the airgap of the machine, hence the name, vector control.

By referring the mmf wave of the stator current to the vector corresponding to the flux wave it becomes apparent that only the quadrature axis component of the stator current mmf wave contributes significantly to developed torque. The direct axis current is seen to contribute to the magnitude of the flux. This makes it convenient to define the stator current in a frame of reference defined by the time-varying field, thus illustrating the close correspondence with dc machines. Such a comparison shows that the d-axis component of stator current in a PMSM is analogous to the field current in the dc machine and the quadrature component of stator current is analogous to the armature current in the dc motor.

While vector control can be implemented in a reference frame fixed to the stator, rotor, or magnetizing flux space vector, with d- and q-axis stator currents defined in that frame, rotor flux oriented control is most commonly used in PMSM drives. This is because in the stator and magnetizing flux oriented control cases there exists a coupling between the torque producing stator current and the stator magnetizing current, whereas with rotor flux oriented control matters are simplified by a natural decoupling that occurs between the d- and q-axis components.

Vector control can be classified as either direct or indirect. Direct vector control, shown in Figure 1.1, depends on the direct measurement of the stator (or

rotor) flux using flux sensors. The d- and q- axis flux components, ψ_{dm} and ψ_{qm}, along with the appropriately calculated command torque and flux and actual torque and flux, are then used to generate the principle control parameters, the rotor flux frame d- and q-axis command currents, i_{dr}^{*} and i_{qr}^{*}. These dc currents, proportional to command torque and flux respectively, are then converted to a stationary reference frame and used to generate phase current commands for the VSI.

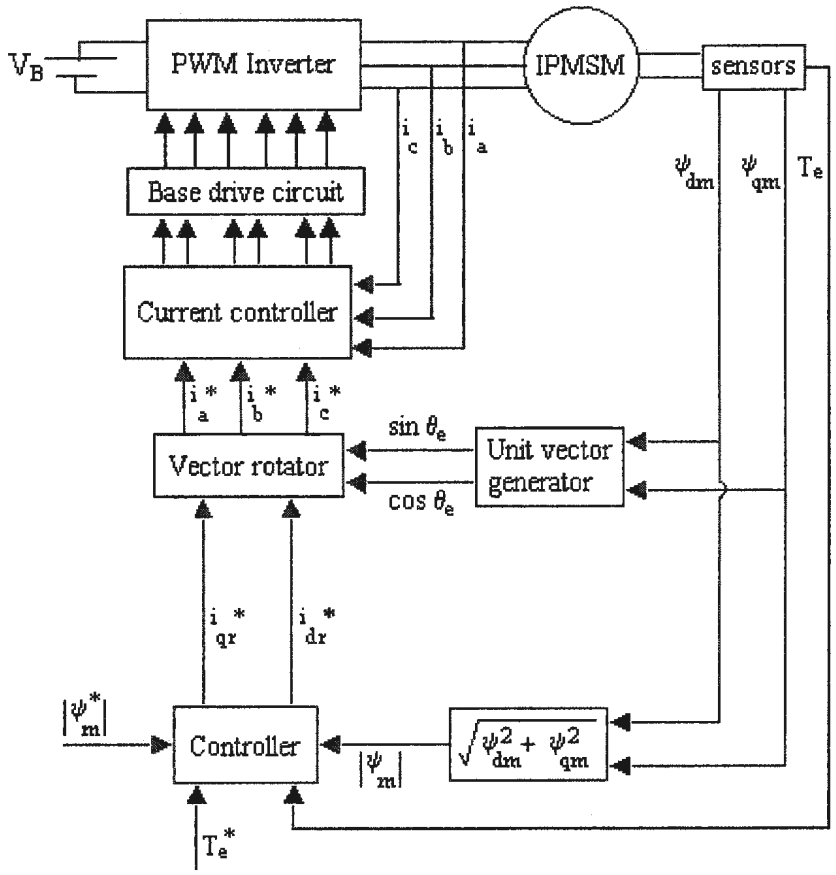

Figure 1.1. Direct vector control scheme of PMSM

The indirect method of vector control, as shown in Figure 1.2, uses sensors to determine rotor position and stator currents. From this, and along with the command speed, the rotor flux frame d- and q-axis command currents, i_{dr}^{*} and i_{qr}^{*}, are calculated. As with the direct method, these currents, after transformation to a stationary reference frame, are then used to generate phase current commands for the VSI. The indirect method of vector control is more sensitive to parameter variations than the direct method, and so motor parameters must be known accurately.

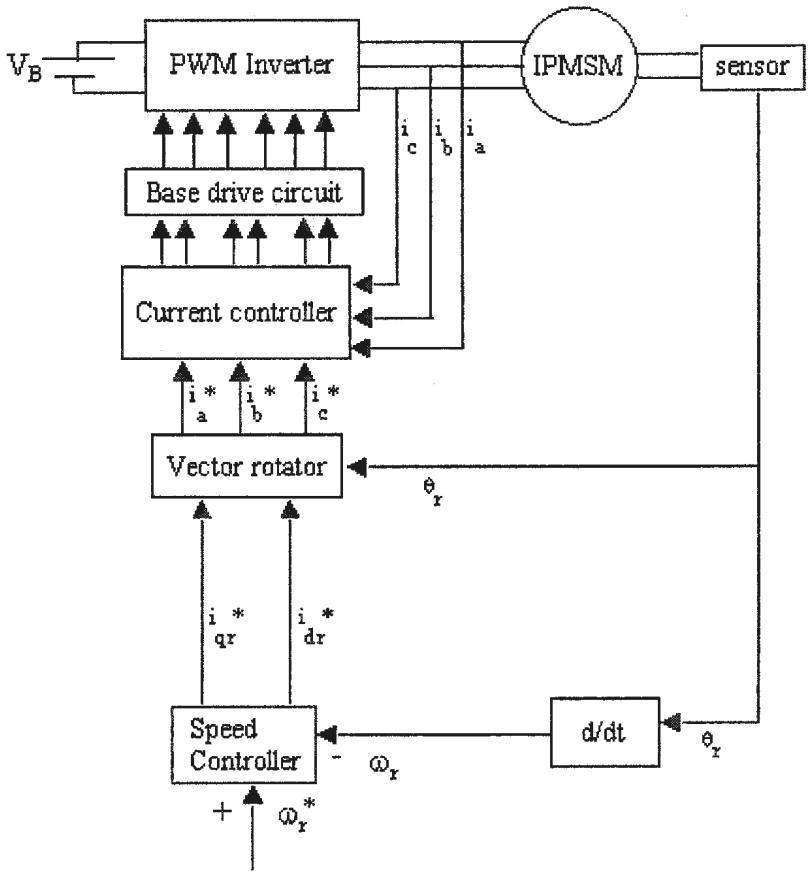

Figure 1.2. Indirect vector control scheme of PMSM

In both of these schemes, a current controlled VSI is used to apply the calculated command currents to the motor stator. This imposes the need for precise and accurate control of the VSI, as the current controller has direct influence on the drive performance. Low-loss current controllers that produce minimal harmonics and noise in the motor, as well as fast responsiveness for high performance under dynamic conditions, are required. The performance of various current control schemes for VSI fed ac and PMSM drives have been investigated [10-17]. Each scheme has been shown to have its own unique drawbacks with regards to accuracy and dynamic response over varying speed ranges. As the purpose of this work is to investigate improvements in control of the motor itself and not the VSI specifically, this work employs a simple fixed band hysteresis current control algorithm for the VSI. This scheme provides fast response and good accuracy in producing a stator current which tracks the command current within a hysteresis band, while avoiding unnecessary complexity. The drawback is that the hysteresis controller generates a random PWM switching pattern, thus producing a switching frequency that varies over the fundamental period [13].

1.3.2 PMSM Drive Controllers

Modern VLSI and advancing power electronic technologies have lead to the utilization of microprocessors in the control of the PMSM. This allows the current advancements in computing power to be applied to PMSM drive control, resulting in the implementation of complex control strategies. Bose and Szczesny originally proposed a microcomputer-based control system of an interior permanent magnet synchronous motor (IPMSM) [18].

Because of the versatility of the IPMSM, it has become essential to develop robust controllers for use in high performance drive (HPD) systems. Various uncertainties like sudden changes of command speed, abrupt load changes and parameter variations have to be handled quickly and accurately in such applications. With this in mind, several types of controllers, including conventional fixed gain types such as proportional-integral (PI), proportional-integral-derivative (PID) and pseudo-derivative-feedback (PDF); adaptive types such as model reference adaptive controllers (MRAC), sliding mode controllers (SMC) and variable structure controllers (VSC); and intelligent types such as artificial neural network (ANN) controllers, fuzzy logic controllers (FLC), and neuro-fuzzy controllers have been used for moderate to high performance drive systems. As my work utilizes the indirect control of an IPMSM through a current controlled VSI, this is where my literature review will focus.

To date, many researchers have reported their work on the development of high performance IPMSM drives, with the majority of the control schemes reported involving the performance of the IPMSM fed by a voltage source or current source inverter. The reader is referred to the indirect vector control scheme shown in Figure 1.2.

Gummaste and Slemon [19] have proposed a vector control scheme to analyze the steady state performance of a VSI-fed PMSM drive. They also presented a similar work utilizing the current source inverter fed PMSM drive [20]. For both schemes they used position feedback control from a shaft position sensor, mounted on the motor shaft, relaying rotor position back to the microcomputer so that the inverter could be operated in a self-controlling mode in real time. The constant torque mode and the constant power mode operations have been investigated, with

strategies having been developed for torque control. They have suggested removing the damper winding for the VSI-fed PMSM drive in order to increase operating stability, as the damper winding provides a path for the flow of harmonic currents induced for non-sinusoidal voltage outputs of the inverter. However, for the current source inverter (CSI) -fed PMSM drive system, the damper windings are helpful in reducing the commutating inductance and, therefore, are not recommended to be removed.

An analysis of a microprocessor-based implementation of the PMSM drive has been presented by Liu et. al., [21]. In their work, the motor is fed by the hysteresis current controlled VSI. To overcome some of the limitations of the hysteresis controller at low speeds, they have proposed a method utilizing the freewheeling period. The downfall of this proposal, however, is that this method reduces the average torque delivered by the motor with only modest performance improvements at low speeds.

Pillay and Krishnan [22-25] have presented a number of papers on modeling, simulation, analysis and controller design for high performance vector controlled PMSM drives using a state space model. They have investigated the transient and steady state performance of the drive using a d-q axis model of the PMSM, and have also investigated the performances of the hysteresis and ramp comparator current controllers for the VSI-fed PMSM drive. In these works, a PID type speed controller, based on the linear model of the PMSM, has been used. This produces error because, in real time, the PMSM torque does not behave linearly [26]. Hence, it is very difficult to predict the performance of the drive accurately using this linear model approximation. In addition, the inherent nature of the PID speed controller makes drive performance very parameter and load sensitive. Pillay

and Krishnan have not reported drive performances over wide speed ranges, but rather only for certain command speeds.

In other work, Pillay et. al., [27] have proposed a control scheme for a PMSM based on dual digital signal processors (DSP). One DSP is used to implement the current controller algorithm and the other the vector control algorithm. The performance of this drive is diminished due to the slower speed of the DSPs employed; and their use of a look-up table in generating command currents may not be suitable for a wide range of speed operations. Therefore, there is a lack of robustness with this drive, and comprehensive test results at different dynamic operating conditions have not been reported. However, the experimental results do show the effectiveness of the controller and its potential.

B.K. Bose [28] has presented a high performance inverter-fed IPMSM drive system using a closed-loop torque control scheme in which command torque is determined using feedback and taking into accounts the effects of saturation, temperature variation and non-linearity. The drive system has been incorporated in the constant torque as well as constant power regions. However, the performance of this drive system has been reported only for a fixed speed, and testing of the drive over a wide speed range and at different dynamic operating conditions is necessary to establish the efficacy of the drive.

An adaptive current control scheme for the PMSM drive has been proposed by Huy and Dessiant [29]. Their controller uses two modes, a hysteresis current control scheme for transient operation and a predictive current control scheme for steady state operation. The performance of this drive at low operating speeds has not been reported.

Huy et. al., [30] have presented an analysis and implementation of a real time predictive current controller for a PMSM synchronous motor servo drive. Although a high performance standard has been obtained with this controller, its implementation requires hardware incorporating an EPROM-based approach, making this scheme less flexible than the microprocessor-based approach.

Bose and Szczesny [31] have proposed a microcontroller-based controller of an IPMSM drive for electric vehicle propulsion. The control system incorporates both the constant torque region as well as the constant power region where the flux weakening mode of operation is used. This drive system has been implemented on a multiprocessor architecture, making the overall system costly.

Jahns et. al., [32] reported an adjustable speed drive using a torque control technique for an IPMSM by providing control of the magnitude and phase angle of the sinusoidal phase currents with respect to the rotor orientation. This method cannot provide a smooth transition from the constant torque mode to the constant power mode while the motor is in operation. In addition, the performance of this drive system has not been investigated over a wide speed range.

Jahns [33] also proposed a flux-weakening mode operating scheme for the IPMSM. This allows for investigation of the performance of the drive over an extended speed range. In this method, the d-axis rotor current is obtained from the sensed stator phase currents and the d-axis command current.

Likewise, Morimoto et. al., [34-39] have proposed a flux-weakening mode-based controller for an IPMSM drive. In this work, the magnetic saturation and demagnetization effects of permanent magnets has been accounted and compensated for. This results in high torque and high efficiency operation within the maximum voltage and current limit ratings of the inverter and the motor. Different

control methods, such as as $i_d = 0$, unity power factor and constant flux linkage schemes have been investigated, and a comparison of the various methods has been made over a wide speed range. Regarding the magnitude and phase errors inherent when using a current controlled VSI, a compensating technique based on a calculated value of q-axis inductance, L_q, from the actual q-axis current has been used. Then, in order to overcome saturation, the d-axis command current is generated from the calculated value of L_q. The shortcoming of this work is that the effects of parameter variations due to noise, temperature, etc. are not considered.

Rahman et. al. [40] have proposed a flux-weakening mode based torque controller for the IPMSM drive for operation exceeding base speed. Maximum voltage and current capabilities of the motor and the inverter during operation are also accounted for in this work. The drive has not been tested for variable speed operation.

Vaez et. al. [41] have proposed a vector control strategy of the IPMSM drive aimed at producing minimum loss operation. They have used a PI-based speed controller, making this scheme sensitive to parameter variations, load changes, etc..

Radwan et. al. [42] have developed a hybrid current controller for the IPMSM drive which incorporates a ramp comparator controller for low speed operation and a hysteresis current controller for high speed operation. This controller produces stable operation over a wide speed range. However, as with Vaez et. al. the speed controller is PI-based.

Hoque et. al. [43] have reported a vector control strategy of the IPMSM drive based on the maximum torque per ampere (MTPA) scheme. In this work, d-axis command current is obtained from q-axis command current by use of a Taylor

series expansion to overcome mathematical difficulties arising from nonlinearities of the model. A PI-based speed controller has been used. This work was done in conjunction with the work presented in this thesis.

Other works [44-47] investigating PMSM drive performance while in flux-weakening mode have been reported. Most of these works are based on conventional PI and PID based speed controllers. These controllers offer the advantages of simplicity and ease of implementation in real time. However, they are very sensitive to parameter variations due to load changes, sudden changes of command speed, saturation, temperature variations and other system uncertainties. Therefore, it is difficult to tune the controller parameters precisely for an optimal implementation. Consequently, these types of controllers are not suitable for high performance applications, and researchers have been prompted to develop adaptive control schemes for PMSM drive systems in which the controller parameters can be adapted in real time in response to system parameter variations and load changes.

1.3.3 PMSM Drives with Adaptive Controllers

To date, adaptive controllers have been used in PMSM drives to achieve fast transient responses, parameter insensitivity, nonlinear load handling capabilities and high adaptabilities to other types of uncertainties.

The model reference adaptive controller (MRAC) is one such scheme in which the drive forces the motor response to follow the output of a reference model regardless of drive parameter changes. A MRAC may be used with a PI controller to adapt the controller parameters compensatively for system parameter changes.

Parameters are adapted by trial and error such that the error between the actual and the desired responses remains within specified limits.

Choy et. al., [48] have proposed a vector control position servo PMSM drive system using a MRAC. In their work a MRAC is used to reactively tune a PI controller. The steady state error gain component of the PI controller is used to compensate the chattering problem that occurs due to discontinuous control inputs. However, this drive still does not completely overcome the chattering problem.

Cerruto et. al., [49] have proposed a MRAC-based PMSM drive for robotic applications. A MRAC has been used to compensate for changes in system parameters such as inertia and torque constant. As explained previously, the error between the reference model speed and the actual speed is used to adjust the parameters. The shortcoming of this model is the computational burden that the algorithm imposes on the microcomputer. This limits the maximum operating speed of the drive.

Sozer and Torrey [50] have proposed a MRAC-based PMSM drive utilizing an adaptive flux weakening mode controller that adjusts the d-axis current i_d compensatively. However, this drive has been reported in simulation only and has not been tested at variable speed conditions.

MRAC is only one of several types of adaptive controllers. Other popular schemes that have been used in PMSM drive systems are the sliding mode controller (SMC) and the variable structure controller (VSC).

Namudri and Sen [51] have presented a SMC-based vector control system of a synchronous motor drive for a position servo drive. In their work a gate turn-off (GTO) inverter and phase-controlled chopper are used to provide the torque

producing current component. The controller accommodates parameter variations and load changes.

Consoli and Antonio [52] have proposed a DSP-based vector control scheme for an IPMSM drive using a SMC for torque control. In this work, both the actual motor currents and terminal voltages are used as feedback signals to generate the torque and flux for flux-weakening mode operation above base speed. The effects of constant acceleration, constant speed and constant deceleration have been accounted for in the design of the SMC. However, this drive system has been presented in simulation only and not in real-time where the parameter variations are not defined.

An ac servo drive using a variable structure controller (VSC) for position and speed control of a PMSM has been presented by Ghirby and Le-Huy [53]. Two control loops have been used, an inner loop for predictive current controllers and an outer loop for a position or speed controller. The performance of the drive has not been reported for wide variable speed operations, and suffers somewhat from chattering.

Sepe and Lang [54] have also proposed an adaptive speed controller for the PMSM drive system in which the mechanical parameters of the motor have been estimated in real-time to continually tune the gain of the controller. As with Ghirby and Le-Huy, the system is composed of two loops: An inner loop consisting of the motor, inverter, current controller, speed controller and filter; and a slower, outer loop consisting of a motor parameter estimator and the control algorithm for the controller. This system has been implemented on a microprocessor of limited computational capacity, therefore the performance of the drive is impaired by significant noise in steady state operation.

Clearly, compared to conventional fixed-gain PI and PID controllers, adaptive controllers show improved performance because of their relative insensitivities to parameter variations, load changes and other uncertainties. However, all of this is achieved at the cost of increased computational burden, hence reducing practicality for real-time implementation. And almost all of the adaptive controller-based systems suffer from chattering, overreaching and steady state errors due to finite switching. In addition, the unavailability of the exact system parameter model makes for cumbersome design approaches for these types of controllers.

1.3.4 PMSM Drives with Intelligent Controllers

To solve some of the problems associated with fixed gain PI, PID and various adaptive controllers, recent researchers have investigated intelligent controllers such as artificial neural network (ANN), fuzzy logic (FL), neuro-fuzzy (NF), and genetic controller-based systems. These controllers are self-adaptive and do not need any advance information about system nonlinearities. They are often called artificial intelligence (AI) controllers, because they involve software programming where the computer mimics human thinking in the control of the motor.

ANNs have been reported for use in controllers for PMSM drives. El-Sarkawi et. al., [55] have proposed one such scheme for a high performance brushless dc motor drive. In their work, a MRAC is used to implement a multi-layer ANN. The inputs of the ANN are the estimated speed from the reference model, three consecutive past samples of actual speed, a past sample of the converter input voltage, and the error between the reference model speed and the actual speed. A back-propagation algorithm is used to train the network. However, the speed con-

trol of this drive is not precise because the ANN must be trained offline. This shortcoming may render the drive incapable of effectively handling different dynamic operating conditions such as load changes, parameter variations and system disturbances.

Similarly, Shigou et. al., [56] have proposed an offline-trained ANN-based controller for a brushless dc servo motor drive system. In their work, they have used an analog speed controller in order to obtain better servo performance. However, they still have not produced satisfactorily precise speed control.

Rahman and Hoque [57] have presented an online ANN-based PMSM drive system utilizing a back-propagation training algorithm and combined offline and online training. There are two artificial neural networks: One to generate the command signal and the other to generate the estimated signal. Controller parameters are then updated in accordance with the error between the two signals. In this work, however, the d-axis command current, i_d^*, is assumed to be zero, which makes it impossible to control the motor above base speed.

Another work, by Y. Yi et. al. [58] has utilized an ANN-based controller for an IPMSM. This work shows encouraging results, but, as with other ANN-based systems, simulation and experimental results show room for improvement in terms of disturbance rejection such as insensitivity to load variations, parameter variations, etc..

Hoque et. al. [59] have reported a similar online ANN-based PMSM drive system using the maximum torque per ampere (MTPA) scheme. Once again, a back-propagation training algorithm making use of combined offline and online training is used, but in this work, d-axis command current is obtained from q-axis command current by use of a Taylor series expansion. This is done to overcome

mathematical difficulties arising from the nonlinearities of the model. The ANN tunes the parameters of a PI-based speed controller. This work was done in conjunction with the work presented in this thesis.

Recently, researchers have developed fuzzy logic controllers (FLC), showing encouraging performances, for use in PMSM drives. In almost all cases the FLC has been used as a speed controller.

Inoue et. al., [60] have presented a fuzzy algorithm for the brushless dc servo motor drive. The fuzzy algorithm is used to tune the gain of the PI controller in response to load changes, parameter changes and system disturbances. The actual speed, reference speed and output of the reference filter are used to generate the membership functions. The experimental results show optimum response after several auto-tuning calculations. However, as the drive system incorporates a reference generator, somewhat complex fuzzy calculations and two PI controllers, the system imposes high computational burden, thus diminishing performance.

Erenay et. al., [61] have proposed a fuzzy logic approach for the brushless dc motor drives used in washing machines. They have made a comparison among various controller techniques namely, conventional PI, fuzzy PI, fuzzy reset rate and fuzzy gain scheduled PI. However, they have investigated the speed responses only for fixed speed conditions. Moreover, because of the large number of fuzzy rules incorporated, high computational burden may render these FLC-based systems incapable of high-speed operations. In experimental results, it is shown that the motor cannot follow the command speed smoothly.

A fuzzy logic-based MRAC for the PMSM drive has been proposed by Koviac et. al. [62]. Simulation results verify the effectiveness of the proposed al-

gorithm, which was designed using the linearized model of the PMSM (the reference model being parameter dependent). This may not translate to real-time implementation where nonlinear load changes and parameter variations exist with different operating conditions.

Uddin and Rahman [63] have presented a FLC-based vector control scheme for the IPMSM. Their work uses a fuzzy algorithm to determine q-axis command current from the error between actual and reference speeds, and the difference between the current and previous speed errors. D-axis command current is set to be zero as a simplifying approximation. Heavy computational burden and the inaccuracy of the $i_{dr}^{*} = 0$ approximation limit the capacity of this scheme.

The application of fuzzy logic for IPMSM drives is in its initial stages. The heavy computational burden imposed by fuzzy algorithms limit these systems to implementation with only the fastest, most resource intensive microprocessors. Therefore, there exists a need to reduce the complexity of these algorithms so they may be implemented more economically. Furthermore, because of mathematical complexity and nonlinearity, the maximum torque per ampere approach for PMSM drives has not been practically implemented. Without this scheme PMSM drives must operate at less than optimum efficiency. Simplified FLC-based controllers, combined with MTPA mode operation, can overcome various drive uncertainties such as unknown nonlinear load characteristics, parameter changes and other system disturbances, as well as provide maximum efficiency operation of the PMSM at and below the rated speed.

1.4 Problem Identification and Thesis Objectives

High performance drive (HPD) systems must provide fast and accurate speed responses, quick recoveries of reference speed from sudden disturbances of all natures, and show insensitivity to parameter variations. Each of the systems presented to date have shortcomings that require remedy if the IPMSM is to be practically implemented under HPD standards. Thus, it is necessary to further develop control algorithms and approaches to produce this high standard of performance in a practical manner.

While the IPMSM has many advantages over conventional motors, its operation is strongly affected by motor magnetic saliency, saturation and armature reaction effects [64]. Particularly, the saturation of the iron portion of the rotor around the permanent magnets produces a distortion of the air-gap flux that affects the reactance parameters of the motor. These reactance changes with different operating conditions and, hence, affect the performance of the drive system if they are not accounted for. This makes the control of the IPMSM for HPD applications an engineering challenge.

The objective of this work is to develop and implement a complete IPMSM drive system to be used in HPD applications. The vector control scheme, incorporating a speed controller and a current controller is used because it decouples the torque and flux, thus providing faster transient responses and making the control task easier. An efficient speed controller, incorporating heretofore undeveloped methods is presented for the high performance IPMSM drive.

As discussed in the literature survey, fixed-gain proportional integral (PI) and proportional integral derivative (PID) controllers, model reference adaptive controllers (MRAC), variable structure controllers (VSC), sliding mode controllers

(SMC) and self-tuning regulators (STR) all require the accurate and precise knowledge of system model parameters. Moreover, the fixed-gain PI and PID controllers are especially sensitive to parameter variations, load changes and other system disturbances. Intelligent controllers, such as the fuzzy logic controller (FLC), do not need any information about the system mathematical model, are self-adaptive to uncertainties and can handle any kind of system non-linearity. However, FLC-based drive systems incorporate complex algorithms that impose such computational burdens that they can only be incorporated by making performance compromises or by use of the latest, most powerful personal computer systems. Therefore, a large part of the purpose of this work is not only the real-time implementation of the IPMSM drive incorporating an intelligent, FLC-based controller, but also to achieve this control with minimal complexity and computational burden. In addition, many researchers have simplified the non-linear model of the IPMSM to a linear one by forcing the d-axis current to zero (i.e. $i_d = 0$). This is not accurate and, as a result, produces a motor control that requires increased stator current to produce a given torque. This work includes the development of a practical implementation of the maximum torque per ampere (MTPA) scheme with the real case of $i_d \neq 0$, which produces motor torque with the minimum possible stator currents.

Laboratory implementation has been carried out to verify theoretical and experimental results. These results have been compared with those obtained using a traditional FLC-based system with $i_d = 0$.

1.5 Thesis Organization

This thesis consists of six chapters. The introduction and literature survey of vector control techniques for permanent magnet synchronous motor drives, as well as the objectives of this thesis have been covered in this chapter.

Chapter two contains the theoretical development of the mathematical model of the interior permanent magnet synchronous motor (IPMSM) and presents the theoretical development of the analysis and modeling of the PWM VSI-fed IPMSM drive with maximum torque per ampere (MTPA) based control.

Chapter three outlines the development of the fuzzy logic based speed controller for the IPMSM drive and presents a simplified fuzzy logic based speed controller incorporating the maximum torque per ampere mode of operation that reduces complexity and computational burden. Ideas developed include linguistic variables, membership functions, fuzzification, rule evaluation and defuzzification. Both controllers are incorporated into problem specific vector control schemes for the IPMSM.

Chapter four presents the simulation results of both of these drives.

Chapter five contains the results of the real-time experimental implementation of the simplified FLC/MTPA drive which has been implemented using a digital signal processor (DSP) based vector control of a laboratory 1 hp IPMSM.

Chapter 6 presents the summary of the contribution of this work and the conclusion.

Finally all pertinent references are listed.

Chapter 2

Analysis and Modeling of the PWM VSI-Fed IPMSM Drive

2.1 General Introduction

This chapter presents the development of the mathematical model of a complete current-controlled voltage source inverter (VSI) -fed interior permanent magnet synchronous motor (IPMSM) drive using the d-q axis model of the IPMSM. A fixed-band hysteresis current controller has been used to apply the correct stator currents to the motor through the VSI.

In order to operate the vector control scheme, a fuzzy logic based speed controller is used. This will be developed in chapter 3.

2.1.1 Mathematical Modeling of the IPMSM

The IPMSM is similar to the conventional synchronous motor with the exception that the field excitation is provided by permanent magnets instead of a wire-wound dc rotor field. Because of this, the mathematical model of the IPMSM can be derived from the standard model of the synchronous motor by removing the equation related to the field current and other associated terms.

The flux linkages in the three stator phase windings due to the permanent magnets of the rotor are given in matrix form as [65]:

$$\begin{bmatrix} \psi_{am} \\ \psi_{bm} \\ \psi_{cm} \end{bmatrix} = \psi_m \begin{bmatrix} \sin\theta_r \\ \sin\left(\theta_r - \frac{2\pi}{3}\right) \\ \sin\left(\theta_r + \frac{2\pi}{3}\right) \end{bmatrix} \tag{2.1}$$

The three phase air gap flux linkage equations are given in matrix form as:

$$\begin{bmatrix} \psi_a \\ \psi_b \\ \psi_c \end{bmatrix} = \begin{bmatrix} L_{aa} & M_{ab} & M_{ac} \\ M_{ba} & L_{bb} & M_{bc} \\ M_{ca} & M_{cb} & L_{cc} \end{bmatrix} \begin{bmatrix} i_a \\ i_b \\ i_c \end{bmatrix} + \psi_m \begin{bmatrix} \sin\theta_r \\ \sin\left(\theta_r - \frac{2\pi}{3}\right) \\ \sin\left(\theta_r + \frac{2\pi}{3}\right) \end{bmatrix} \tag{2.2}$$

where i_a, i_b, i_c are the three phase currents, L_{aa}, L_{bb}, L_{cc} are the self inductances and M_{ab}, M_{bc}, M_{ca} are the mutual inductances, respectively, ψ_m is the constant flux sup-

plied by the permanent magnets and θ_r is the rotor position angle. Rotor position angle θ_r is defined as,

$$\theta_r = \int_0^t \omega_r(t)dt + \theta_r(0) \tag{2.3}$$

The voltage equations of the three phases of the IPMSM can be defined as,

$$v_a = r_a i_a + \frac{d\psi_a}{dt} \tag{2.4}$$

$$v_b = r_b i_b + \frac{d\psi_b}{dt} \tag{2.5}$$

$$v_c = r_c i_c + \frac{d\psi_c}{dt} \tag{2.6}$$

where v_a, v_b, v_c are the three phase voltages and r_a, r_b, r_c are the three stator phase resistances. In matrix form, this is,

$$\begin{bmatrix} v_a \\ v_b \\ v_c \end{bmatrix} = \begin{bmatrix} r_a & 0 & 0 \\ 0 & r_b & 0 \\ 0 & 0 & r_c \end{bmatrix} \begin{bmatrix} i_a \\ i_b \\ i_c \end{bmatrix} + p \begin{bmatrix} \psi_a \\ \psi_b \\ \psi_c \end{bmatrix} \tag{2.7}$$

where p is the time differential operator, $\frac{d}{dt}$. Inspection of Eqn. (2.2) reveals that the flux linkages are functions of rotor position and, therefore, functions of rotor speed. This means that the coefficients of the voltage equations are time varying (except, of course, when the motor is stationary). In order to avoid the complexity

of calculations, all of the equations can be transformed to the synchronously rotating rotor reference frame where the machine equations are no longer dependent on the rotor position. This is accomplished using Park's transformation equations [65]. First, the machine equations are transformed from the stationary a-b-c frame to the stationary d-q frame, then they are transformed from the stationary d-q frame to the synchronously rotating d^r-q^r frame. Using x to represent the machine phase variables, the inverse Park's transform gives,

$$\begin{bmatrix} x_a \\ x_b \\ x_c \end{bmatrix} = \begin{bmatrix} \cos\theta_r & \sin\theta_r & 1 \\ \cos\left(\theta_r - \frac{2\pi}{3}\right) & \sin\left(\theta_r - \frac{2\pi}{3}\right) & 1 \\ \cos\left(\theta_r + \frac{2\pi}{3}\right) & \sin\left(\theta_r + \frac{2\pi}{3}\right) & 1 \end{bmatrix} \begin{bmatrix} x_q \\ x_d \\ x_o \end{bmatrix} \tag{2.8}$$

The corresponding Park transform is,

$$\begin{bmatrix} x_q \\ x_d \\ x_o \end{bmatrix} = \frac{2}{3} \begin{bmatrix} \cos\theta_r & \cos\left(\theta_r - \frac{2\pi}{3}\right) & \cos\left(\theta_r + \frac{2\pi}{3}\right) \\ \sin\theta_r & \sin\left(\theta_r - \frac{2\pi}{3}\right) & \sin\left(\theta_r + \frac{2\pi}{3}\right) \\ \frac{1}{2} & \frac{1}{2} & \frac{1}{2} \end{bmatrix} \begin{bmatrix} x_a \\ x_b \\ x_c \end{bmatrix} \tag{2.9}$$

where x_o is the zero sequence component. The matrix element x may represent either voltage or current. Eqns. (2.8 -2.9) are both in a stationary reference frame, so θ_r is only the initial rotor position $\theta_r(0)$ which is also the angle difference between

the q-axis and a-phase. For balanced 3-phase, x_o does not exist and it is also convenient to set $\theta_r(0) = 0$ so that the q-axis coincides with the a-phase. Under these conditions, Eqns. (2.8) and (2.9) become,

$$\begin{bmatrix} x_a \\ x_b \\ x_c \end{bmatrix} = \begin{bmatrix} 1 & 0 \\ \frac{-1}{2} & \frac{-\sqrt{3}}{2} \\ \frac{-1}{2} & \frac{\sqrt{3}}{2} \end{bmatrix} \begin{bmatrix} x_q \\ x_d \end{bmatrix} \tag{2.10}$$

and

$$\begin{bmatrix} x_q \\ x_d \end{bmatrix} = \begin{bmatrix} \frac{2}{3} & \frac{-1}{3} & \frac{-1}{3} \\ 0 & \frac{-1}{\sqrt{3}} & \frac{1}{\sqrt{3}} \end{bmatrix} \begin{bmatrix} x_a \\ x_b \\ x_c \end{bmatrix} \tag{2.11}$$

To convert these variables to the rotating d-q frame we use Fig 2.1 as reference. From this, we see that the quantities in the stationary d-q frame can be converted to the synchronously rotating frame as follows:

$$\begin{bmatrix} x_q^r \\ x_d^r \end{bmatrix} = \begin{bmatrix} \text{Cos}\theta_r & -\text{Sin}\theta_r \\ \text{Sin}\theta_r & \text{Cos}\theta_r \end{bmatrix} \begin{bmatrix} x_q \\ x_d \end{bmatrix} \tag{2.12}$$

The inverse relation can be written as,

$$\begin{bmatrix} x_q \\ x_d \end{bmatrix} = \begin{bmatrix} \text{Cos}\theta_r & \text{Sin}\theta_r \\ -\text{Sin}\theta_r & \text{Cos}\theta_r \end{bmatrix} \begin{bmatrix} x_q^r \\ x_d^r \end{bmatrix} \tag{2.13}$$

Now, using equations (2.7)-(2.8) and (2.13) the d^r-q^r model of the IPMSM can be written as,

$$v_q^r = r_s i_q^r + p\psi_q^r + \omega_s \psi_d^r \tag{2.14}$$

$$v_d^r = r_s i_d^r + p\psi_d^r - \omega_s \psi_q^r \tag{2.15}$$

where v_d^r and v_q^r are the d and q axis voltages, i_d^r and i_q^r are the d and q axis currents, respectively, r_s is the per phase stator resistance and ω_s is the stator frequency.

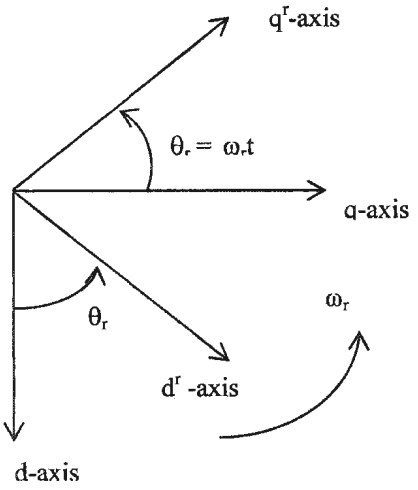

Fig. 2.1 Relative positions of stationary d-q axes and rotating d^r-q^r axes.

The following assumptions have, thus far, been made:

(a) The eddy current and hysteresis losses are negligible.

(b) There is no squirrel cage on the rotor side.

(c) The induced emf is sinusoidal.

(d) The saturation is neglected.

(e) There are no field current dynamics or magnet imperfections.

(f) The stator resistances of the three phases are balanced.

The q-axis flux linkage ψ_q^r and the d-axis flux linkage ψ_d^r can be written as,

$$\psi_q^r = L_q i_q^r \tag{2.16}$$

$$\psi_d^r = L_d i_d^r + \psi_m \tag{2.17}$$

where,

$$L_q = L_l + L_{mq} \tag{2.18}$$

$$L_d = L_l + L_{md} \tag{2.19}$$

L_d and L_q are the d and q axis inductances, L_{md} and L_{mq} are the d- and q-axis magnetizing inductances, respectively, and L_l is the leakage inductance per phase. The stator frequency ω_s is related to the rotor frequency ω_r as,

$$\omega_s = P\omega_r \tag{2.20}$$

where P is the number of pole-pairs. Therefore, Eqns. (2.14)-(2.15) can be rewritten as,

$$\begin{bmatrix} v_q^r \\ v_d^r \end{bmatrix} = \begin{bmatrix} r_s + pL_q & P\omega_r L_d \\ -P\omega_r L_q & r_s + pL_d \end{bmatrix} \begin{bmatrix} i_q^r \\ i_d^r \end{bmatrix} + \begin{bmatrix} P\omega_r \psi_m \\ 0 \end{bmatrix} \tag{2.21}$$

Consequently, the IPMSM can be represented by the d^r and q^r axis equivalent circuit diagrams shown in Fig. 2.2, where the permanent magnet is represented as a current source [66] in Fig. 2.2(a).

From these equivalent circuits, the power developed per phase is given by,

$$P_{phase} = \left(-P\omega_r L_q i_q^r i_d^r + P\omega_r L_d i_d^r i_q^r + P\omega_r \psi_m i_q^r\right)\left(\frac{1}{2}\right) \tag{2.22}$$

So, the total power developed by the machine is,

$$P_{mach} = \frac{3P\omega_r}{2}\left\{\psi_m i_q^r + \left(L_d - L_q\right) i_d^r i_q^r\right\} \tag{2.23}$$

And the developed electromagnetic torque is given by,

$$T_e = \frac{P_{mach}}{\omega_r} = \frac{3P}{2}\left[\psi_m i_q^r + \left(L_d - L_q\right) i_d^r i_q^r\right] \tag{2.24}$$

which can also be represented as,

$$T_e = T_L + B_m\omega_r + J_m p\ \omega_r \tag{2.25}$$

where T_L is the load torque, P is number of pole pairs of the motor, p is the differential operator, B_m is the friction damping coefficient and J_m is the rotor inertia constant.

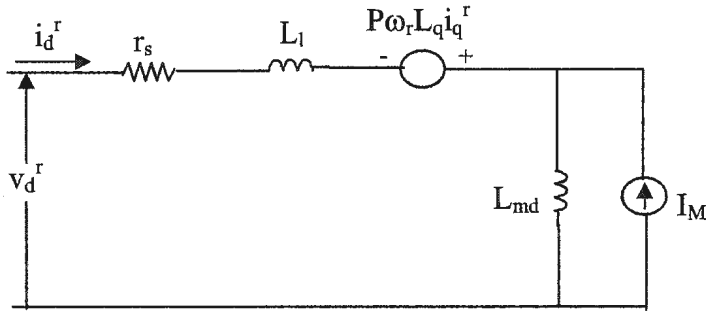

(a)

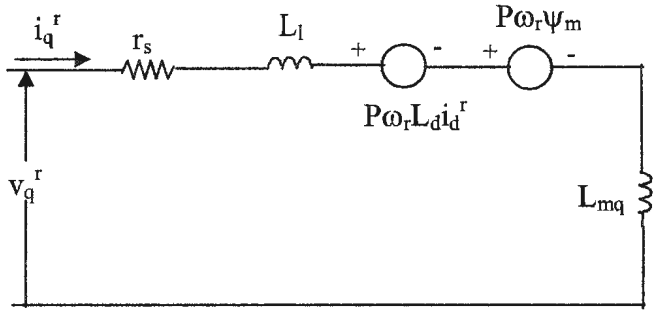

(b)

Fig. 2.2. Equivalent circuit model of the IPMSM: (a) d-axis, (b) q-axis.

So, finally, the IPMSM model equations may be expressed as follows:

$$pi_q^r = (v_q^r - R\, i_q^r - P\omega_r L_d\, i_d^r - P\omega_r \psi_m)/ L_q \tag{2.26}$$

$$pi_d^r = (v_d^r - R\, i_d^r + P\omega_r L_q\, i_q^r)/ L_d \tag{2.27}$$

$$p\omega_r = (T_e - T_L - B_m\, \omega_r)/J_m \tag{2.28}$$

The above three fundamental equations are used to model the IPMSM. The specific motor parameters used for simulation are given in Appendix A.

2.2 Vector Control of the IPMSM Drive

From equation (2.24) one obtains the expression of torque,

$$T_e = \frac{P_{mach}}{\omega_r} = \frac{3P}{2}\left[\psi_m i_q^r + \left(L_d - L_q\right) i_d^r i_q^r\right] \tag{2.29}$$

we see that the second term in the electrical torque equation (2.29) represents a complex interaction of inductances, L_d and L_q and also the currents, i_d^r and i_q^r. However, in the case of the IPMSM, L_q is larger than L_d, and both undergo significant variations under different steady state and dynamic loading conditions [64]. So the complexity of the control of the IPMSM drive arises due to the nonlinear nature of the torque Eqn. (2.29).

Using phasor notations, and taking the d^r axis as reference, the steady state phase voltage V_a can be derived from the steady state d^r-q^r axis voltages described in Eqn. (2.21) as,

$$V_a = v_d^r + j\, v_q^r = r_s I_a - \omega_s L_q i_q^r + j\omega_s L_d i_d^r + j\omega_s \psi_m \qquad (2.30)$$

In the case of the IPMSM motor, the d^r-axis current is negative and it demagnetizes the main flux provided by the permanent magnets. Thus, in order to take only the absolute value of i_d^r one can re-write the Eqn. (2.30) as follows:

$$V_a = r_s I_a - \omega_s L_q i_q^r - j\omega_s L_d i_d^r + j\omega_s \psi_m \qquad (2.31)$$

where, the phase current, I_a is given as,

$$I_a = -i_d^r + j\, i_q^r \qquad (2.32)$$

Based on Eqn. (2.30) the vector diagram of the IPMSM is shown in Fig. 2.3. It can be seen that the stator current can be controlled by the d^r and q^r axis current components, hence, the basis of the vector control scheme is illustrated. A complete indirect vector control scheme for the current controlled VSI-fed IPMSM drive is shown in Fig. 2.4.

The IPMSM drive consists of the current controller and the speed controller. The speed controller generates the torque command from the command speed and the actual speed samples. Then the command phase currents i_a^*, i_b^* and i_c^* are generated from i_q^{r*} and i_d^{r*} using Park's transformation. From these command currents and the actual motor stator currents, i_a, i_b and i_c, the current controller provides the appropriate operating gating signals to the current-controlled voltage source pulse width modulated (PWM) 3-phase, 6-pulse inverter, forcing the actual

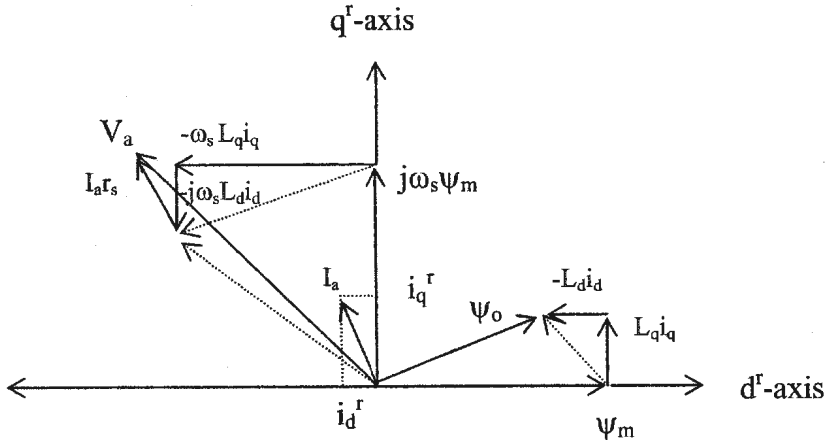

Fig. 2.3. Vector diagram of IPMSM parameters.

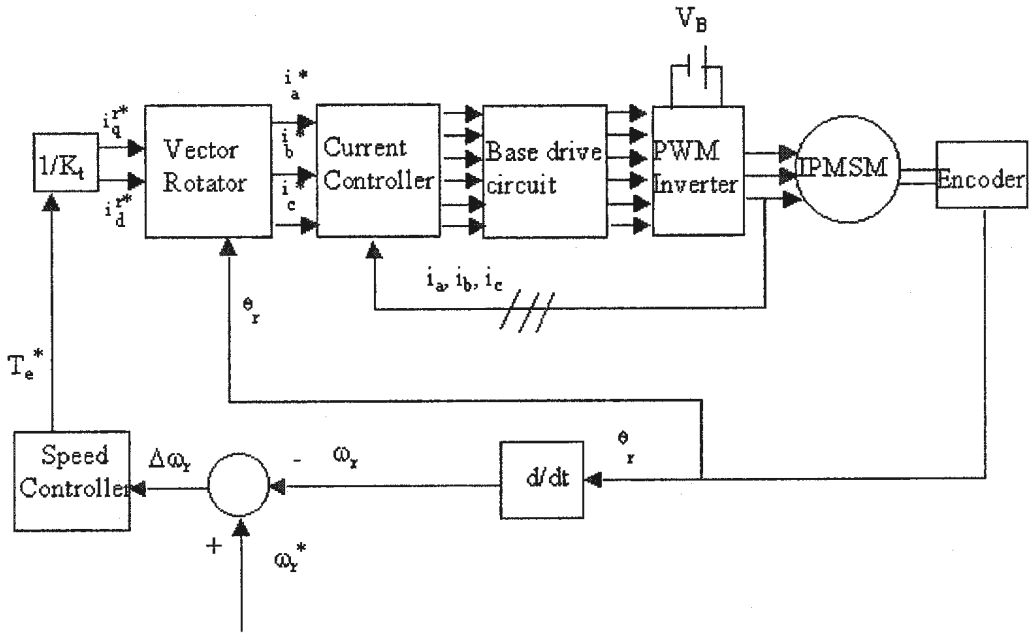

Fig. 2.4. Block diagram of complete current-controlled VSI-fed IPMSM drive.

motor currents to follow the command currents as closely as possible and, hence, forcing the motor to follow the command speed by feedback control.

Therefore, in order to operate the motor in a vector control scheme the feedback quantities will be the rotor angular position and the actual motor currents.

2.2.1 Maximum Torque Per Ampere Speed Controller

The speed controller generates the torque command from the command speed and the actual speed samples. Traditionally, this has been accomplished by use of PI and PID controllers. However, these controllers produce unsatisfactory performance for high performance drive systems, so alternatives must be found (as covered in Chapter 1). In this work, Fuzzy Logic Controllers have been used to design the speed controllers. Their development will be detailed in Chapter 3.

In addition, the d-q axis command currents, i_d^{r*} and i_q^{r*} are determined from command torque by manipulation of Eqn. (2.29). One of the main problems associated with the control of the IPMSM is the non-linearity arising out of the developed torque, as can be seen from the torque equation (2.29). Many researchers have focused their attention on the vector control of the IPMSM drive by forcing $i_d = 0$, which linearizes the torque equation [25, 28, 32, 34]. However, in real-time the electromagnetic torque truly is non-linear in nature. In order to incorporate this non-linearity in a practical IPMSM drive, a control technique known as maximum torque per ampere (MTPA) has been derived which provides maximum motor torque with minimum stator current [25, 28, 32, 40, 67]. This MTPA strategy is very important from the limitation of IPMSM and inverter rating points of view, which optimizes the drive efficiency. Figure 2.5 shows the

maximum torque per ampere trajectory that provides information for the control strategy.

The problem associated MTPA control technique is that its implementation in real time becomes complicated because of the complex relationship between d-axis and q-axis currents. Some researchers have solved this problem by use of look-up tables, based on this trajectory, for d- and q-axis currents [40, 43].

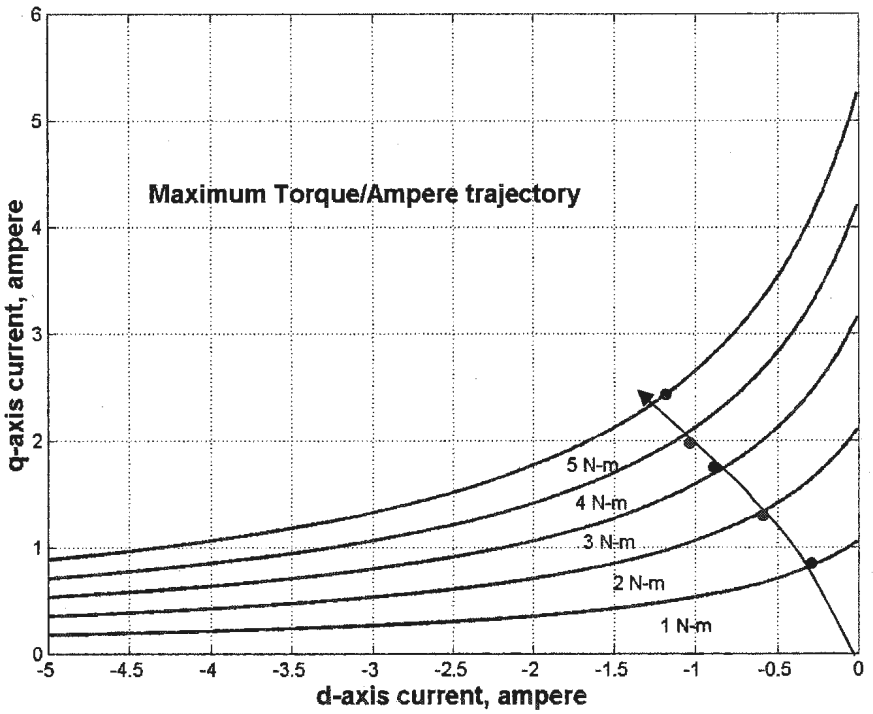

Fig. 2.5. Maximum torque per ampere (MTPA) trajectory on constant torque loci.

For application of the MTPA technique, the relation between i_d and i_q can be obtained by differentiating Eqn. (2.29) with respect to i_q and setting the resulting expression to zero. The relation between i_d, i_q and I_a can be derived from Eqn. (2.32) as

$$i_d = \sqrt{I_a^2 - i_q^2}. \tag{2.33}$$

Giving,

$$\frac{dT_e}{di_q} = \frac{3P}{2}\left(\psi_m + (L_d - L_q)i_d - (L_d - L_q)i_q^2 \frac{1}{\sqrt{I_a^2 - i_q^2}}\right) = 0, \tag{2.34}$$

$$\psi_m + (L_d - L_q)i_d - (L_d - L_q)\frac{i_q^2}{i_d} = 0. \tag{2.35}$$

Rearranging the order of L_d and L_q and solving for i_d gives,

$$i_d = \frac{\psi_m}{2(L_q - L_d)} - \sqrt{\frac{\psi_m^2}{4(L_q - L_d)^2} + i_q^2} \tag{2.36}$$

Substituting Eqn. (2.36) into Eqn. (2.29), one can get a non-linear relationship between i_q and T_e as,

$$T_e = \frac{3P}{2}\left(\psi_m i_q - \frac{\psi_m i_q}{2} - \left(L_d - L_q\right)\sqrt{\frac{\psi_m^2 i_q^2}{4\left(L_q - L_d\right)^2} + i_q^4}\right) \tag{2.37}$$

Because of the square root terms, the real-time implementation of the drive system becomes difficult using Eqns. (2.36) and (2.37). This work presents a simplified relationship between the d-q axis currents, which is obtained by expanding the square root term of Eqn. (2.36) using a Taylor series expansion around a point approaching zero. (Zero itself was not used because, practically, it is desired to have the approximation most accurate for small values of i_q but not exactly zero.) Substituting the appropriate experimental machine parameters given in Appendix A into Eqn. (2.36) gives,

$$i_d = 4.22839 - \sqrt{17.87925 + i_q^2} \tag{2.38}$$

and expanding Eqn. (2.38) in a Taylor series about $i_q = 0.001$ gives,

$$i_d = -0.11825\,(i_q - 0.001)^2 - 0.00024\,(i_q - 0.001) - 0.118 \times 10^{-6} \tag{2.39}$$

Substituting Eqn. (2.39) into Eqn. (2.29) and solving for i_q gives,

$$i_q = -0.000047\,(T_e - 0.000942)^2 + 1.06157\,(T_e - 0.000942) + 0.001 \tag{2.40}$$

Equations (2.39) and (2.40) are used in the speed controller to determine the rotating frame d-q axis command currents for the MTPA control of the IPMSM.

2.2.2 Vector Rotator

The command current outputs of the speed controller are in the rotating rotor reference frame. Therefore, they must be transferred to the stator reference frame. The inputs of the vector rotator block are the d-q axis command currents, i_d^{r*} and i_q^{r*}, from the speed controller and the rotor position θ_r from the sensor on the motor. The outputs are the three phase command currents i_a^*, i_b^* and i_c^*.

The transformation is done by first converting the synchronously rotating $d^r - q^r$ axis quantities to the stationary d-q axis quantities and then transforming these stationary d-q axis quantities into the corresponding a-b-c phase currents.

2.2.3 Current Controller and Voltage Source Inverter

Once the appropriate a-b-c phase command currents are generated by the vector rotator a current controller is used to control the voltage source inverter (VSI) to produce these command currents on the motor stator. The outputs of the current controller are the firing pulses for the inverter switches. Therefore, the VSI forces the motor to follow the command speed by feedback control.

The current control principle for the VSI used in this work is the based on the fixed-band hysteresis controller. The hysteresis current controller is most commonly used for high performance drive applications because of its simplicity and ease of implementation while providing acceptable results.

2.3 Current Control of the Voltage Source Inverter

The purpose of the current controller is to force the motor stator currents to follow the a-b-c phase command currents as closely as possible. These command currents are produced from the error between the command speed and samples of the actual speed of the motor with the intent of producing a motor speed identical to that of the command speed. Therefore, under the scheme of speed control, the current controller forces the motor to follow the command speed.

The current-controlled VSI operation can be described, with reference to Fig. 2.6, as follows: The errors between the actual motor currents and the command currents are processed by the hysteresis current controller to generate the firing pulses for the transistors of the inverter. Each stator phase of the motor is

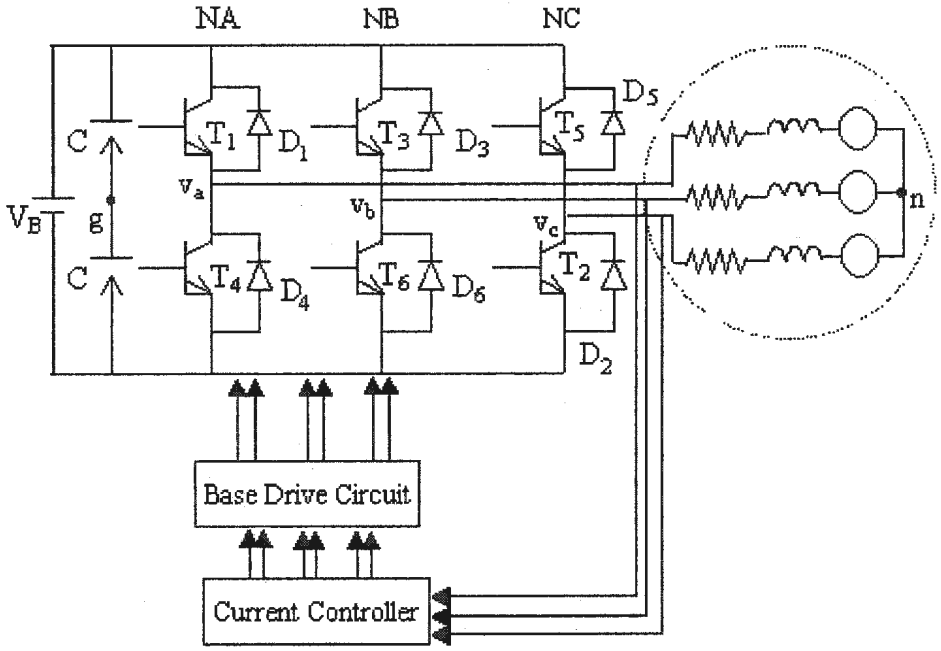

Fig. 2.6. Current controlled voltage source inverter for the IPMSM drive.

connected to the corresponding leg of the three-phase VSI. The center point of the two equal-valued capacitors is considered ground. The neutral of the stator is not connected to this ground.

In the figure NA, NB and NC represent three binary logic variables of the three legs of the inverter, respectively. These logic variables determine the conduction state of the inverter. When NA is 1, T_1 is conducting and T_4, is not, and when NA is 0, T_4 is conducting and T_1 is not. NB and NC produce similar conduction patterns in the other two legs.

To simplify the analysis of the three phase voltages, the concept of voltage and space vectors are used to analyze the current controller. The inverter voltage vector is defined as [14],

$$v = (2/3)\,(v_a + a v_b + a^2 v_c) \tag{2.41}$$

where $a=e^{j2\pi/3}$, and v_a, v_b, v_c are the phase voltages. The phase voltages v_a, v_b and v_c are expressed as functions of bus voltage, V_B, and the logic variables as,

$$\begin{bmatrix} v_{an} \\ v_{bn} \\ v_{cn} \end{bmatrix} = \frac{1}{3}\begin{bmatrix} 2 & -1 & -1 \\ -1 & 2 & -1 \\ -1 & -1 & 2 \end{bmatrix}\begin{bmatrix} NA \\ NB \\ NC \end{bmatrix} V_B\,. \tag{2.42}$$

There are eight switch combinations for the six switches of the inverter. Using Eqn. (2.41) the inverter voltage vector can be written as,

$$\begin{aligned} v_L &= (2/3)\, V_B\, e^{j(L-1)\pi/3} \quad \text{for } L= 1,2,\ldots,6 \\ &= 0 \qquad\qquad\qquad\qquad\quad \text{for } L= 0,7. \end{aligned} \tag{2.43}$$

The logic operation of the current-controlled VSI is summarized in Table 2.1.

The voltage vectors corresponding to the six active states are shown in Fig. 2.7. The magnitude of each voltage vector is $(2/3)V_B$. The magnitudes of the volt-

Table 2.1. Conduction modes of the VSI under current control

State, L	Leg 'a'		Leg 'b'		Leg 'c'		Operating modes	Voltage phasor
	T_1	T_4	T_3	T_6	T_5	T_2		
0	0	1	0	1	0	1	Freewheeling	v_o
1	1	0	0	1	0	1	Active	v_1
2	0	1	1	0	0	1	Active	v_2
3	1	0	1	0	0	1	Active	v_3
4	0	1	0	1	1	0	Active	v_4
5	1	0	0	1	1	0	Active	v_5
6	0	1	1	0	1	0	Active	v_6
7	1	0	1	0	1	0	Freewheeling	v_7

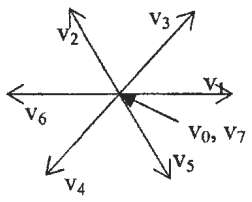

Fig. 2.7. VSI voltage vectors.

age vectors corresponding to the freewheeling states, v_0 and v_7, are zero. In these cases, no voltage is applied to the motor because in these states no conduction path exists across any leg of the inverter.

2.3.1 Effect of Unconnected Neutrals

If the neutral of the motor stator is not connected to the dc bus midpoint, the switching of any one phase depends on the states of the other two phases. This means that the individual line-to-neutral voltages are dependent on each other and each line current will depend not only on the corresponding inverter phase but also on the state of the other two phases. Therefore, the current controller experiences interaction between the phases of the inverter, and the actual current potentially may not follow the command current accurately and precisely.

2.3.2 Limitation of dc Bus Voltage and Inverter Switching frequency

In order for the inverter to produce and follow the command currents there must be sufficient dc voltage across the inverter terminals to force the line currents in the desired direction. As the back emf from the motor stator is increased a point is reached where the dc bus voltage is insufficient, and the line-to-neutral voltage of the inverter (and therefore also the stator) becomes a six-step quasi-square wave. At this point the current controller is saturated and actual stator current is not able to follow command current.

Inverter switching frequency, which depends on the type of current controller used, also imposes a limitation on the operation of the motor. In the case of the hysteresis controller, the switching frequency depends on several factors that can be described by the following equation representing one phase of the motor:

$$L\frac{di_a}{dt} = v_a - Ri_a - e_a, \tag{2.44}$$

where L is phase inductance, i_a is phase current, R is per-phase resistance, v_a is phase voltage and e_a is phase back emf. The actual switching pattern is shown in Fig. 2.8. In this figure, Δt_1 represents the time during which the line current will increase by Δi_{a1}, and Δt_2 is the time during which the current will decrease by Δi_{a2}. Assuming v_a and e_a are constant during the interval $\Delta t_1 + \Delta t_2$, and since inverter dc bus voltage, V_B, is equal to stator phase voltage, v_a, the equation describing Δt_1 and Δt_2 can be written as,

$$\Delta t_1 = \frac{L\Delta i_{a1}}{V_B - Ri_a - e_a}; \quad \Delta t_2 = \frac{L\Delta i_{a2}}{V_B - Ri_a - e_a}, \tag{2.45}$$

Inverter switching frequency can be expressed as,

$$f = 1/(\Delta t_1 + \Delta t_2). \tag{2.46}$$

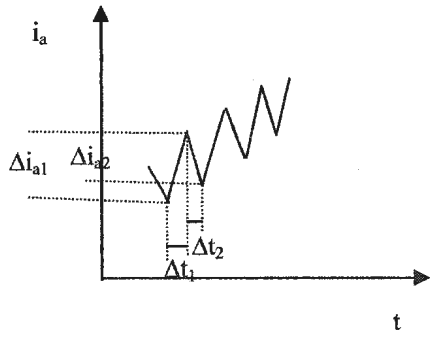

Fig.2.8. Hysteresis current controller switching pattern.

Therefore, switching frequency depends on the dc bus voltage, the inductance, and the magnitude and ripple content of the motor current. As the line-to-neutral fundamental voltage varies periodically, so the inverter switching frequency will vary over the fundamental period.

2.4 Hysteresis Current Controller

The block diagram of a typical three-phase hysteresis current controller scheme is shown in Fig. 2.9. The hysteresis controller is used to control the stator current in such a way that it can follow the command current within a hysteresis band, but the switching frequency of the inverter varies over the fundamental period. This results in an irregular operation of the inverter with time and, therefore, the switching losses are increased as compared to some other types of current controllers. Still, this type of controller is the most extensively used because of its simplicity and excellent dynamic response.

There are conventionally two types of hysteresis controllers: Sinusoidal-band and fixed-band hysteresis controllers. In the sinusoidal-band type, the hysteresis band varies sinusoidally over the fundamental period. The advantage of this scheme is that the harmonic content of the current is low, but this scheme produces very high switching frequencies near zero crossings. As a result, the maximum switching frequency of the inverter increases substantially when this type of controller is used.

With the fixed-band hysteresis controller the hysteresis band is maintained constant. This reduces the maximum switching frequency of the inverter but the harmonic current is increased. This is the type of current controller used in this work.

Fig. 2.9 illustrates the operating principle of the fixed-band hysteresis controller. In the figure, N1, N3 and N5 are the logic signals for the high transistors of the inverter and N4, N6 and N2 are the logic signals for the corresponding low transistors of the inverter. When the logic signal N1 is 1 then transistor T_1 is on and when it is 0 then T_1 is off. The other transistors follow logic signals likewise.

The operational logic of the fixed-band hysteresis controller is illustrated in Fig. 2.10. It can be described as follows:

(i) For $i_a^* > 0$, $N_4=0$: if $i_a > i_{up}$, then $N_1=0$, else if $i_a < i_{lo}$, then $N_1 =1$.

(ii) For $i_a^* < 0$, $N_1=0$: if $i_a > i_{up}$, then $N_4=1$, else if $i_a < i_{lo}$, then $N_4 =0$.

where i_a is actual 'a' phase current, i_a^* is command current, $i_{up}=i_a^* + H$ is the upper band, $i_{lo}=i_a^* - H$ is the lower band, and H is the fixed hysteresis band.

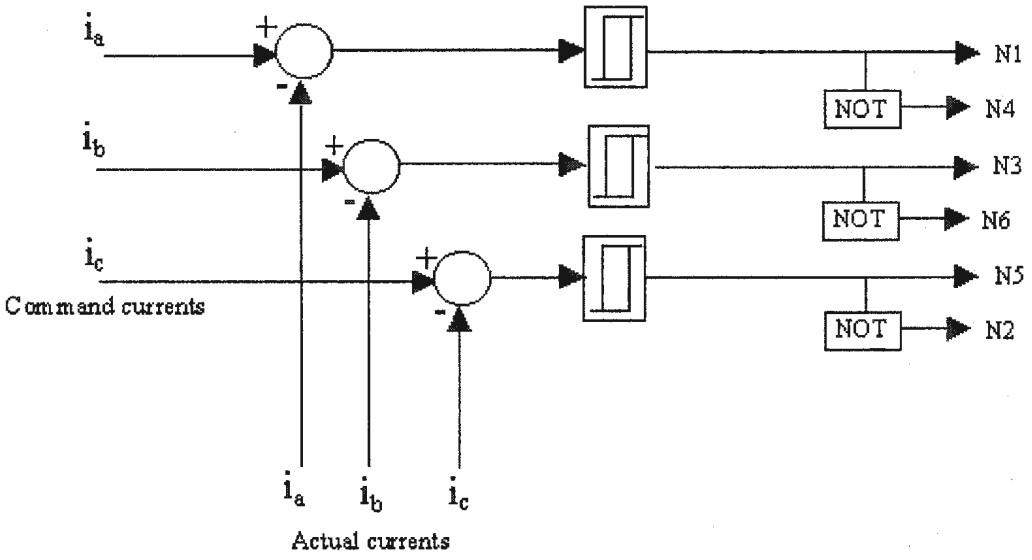

Fig.2.9. Fixed-band hysteresis current controller scheme.

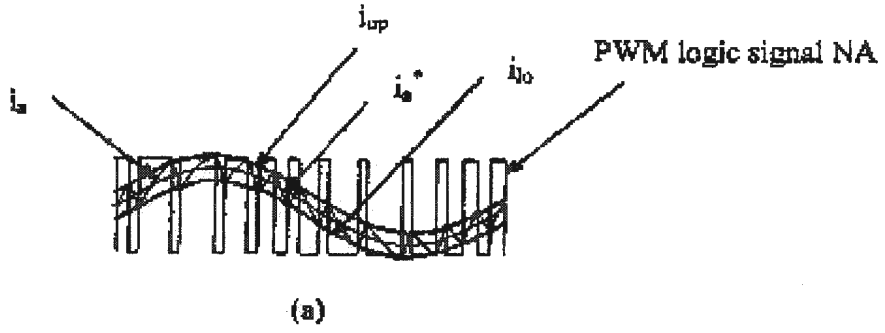

Fig 2.10 Fixed-band hysteresis current controller waveforms.

Chapter 3

Fuzzy Logic Based Speed Controller

3.1 General Introduction

The two most commonly implemented command current generating algorithms for controlling the current-controlled VSI are PI and PID schemes. In these schemes the speed error (command speed – actual speed) is used to generate the command torque necessary in order to return the rotor to the command speed. The stator currents that must be applied to the motor in order to produce this desired speed are obtained from the required torque, and then the VSI is used to apply these currents to the stator windings. By continuously adjusting the applied stator currents, under the influence of the command currents, the rotor speed is made to track the command speed.

The calculations of command torque, however, rely upon mathematical modeling equations of the IPMSM that are dependent upon the internal motor parameters of d- and q-axis reactances. This leads to problems because, in the IPMSM, the rotor magnetic saliency, saturation and armature reaction vary during operation under different speed and loading conditions and thus affect the air gap flux and reactance parameters. Therefore, under operating conditions, the IPMSM

model contains unknown dynamics. This affects the performance of PI and PID based control systems at different operating conditions, because in these controllers the d-q axis parameters are assumed to be constant. In addition, conventional PI and PID controllers are very sensitive to step changes of command speed and load disturbances. Thus, the effective control of the IPMSM needs a complex structure for high performance applications, where rapid speed response, fast and precise handling of load changes and parameter variations, overload capacity, maintenance free operation, size, weight and robustness are all of primary concern.

The use of fuzzy logic controllers (FLC) eliminates much of these problems and makes the control system more generic. The FLC has the advantage over conventional controllers because it does not need the exact system mathematical model, and therefore it does not rely upon knowledge of dynamically changing parameters, such as reactances [76]. Thus, it can handle nonlinear functions of any arbitrary complexity, and it is easily expanded and modified.

3.2 Fundamentals of Fuzzy Logic Control

Fuzzy logic is an extension of Boolean logic that is designed to handle the concept of partial truth - truth values between "completely true" and "completely false" – between 0 and 1 [68]. For instance, in fuzzy logic a statement may be true to a degree of 0.7, not just 1 or 0.

The fuzzy set (subset) A on the universe (set) X is defined by a membership function, m_A from X to the real interval [0,1], which associates a number $m_A(x) \in [0,1]$ to each element x of universe X. $m_A(x)$ represents the degree of membership

of the element x to the fuzzy set A. For example, the equation $m_A(x) = 0.5$ means x has A-ness of about 50%.

A fuzzy singleton $S(x_o) = m(x)|_{x_o}$ is a fuzzy set that supports only one element x_o. Therefore, the fuzzy set (A in this discussion) is the union of the fuzzy singletons of all its constituent elements (here, all the elements x of universe X). However, in fuzzy set theory, the boundaries of the fuzzy sets can be vague and ambiguous, making it useful for approximate systems.

Fuzzy sets are represented graphically by means of their membership functions. The four most popularly used membership functions are shown in Figure 3.1 (although there are numerous others).

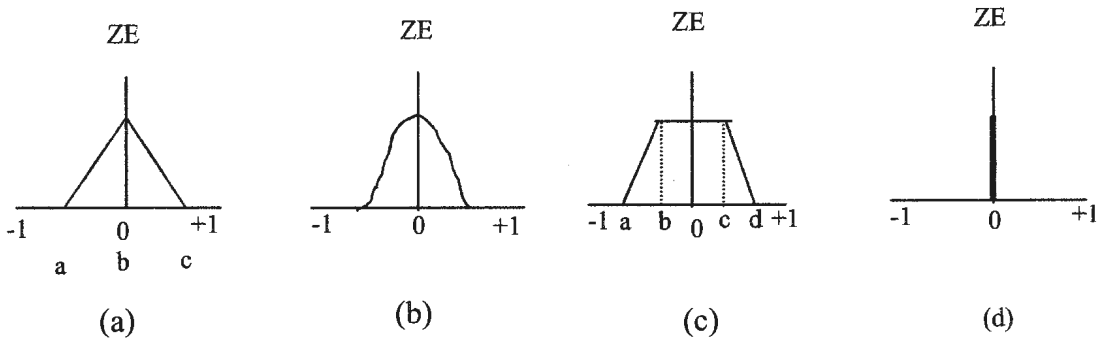

Figure 3.1. Membership functions of linguistic value ZE: (a) triangular, (b) Gaussian function, (c) trapezoidal and (d) singleton.

Mathematically, these membership functions can be defined as,

a) triangular:
$$f(x;a,b,c)=\begin{cases}0, & x\le a\\ \dfrac{x-a}{b-a}, & a\le x\le b\\ \dfrac{c-x}{c-b}, & b\le x\le c\\ 0, & x\ge c\end{cases} \tag{3.1}$$

b) Gaussian function:
$$f(x;\sigma,c)=e^{\frac{-(x-c)^2}{2\sigma^2}} \tag{3.2}$$

c) trapezoidal:
$$f(x;a,b,c)=\begin{cases}0, & x\le a\\ \dfrac{x-a}{b-a}, & a\le x\le b\\ 1 & b\le x\le c\\ \dfrac{d-x}{d-c}, & c\le x\le d\\ 0, & x\ge d\end{cases} \tag{3.3}$$

d) singleton:
$$f(x)=\begin{cases}1, & x=x_o\\ 0, & x\ne x_o\end{cases} \tag{3.4}$$

Fig. 3.1 shows some possible choices of membership functions for a fuzzy set associated with the linguistic value ZE in the universe X = [-1, 1]. In these examples we see that the number 0 fully belongs to the fuzzy sets while the numbers -1 and +1 do not. This need not necessarily be the case for all possible choices of membership functions. The choice of fuzzy logic membership functions depends on the designer's preference and/or experience, and the designer has the option of specifying his or her own membership functions.

The complete process of formulating the mapping from a given input to an output using fuzzy logic is known as fuzzy inference. There are two types of fuzzy

inference methods: Mamdani and Sugeno types [69]. The difference between the two methods is only in the way the output is defined. In control applications, Mamdani type fuzzy inference is the most commonly used method and is the one utilized for this work. The process of fuzzy inference consists of three main components. These are given as follows:

(1) fuzzification,

(2) rule evaluation

(3) defuzzification.

3.2.1 Fuzzification

The first step of fuzzy inference is to take the inputs and apply the appropriate membership functions to them to determine the degree to which they belong to each of the appropriate fuzzy sets. This process of converting a numerical variable (real number) into a linguistic variable (fuzzy number) is called fuzzification. In the FLC, the input is a numerical value limited to the prescribed universe and the output is a value between 0 and 1 that represents the input's degree of membership to the qualifying linguistic set.

3.2.2 Rule Evaluation

In a fuzzy logic controller, the rule evaluation process involves the application of conditional statement (such as if..., then...,) where both the antecedent (if...) and the consequent (then...) are expressed in linguistic form. The rule evaluation consists of two processes: first the application of the fuzzy operator (AND or OR) in the antecedent, then implication from the antecedent to the consequent. A typical rule can be written as follows:

Rule R_i : If $\Delta\omega$ is A and Δe is B then T_e is C.

where speed error $\Delta\omega$ and change of speed error Δe are the input linguistic variables, current I is the output linguistic variable and A_i, B_i, and C_i are the labels of linguistic variables $\Delta\omega$, Δe and I, respectively. If the antecedent is true to some degree of membership then the consequent is also true to that same degree. The fuzzy operators used for fuzzy rules are AND ($\cap$), OR ($\cup$) and NOT ($\bar{}$). They are defined as follows:

a) AND means classical intersection: $m_{A\cap B} = \min\{m_A(x), m_B(x)\}$

b) OR means classical union: $m_{A\cup B} = \max\{m_A(x), m_B(x)\}$

c) NOT means classical complement: $\bar{m}_A = 1 - m_A(x)$.

Therefore, according to rule, the rule R_i, $m_{ci}(x)=\min\{m_{Ai}(x), m_{Bi}(x)\}$.

3.2.3 Aggregation and Defuzzification

Defuzzification is the process of fuzzy inference that generates the final output. But before the process of defuzzification can be completed, there is another process, called the aggregation process, which must be evaluated.

The resultant decisions made by the FLC are based on the testing and combining of all the rules in the fuzzy inference system. The process of combining the fuzzy sets that represents the output of each rule into a single fuzzy set is called the aggregation process.

The defuzzification process is the reverse of the fuzzification process. The input for defuzzification is the combined output of each rule (the result of aggregation process) and the output is a single number. Several different defuzzification methods exist. In this work, the method was chosen by compromising the accuracy of the outcome to reduce the computational burden

imposed in calculating it. The centre of gravity method was used, which is evaluated as,

$$\text{output } I = \frac{\sum_{i=1}^{N} I_i m_{ci}(I_i)}{\sum_{i=1}^{N} m_{ci}(I_i)} \tag{3.5}$$

where N is the total number of rules, $m_{ci}(I_i)$ denotes the output membership grade for the i^{th} rule with the output subset of I_i. An illustration of this process is shown in Fig. 3.2.

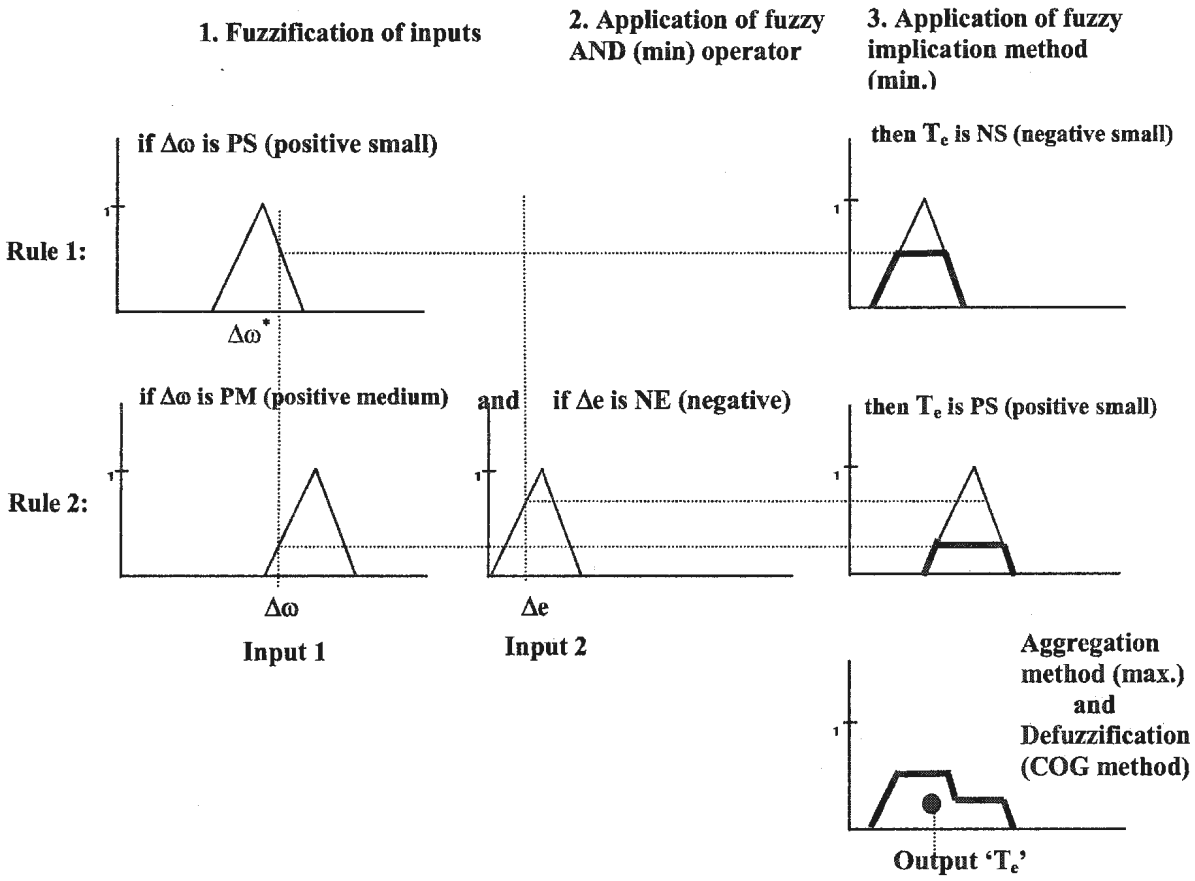

Fig. 3.2. Overview of the complete fuzzy inference.

3.3 Fuzzy Logic Controller for IPMSM Drive

In the interior permanent magnet synchronous motor, the permanent magnets are buried within the rotor core in order to produce a smooth rotor surface and reduced air gap between the stator and the rotor. This allows the motor to be used at high speeds with improved dynamic performance compared to other types of permanent magnet motors. However, the operation of IPMSM is strongly affected by rotor magnetic saliency, core saturation and armature reaction effects due to the d-axis stator current i_d. The saturation of the rotor iron around the permanent magnets produces significant distortion of the air gap flux and causes the reactance parameters to vary with different operating conditions. These nonlinearities affect the performance of the drive at different dynamic operating conditions.

These factors can be overcome by use of artificial intelligence based controllers, capable of handling any nonlinear functions of arbitrary complexity. A fuzzy logic controller has been proposed for the IPMSM drive. The use of a fuzzy logic controller (FLC) for the IPMSM drive in high performance applications has the following benefits:

(a) The system mathematical model is not required**:** The FLC does not need any information of the exact system mathematical model. This makes it one of the best approaches for control of an IPMSM motor drive, where the exact system mathematical model is difficult to obtain and includes dynamically changing parameters.

(b) The FLC is self-adaptive**:** In the real-time IPMSM drive reactance parameters change with operating conditions, resistance changes with

temperature, inertia changes with mechanical load variation and command speed may be changed on demand. The FLC self-adapts to these changing conditions and hence can be used as a robust controller for the IPMSM drive.

(c) Reasonable cost: The application of other types of intelligent controllers to the IPMSM drive for high performance applications requires sophisticated, and often expensive, hardware. While the use of the FLC also requires a degree of specialized hardware, it is less complex than other intelligent controllers and therefore is considered cost effective.

3.3.1 FLC Structure for the IPMSM Drive

The motor dynamics can be represented by the following equation:

$$T_e = T_L + B_m\omega_r + J_m p\omega_r \tag{3.6}$$

where T_e is the electrical torque, T_L is the load torque, B_m is the friction damping coefficient, J_m is the rotor inertia constant, p is the differential operator and ω_r is rotor speed.

The dynamic model of the IPMSM can be rewritten from Eqns. (2.21) and (3.6) as,

$$L_q p i_q + L_d P \omega_r i_d = v_q - r_s i_q - K_b \omega_r \tag{3.7}$$

$$p\omega_r = (T_e - T_L - B_m \omega_r)/J_m \tag{3.8}$$

where $K_b = P\psi_m$. As the FLC can handle any non-linearity, one can consider the load as having unknown nonlinear mechanical characteristics. The load can be modeled using the following equation as [70],

$$T_L = A\omega_r^2 + B\omega_r + C \tag{3.9}$$

where A, B and C are arbitrary constants. To make the control task easier, the equations of an IPMSM are expressed as a single input and single output system by combining Eqns. (3.8 and 3.9) in continuous time domain form as,

$$J_m \frac{d\omega_r}{dt} = T_e - (B_m + B)\omega_r - A\omega_r^2 - C. \tag{3.10a}$$

A small increment ΔT_e in T_e causes a small increment $\Delta\omega_r$ in ω_r:

$$J_m \frac{d(\omega_r + \Delta\omega_r)}{dt} = (T_e + \Delta T_e) - (B_m + B)(\omega_r + \Delta\omega_r) - A(\omega_r + \Delta\omega_r)^2 - C. \tag{3.10b}$$

Subtracting Eqn. (3.10a) from (3.10b) gives,

$$J_m \frac{d(\Delta\omega_r)}{dt} = \Delta T_e - (B_m + B + 2A\omega_r)(\Delta\omega_r) - A(\Delta\omega_r)^2 \tag{3.11}$$

By replacing all the continuous quantities of Eqn. (3.11) by their finite differences, the discrete time small signal model of the simplified IPMSM with nonlinear load can be given as,

$$\Delta T_e(n) = \frac{J_m}{t_s}\Delta e(n) + \left(B_m + B + 2A\omega_r(n)\right)\Delta\omega_r(n) + A\{\Delta\omega_r(n)\}^2 \qquad (3.12)$$

Hence,

$$T_e(n) = \int_{\text{discrete}} \Delta T_e(n) = f(\Delta e(n),\ \Delta\omega_r(n),\ \omega_r(n)) \qquad (3.13)$$

where, $\Delta e(n) = \Delta\omega_r(n) - \Delta\omega_r(n-1)$ is the change of speed error, $\Delta\omega_r(n) = \omega_r^*(n) - \omega_r(n)$ is the present sample of speed error, $\Delta\omega_r(n-1)$ is the past sample of speed error, $\omega_r(n)$ is the present sample of actual speed, $\omega_r^*(n)$ is the present sample of command speed, t_s is the sampling time interval and f denotes the nonlinear function. Thus, the purpose of using the FLC is to map the nonlinear functional relationship between electrical torque T_e and rotor speed ω_r.

From this command torque T_e, Eqns. (2.36) and (2.37) are used to calculate the necessary q- and d-axis currents to produce the rotor speed ω_r. In real-time, the motor position information and the output of the simplified FLC in terms of the command q-axis and d-axis currents i_q^* and i_d^* are used to get the motor command phase currents i_a^*, i_b^* and i_c^* by using Park's transformation.

3.3.2 Simplified FLC for the IPMSM Drive

The model of the IPMSM expressed by Eqn. (3.13) defines the input and output linguistic variables for the FLC of the IPMSM drive. According to Eqn. (3.13), the inputs of the proposed FLC are the present samples of speed error, change of speed error (which is the difference between the present and past samples of speed error) and present rotor speed. However, it has been observed that the effect of the inclusions of the rotor speed and change of speed error on motor speed response is negligible, not producing an improvement in drive performance commensurate with the resulting increase in computational burden as compared to the case when it is omitted. The omission of the $\omega_r(n)$ and $\Delta e(n)$ terms produces a proportional-type FLC-based drive with acceptably responsive and accurate tracking of the command speed. Thus, the input vectors of the FLC can be reduced to only $\Delta\omega_r(n)$, producing a much-simplified FLC as compared to input vectors of $\Delta\omega_r(n)$, $\Delta e(n)$ and $\omega_r(n)$ with the non-simplified system. These simplifications significantly reduce computational burden and lower the computer memory and power required to implement the FLC scheme in real time. Thus, this simplified FLC is a significant factor for real-time implementation of the laboratory IPMSM drive system, if a fuzzy-based controller is to be employed. The block diagram of the proposed FLC based IPMSM drive incorporating MTPA is shown in Fig. 3.3.

Next, scaling factors, K_ω and K_i, are chosen for fuzzification and obtaining the appropriate actual output of the command current. The factor K_ω is chosen so that the normalized value of speed error, $\Delta\omega_m$, remains within the limits of $\pm$ 1. The factor K_i is chosen so that rated current is produced by the controller at rated conditions. The constants are taken as $K_\omega = \omega_r^*$(command speed) and K_i = 10 in order to get the optimum drive performance.

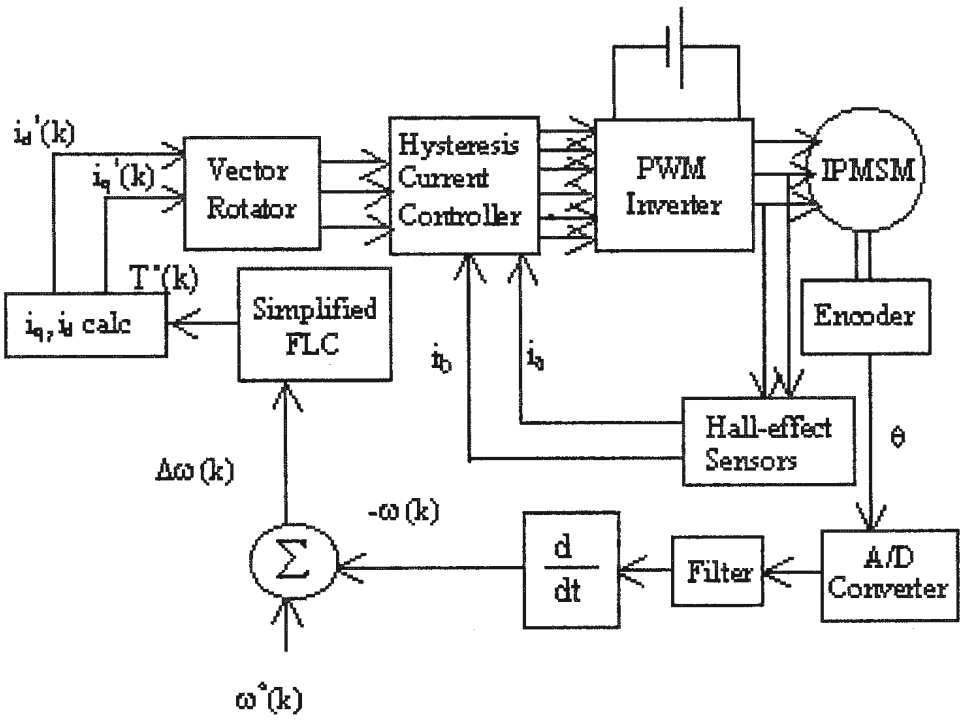

Fig. 3.3. Block diagram of proposed simplified FLC -based IPMSM drive with MTPA control.

After selecting the scaling factors, the next step is to choose the membership functions of $\Delta\omega_m$ and the normalized command torque T_{en}^*, which form an important element of the FLC.

The membership functions used for the input and output fuzzy sets are shown in Fig. 3.4. Trapezoidal functions are used as membership functions for all the fuzzy sets with the exception of the fuzzy set ZE (zero) of the input vector. Triangular membership functions are used for the fuzzy set ZE of the input vector and all the fuzzy sets of the output vector. The trapezoidal and the triangular functions are used because of their mathematical simplicity, and thus to simplify

implementation and reduce computational burden for real-time implementation. The non-symmetrical nature of the membership functions were arrived at by trial and error.

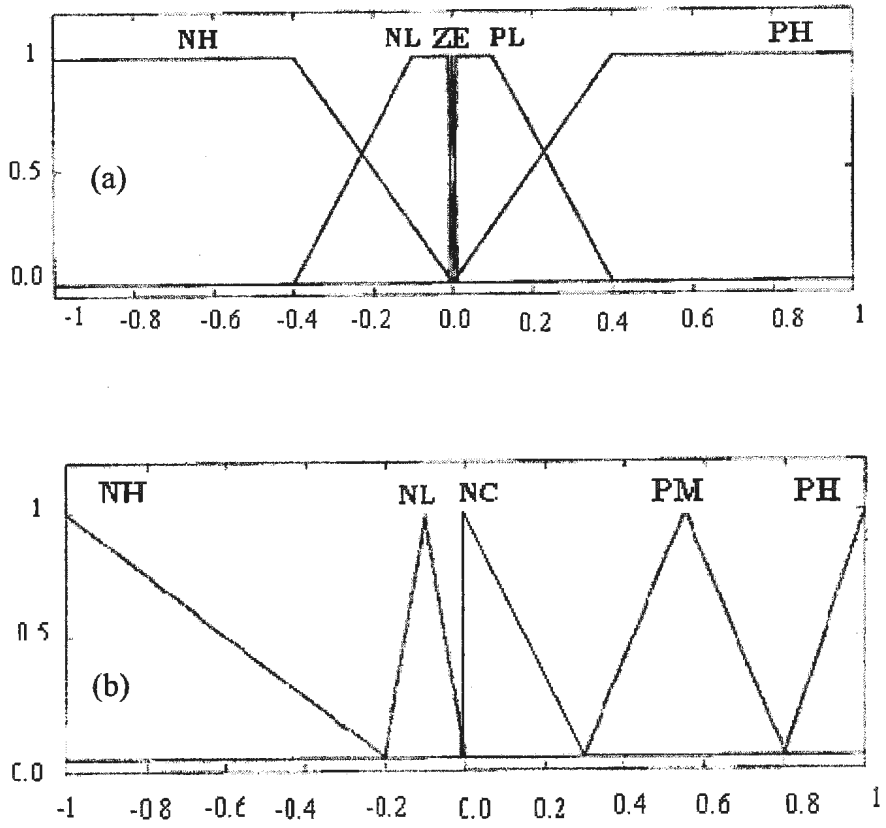

Fig. 3.4. Membership functions for: (a) normalized speed error $\Delta\omega_m$, (b) normalized command torque T_{en}^*.

The rules used for the proposed FLC algorithm are as follows:

i) if $\Delta\omega_{rn}$ is PH (positive high), T_{en} is PH (positive high).

ii) if $\Delta\omega_{rn}$ is PL (positive low), T_{en} is PM (positive medium).

iii) if $\Delta\omega_{rn}$ is NL (negative low), T_{en} is NL (negative low).

iv) if $\Delta\omega_{rn}$ is NH (negative high), T_{en} is NH (negative high).

v) if $\Delta\omega_{rn}$ is ZE (zero), T_{en} is NC (no change).

In this work, the values of the constants, membership functions, fuzzy sets for the input/output variable and the rules used were selected by trial and error in order to obtain the optimum drive performance.

3.4 Concluding Remarks

The principles of the fuzzy logic controller for IPMSM control applications have been presented in this chapter. A specific simplified fuzzy logic controller is proposed for the IPMSM motor drive as a robust speed controller in order to overcome the problems caused by real-time motor parameter variations, load changes and system disturbances.

Chapter 4

Simulation of the FLC Based Vector Control of the IPMSM

4.1 General Introduction

This chapter presents a neoteric speed control technique for the IPMSM based around both fuzzy logic and the maximum torque per ampere (MTPA), with Taylor series approximation, mode of operation. For comparison purposes, two separate fuzzy logic based speed controllers have been implemented. The first is a FLC based controller operating under the $i_d = 0$ assumption, based on previous work by M. N. Uddin [63]. The second is a new, simplified FLC/MTPA based system designed around the mathematical model of the IPMSM, the appropriate motor dynamics and the nonlinear load model. This design has been developed in chapter 3, is illustrated in Fig. 3.4 and simulation model details are presented in Appendix B.

Extensive simulations have been done in order to predict the performances of the drives using the two FLC based systems at different dynamic operating conditions.

Finally the simulation results have been presented and discussed.

4.2 Current Controller and Voltage Source Inverter

In this work, the fixed-band hysteresis controller is used is as the current controller due to its fast transient response, accurate steady-state response and its high performance characteristics over the entire speed range when used in the IPMSM drive. This is especially true when the fixed-band hysteresis controller is used in tandem with a voltage source inverter (VSI) employing fast switching devices like insulated gate bipolar transistors (IGBTs).

Consequently, an IGBT based VSI and base drive unit have been utilized in this work. The details of the IGBT inverter with its snubber circuits and base drive circuit for the inverter switches are given in Appendix C. The details of the current control technique for the VSI and the principle of the hysteresis current controller have been presented in chapter 2.

4.3 Simulation Results and Discussion

Simulations have been carried out using the Matlab Fuzzy Logic Toolbox. Some simulation results are presented here. The laboratory experimental IPMSM is a 1 hp, 4-pole machine with 2 N-m as full load, fed by a current-controlled VSI. The capability of the motor to run at different loading conditions is one of the main criteria of the control system. Others include the ability to run at different command speeds and with sudden changes in motor parameters.

The speed response, corresponding command phase current, command q-axis current and actual steady-state 'a' phase current for the FLC based/i_d=0 IPMSM drive are shown in Figs. 4.1 (a)-(d), respectively, for no load and rated speed conditions. The results show that the drive follows the command speed very

quickly without any overshoot and nearly zero steady-state error. The command q-axis current, which also represents the command torque (since i_d has been forced to zero in this scheme), however, oscillates significantly at steady-state conditions. This does not appear to significantly impact operational performance.

Figs. 4.2 (a)-(d) show the speed response, command phase current i_a^*, q-axis command current and steady-state phase current i_a, respectively, for the FLC based/i_d=0 IPMSM at half load and rated speed conditions. Again the drive follows the command speed without any overshoot or steady-state error, but the command q-axis current, and hence the command torque, oscillates greatly at steady-state, although the actual phase current is almost sinusoidal.

The similar responses of the FLC based/i_d = 0 IPMSM drive at full load and rated speed conditions are shown in Figs. 4.3 (a)-(d). Under these conditions, phase current magnitude peaks at 3.3 amperes, which is 10% in excess of the rated current of 3 amperes. This is due to the fact that the i_d = 0 approximation induces a higher stator command current than ideally with i_d not forced to zero. Once again, it is shown that the drive can follow the command speed smoothly without any overshoot and steady state error. These results verify that the FLC/ i_d=0 based IPMSM drive can follow the command rated speed at various loading conditions.

A step change of command speed is applied to the FLC based/i_d=0 drive in order to evaluate drive performance in terms of response time, speed overshoot, transient and steady state errors and stability. This is necessary because in high performance drive applications it is essential to change command speeds with situational demands. The responses of the drive including speed, 'a' phase command current, q-axis command current and steady-state actual phase current are shown in Figs. 4.4 (a)-(d), respectively, for a step change of command speed at

half load conditions. The results show that the drive can follow the command speed without overshoot and steady-state error during a step increase of speed (100 rad./sec.→188.5 rad./sec.) but there is a small, but acceptable, undershoot during a step decrease of speed (188.5rad./sec.→100rad./sec.). Again, q-axis command current, and hence command torque, oscillates significantly, though this does not appear to significantly impact drive performance. The results show that the FLC based/i_d=0 drive can follow the command speed even after a step change of command speed.

The ability of the drive to withstand disturbances is another important feature of the control system. Change of load is a typical external disturbance and is a very common occurrence for a high performance drive. The speed and corresponding command a-phase current of the motor, q-axis command current and steady-state actual a-phase current responses for the FLC based/i_d=0 drive are shown in Figs. 4.5 (a)-(d), respectively, for a sudden increase of load at the rated speed. The motor is started with half load and at t = 0.25 sec. the load is suddenly increased to full load. It is shown that drive speed is reduced transiently, and only modestly, and that command speed is quickly recovered even under this relatively dramatic increase of load. The current response is almost sinusoidal and follows command current. Command torque, as indicated by i_q^* oscillates greatly, but this does not appear to negatively effect drive performance.

The speed response, corresponding command phase current, command q-axis current and actual steady-state 'a' phase current for the simplified FLC based/MTPA IPMSM drive are shown in Figs. 4.6 (a)-(d), respectively, for no load and rated speed conditions. The results show that the drive follows the command

speed very quickly with only a minute overshoot which is recovered promptly and steady-state reached. Steady-state error is almost zero. i_q has a much lower magnitude of oscillation than for the FLC/i_d=0 based drive, and i_d has a yet further smaller magnitude of oscillation. This is explained by the fact that, with i_d not forced to zero, both the q and d-axis components of current contribute to the command torque rather than just i_q alone. It can also be observed that i_d is a smaller magnitude, scaled opposite of i_q.

Figs. 4.7 (a)-(d) show the speed response, actual phase current i_a, q- and d-axis command currents and steady-state phase currents i_a and i_b, respectively, for the simplified FLC based/MTPA IPMSM drive at half load and rated speed conditions. Again the drive follows the command speed without detectable steady-state error, but this time the short transient overshoot is even less. Again, i_q has a much lower magnitude of oscillation than for the FLC/i_d=0 based drive, and i_d is observed to be a smaller magnitude, scaled opposite of i_q. The actual phase currents are almost, but not purely, sinusoidal.

The similar responses of the simplified FLC based/MTPA IPMSM drive at full load and rated speed conditions are shown in Figs. 4.8 (a)-(d). The maximum phase current magnitude achieved under these conditions is 2.85 amperes. This is 5% below the rated current of 3 amperes. In comparison, the FLC based/i_d=0 scheme required a maximum stator current magnitude of 3.3 amperes to follow the command speed at this load. Once again, it is shown that the FLC based/MTPA drive can follow the command speed smoothly, and this time transient overshoot is nearly completely eliminated and steady-state achieved even more quickly. The actual phase currents are almost, but not purely, sinusoidal. Heretofore, the simplified FLC based/MTPA drive achieves steady-state command speed faster than the FLC based/i_d=0 drive, and with lower peak phase currents, in all cases.

These results verify that the FLC based/MTPA IPMSM drive can quickly achieve and follow the command rated speed under various loading conditions.

Figs. 4.9 (a)-(d) show the speed response, actual phase current i_a, q- and d-axis command currents and steady-state phase currents i_a, i_b and i_c, respectively, for the simplified FLC based/MTPA IPMSM drive at full load + 25% and rated speed conditions. Command speed is achieved very quickly, with practically no overshoot or oscillation. Maximum phase current magnitude under these conditions is 3.3 amperes, the same magnitude required by the FLC based/i_d=0 drive to achieve rated speed at full load conditions.

Figs. 4.10 (a)-(d) show the speed response, actual phase current i_a, q- and d-axis command currents and steady-state phase currents i_a, i_b and i_c, respectively, for the simplified FLC based/MTPA IPMSM drive at full load and low speed conditions (75 rad./sec.). There is some oscillation in reaching command speed but this is quickly damped and steady-state reached in under 0.05 sec. The actual phase currents exhibit almost, but not purely, sinusoidal behavior with peak values well below rated current.

The responses of the FLC based/MTPA drive including speed, 'a' phase actual current, q- and d-axis command currents and steady-state actual phase currents to a step change of command speed at half load are shown in Figs. 4.11 (a)-(d), respectively. The results show that the drive can follow the command speed quickly and accurately during a step increase (100 rad./sec.→188.5 rad./sec.) and decrease (188.5rad./sec.→100rad./sec.) of speed, but there are small, but acceptable, overshoots and undershoots which are recovered promptly.

Figs. 4.12 (a)-(d) show the speed response, actual phase current i_a, q- and d-axis command currents and command phase current imposed over actual phase current, respectively, for the simplified FLC based/MTPA IPMSM drive to a step

change of command speed at full load conditions. Once again, it is shown that the drive quickly and accurately follows command speed. It can also be observed that actual phase current follows command current. The results show that the FLC based/MTPA drive can follow the command speed even after a step change of command speed at different loading conditions.

The ability of the drive to withstand disturbances is another important feature of the control system. Change of load is a typical external disturbance and is a very common occurrence for a high performance drive. The speed and corresponding actual a-phase current of the motor, q- and d-axis command currents and steady-state actual a-phase current responses for the FLC based/MTPA drive are shown in Figs. 4.13 (a)-(d), respectively, for a sudden increase of load at rated speed. The motor is started with half load and at t = 0.25 sec. the load is suddenly increased to full load. It is observed that drive speed is reduced transiently, and only very slightly, and that command speed is recovered extremely quickly, even under this relatively dramatic increase of load. The current response is almost sinusoidal and follows command current.

Because IPMSM parameters are affected significantly by saturation and temperature, one of the most important criteria of the control system for the IPMSM drive is the ability to withstand motor parameter variations. The change of stator resistance with temperature is a common phenomenon in such machines. The speed and corresponding actual phase current responses of the FLC based/MTPA drive are shown in Figs. 4.14 (a) and (b), respectively, for doubled stator resistance at no load and rated speed conditions. The similar responses for full load conditions are shown in Figs. 4.15 (a) and (b). In both cases it is shown

that the drive follows the command speed even after a sudden and dramatic change of armature resistance.

Additionally, the inertia of the motor may change at different loading conditions, so it is important to investigate the response of the drive to inertia variations. Figs. 4.16 (a) and (b) show the speed and corresponding actual 'a' phase current responses, respectively, to a sudden doubling of rotor inertia under no load conditions at rated speed. Figs. 4.17 (a) and (b) show the similar responses under full load conditions. These results indicate that the FLC based/MTPA drive follows the rated command speed accurately and smoothly even when subjected to a sudden doubling of rotor inertia under different loading conditions.

In the IPMSM changes in d- and q-axis reactance parameters during operation can significantly affect drive performance. This can be easily understood as the torque equation (2.29) contains both the d- and q-axis inductance parameters. Therefore, high performance drives must be able to respond quickly and accurately to variations in L_q and L_d. Figs. 4.18 (a) and (b) show the speed and corresponding actual 'a' phase current responses, respectively, to a sudden 50% decrease in L_q under no load at rated speed. Figs. 4.19 (a) and (b) show the similar responses under full load conditions. These results indicate that the FLC based/MTPA drive follows the rated command speed accurately and smoothly even when subjected to a sudden 50% decrease of L_q under different loading conditions.

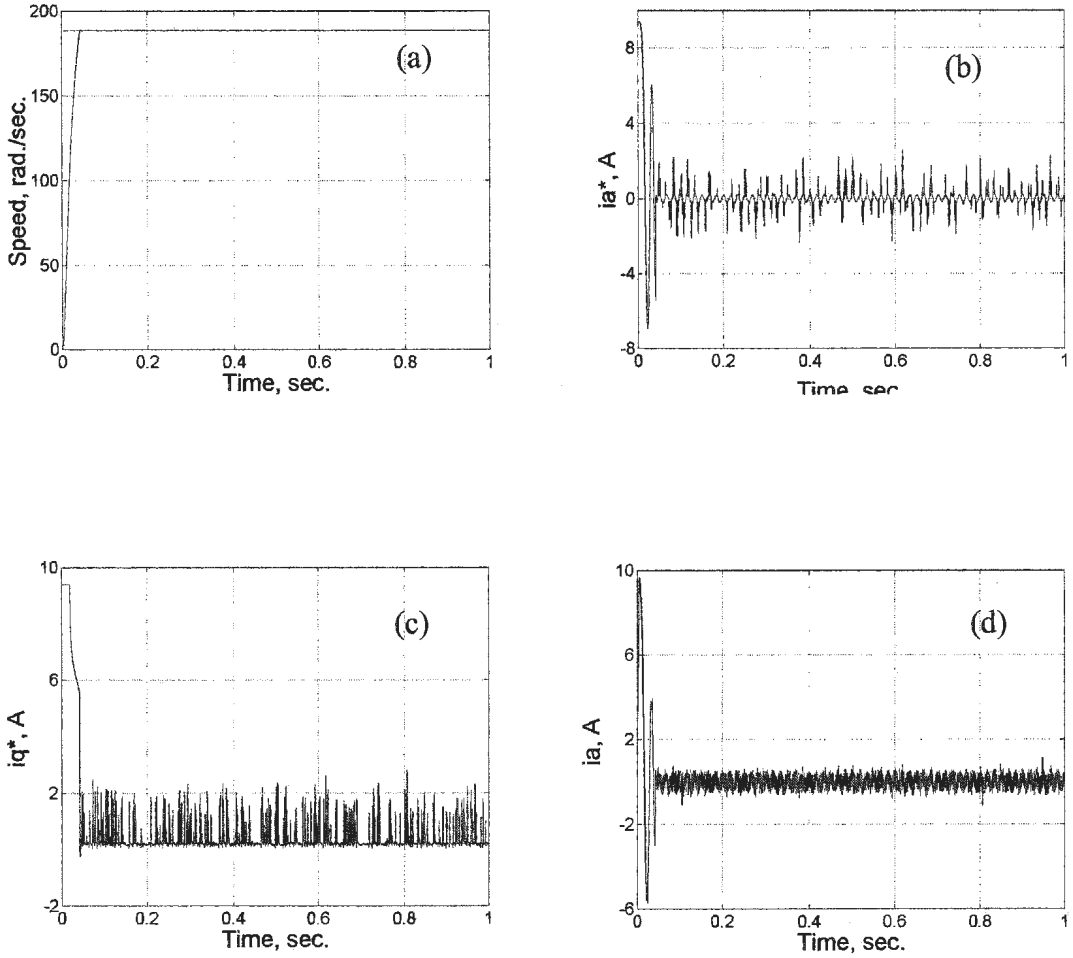

Fig. 4.1. Simulated responses of the FLC based/i_d=0 IPMSM drive: a) speed, (b) command phase current, (c) q-axis command current and (d) steady-state actual phase current at no load and rated speed conditions.

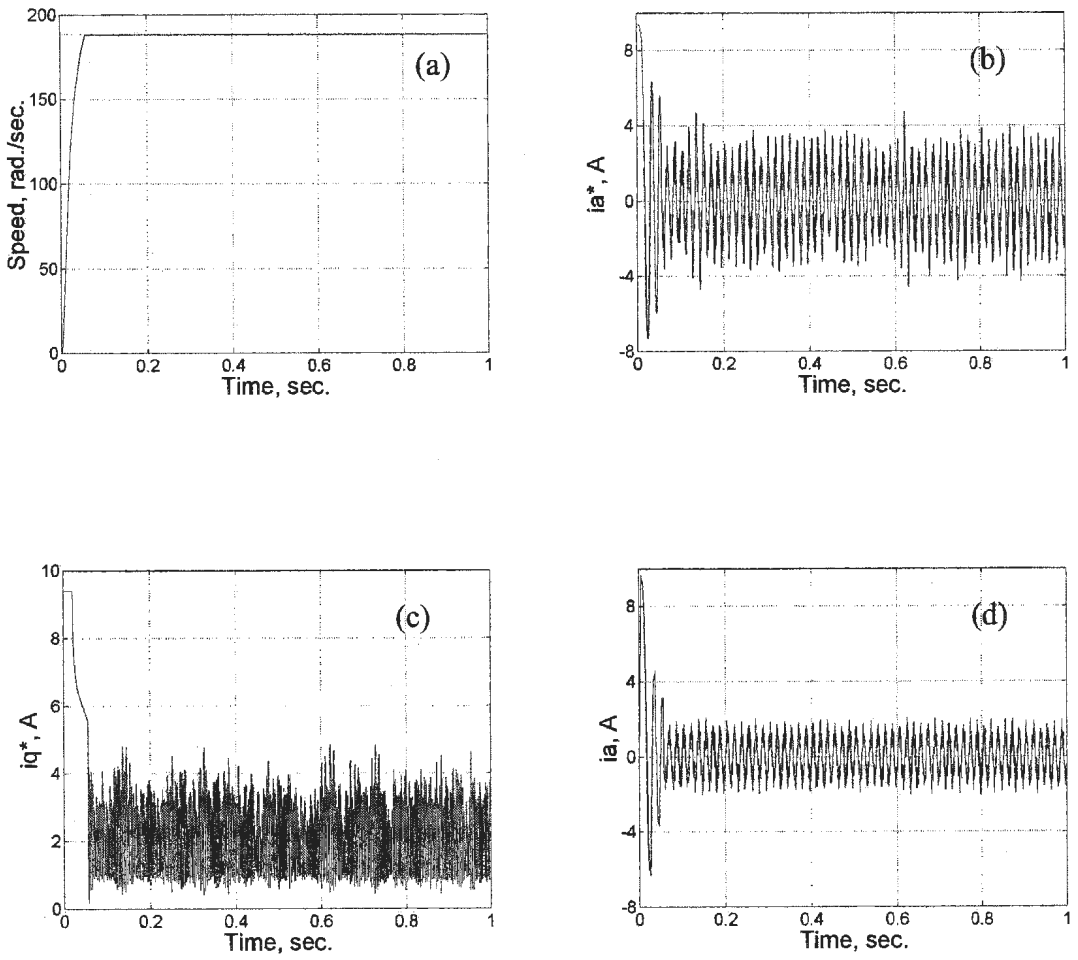

Fig. 4.2. Simulated responses of the FLC based/i_d=0 IPMSM drive: a) speed, (b) command phase current, (c) q-axis command current and (d) steady-state actual phase current at half load and rated speed conditions.

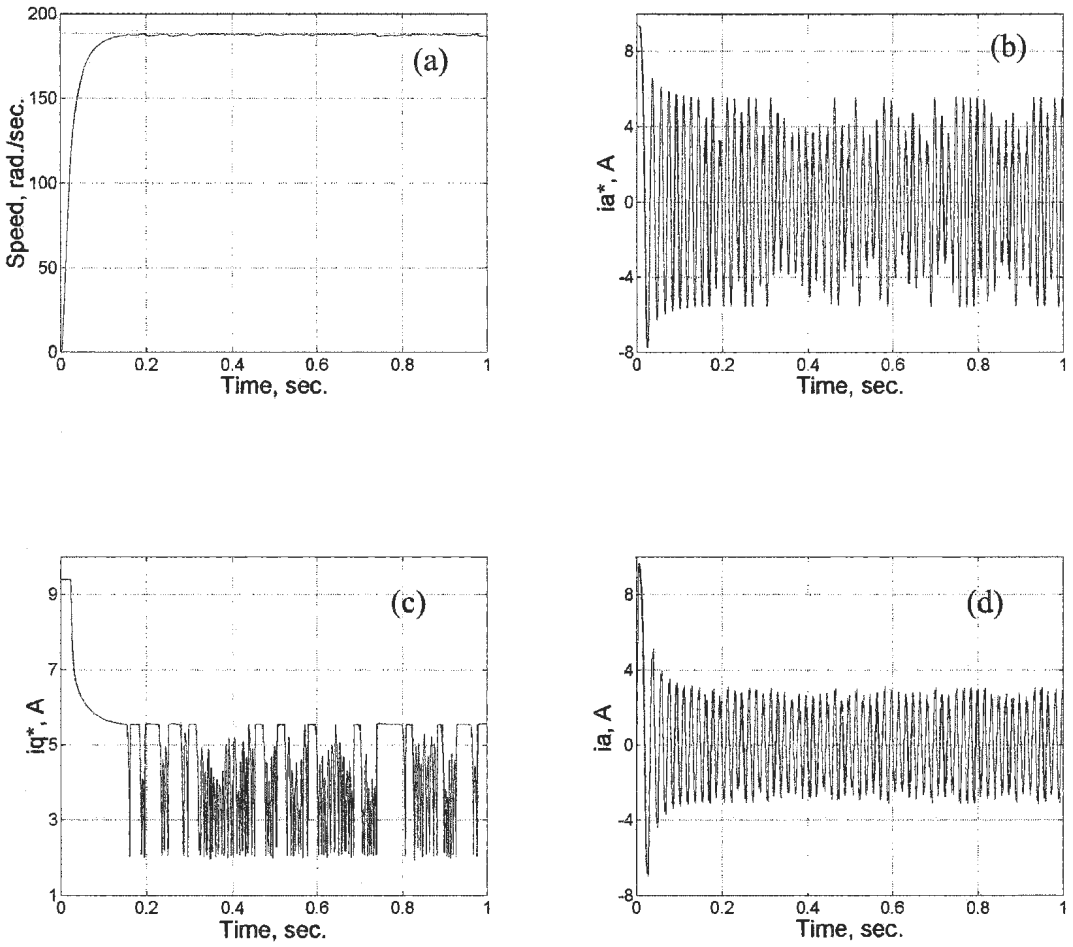

Fig. 4.3. Simulated responses of the FLC based/i_d=0 IPMSM drive: a) speed, (b) command phase current, (c) q-axis command current and (d) steady-state actual phase current at full load and rated speed conditions.

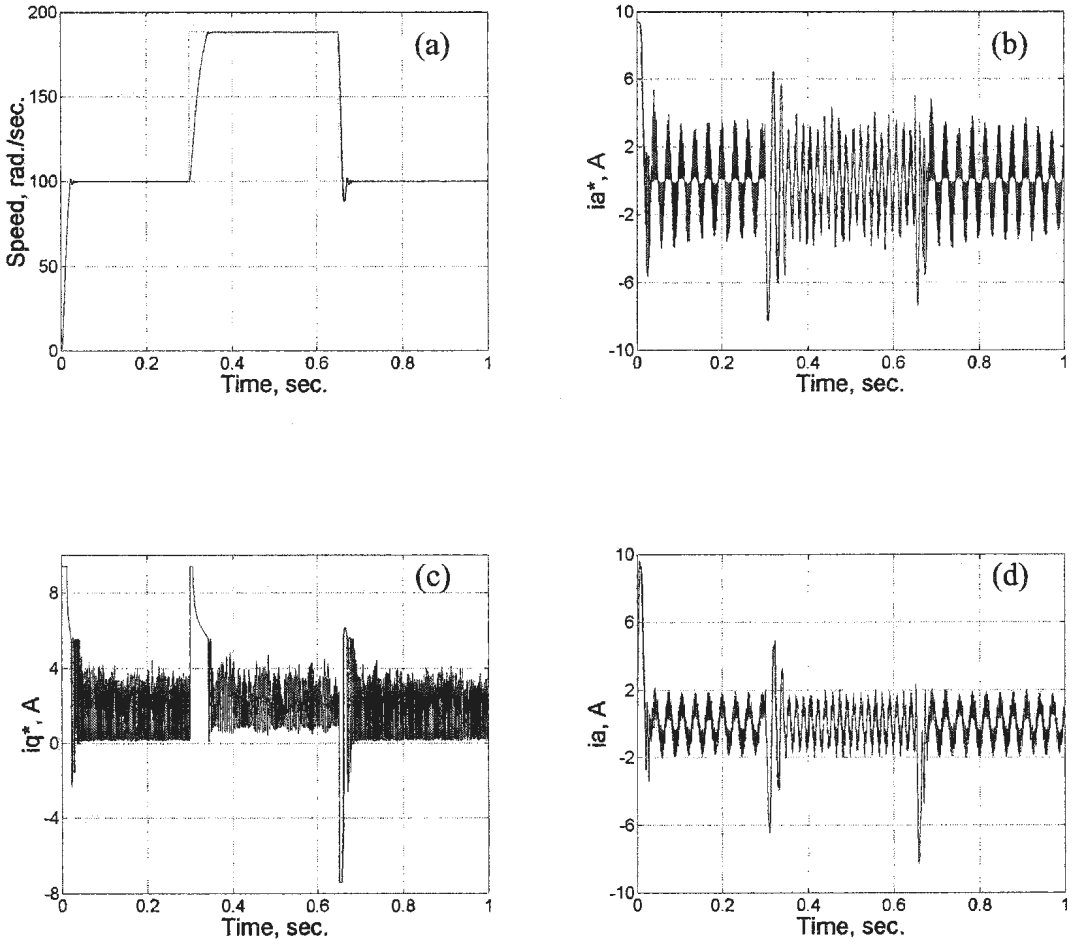

Fig. 4.4. Simulated responses of the FLC based/i_d=0 IPMSM drive: a) speed, (b) command phase current, (c) q-axis command current and (d) steady-state actual phase current for a step change of speed at half load conditions.

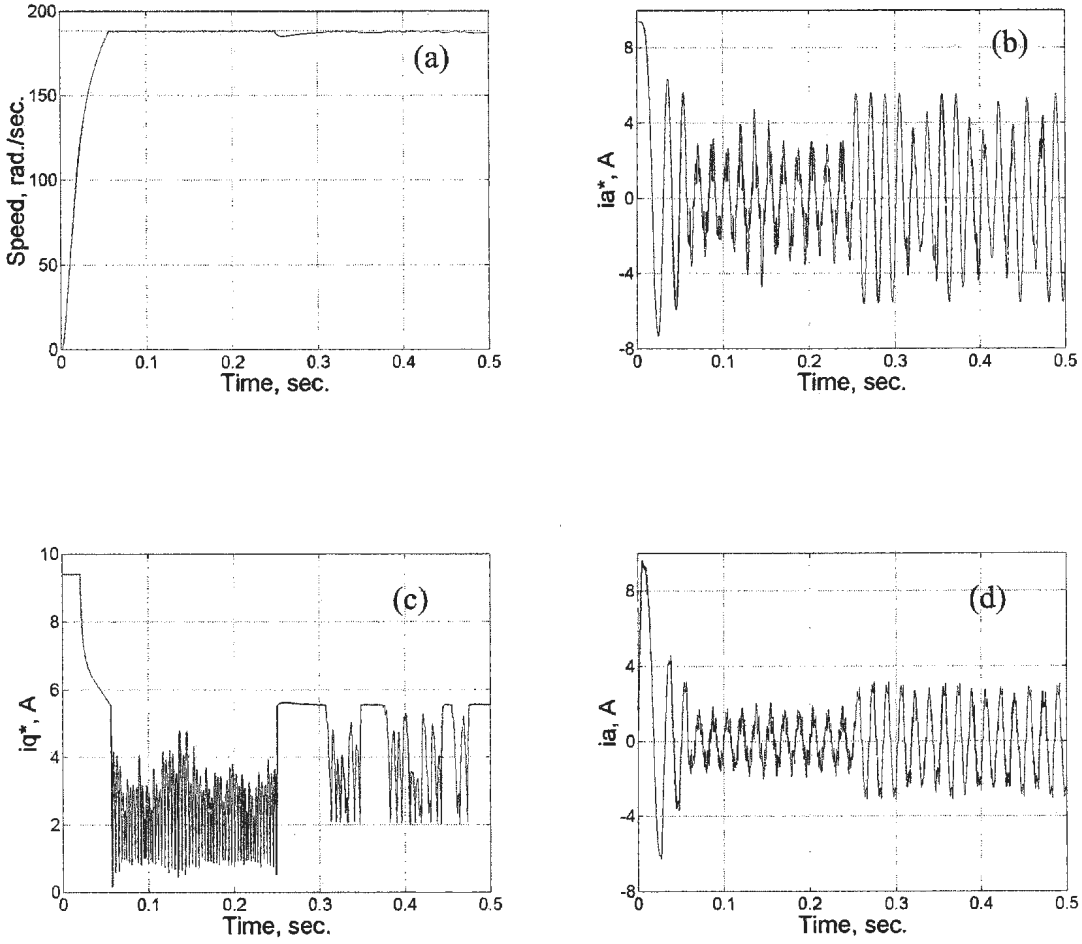

Fig. 4.5. Simulated responses of the FLC based/i_d=0 IPMSM drive: a) speed, (b) command phase current, (c) q-axis command current and (d) steady-state actual phase current for a sudden change of load (from half load to full load) at rated speed.

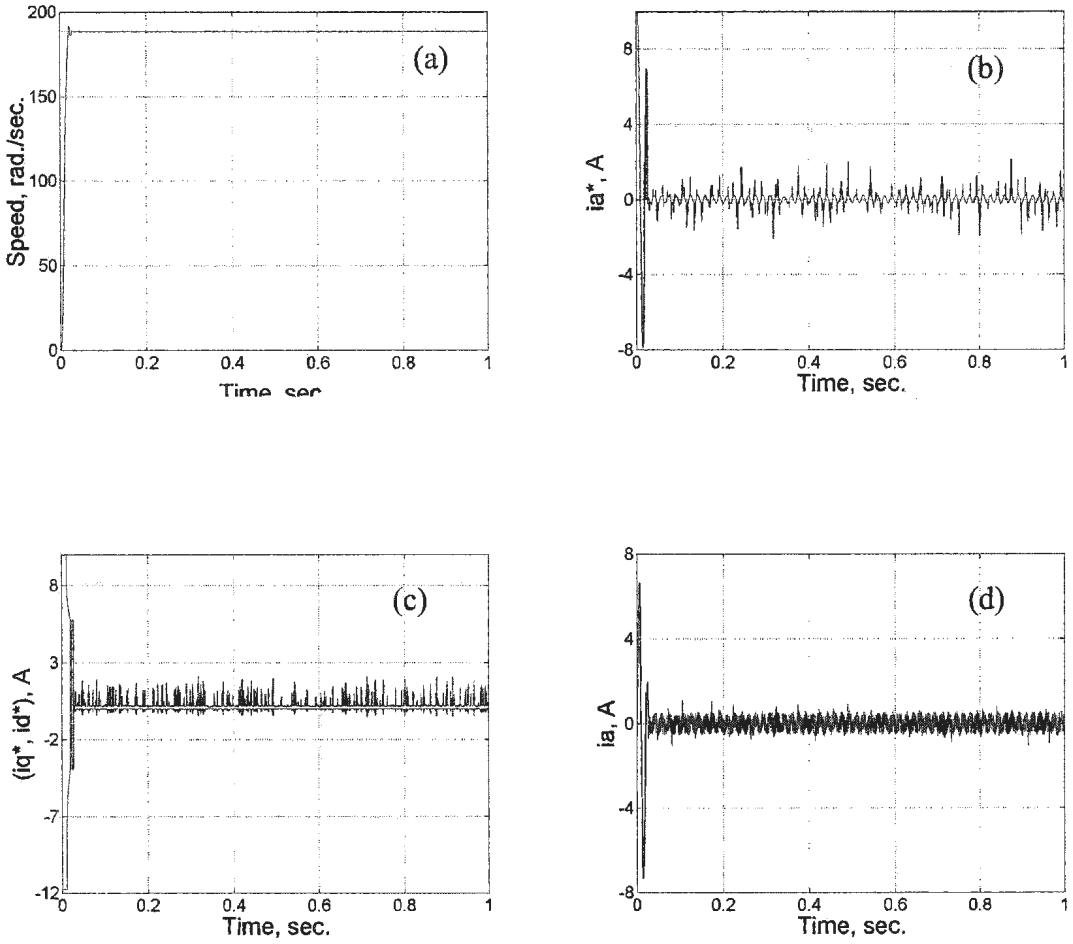

Fig. 4.6. Simulated responses of the simplified FLC based/MTPA IPMSM drive: a) speed, (b) command phase current, (c) q-axis and d-axis command currents and (d) steady-state actual phase current at no load and rated speed conditions.

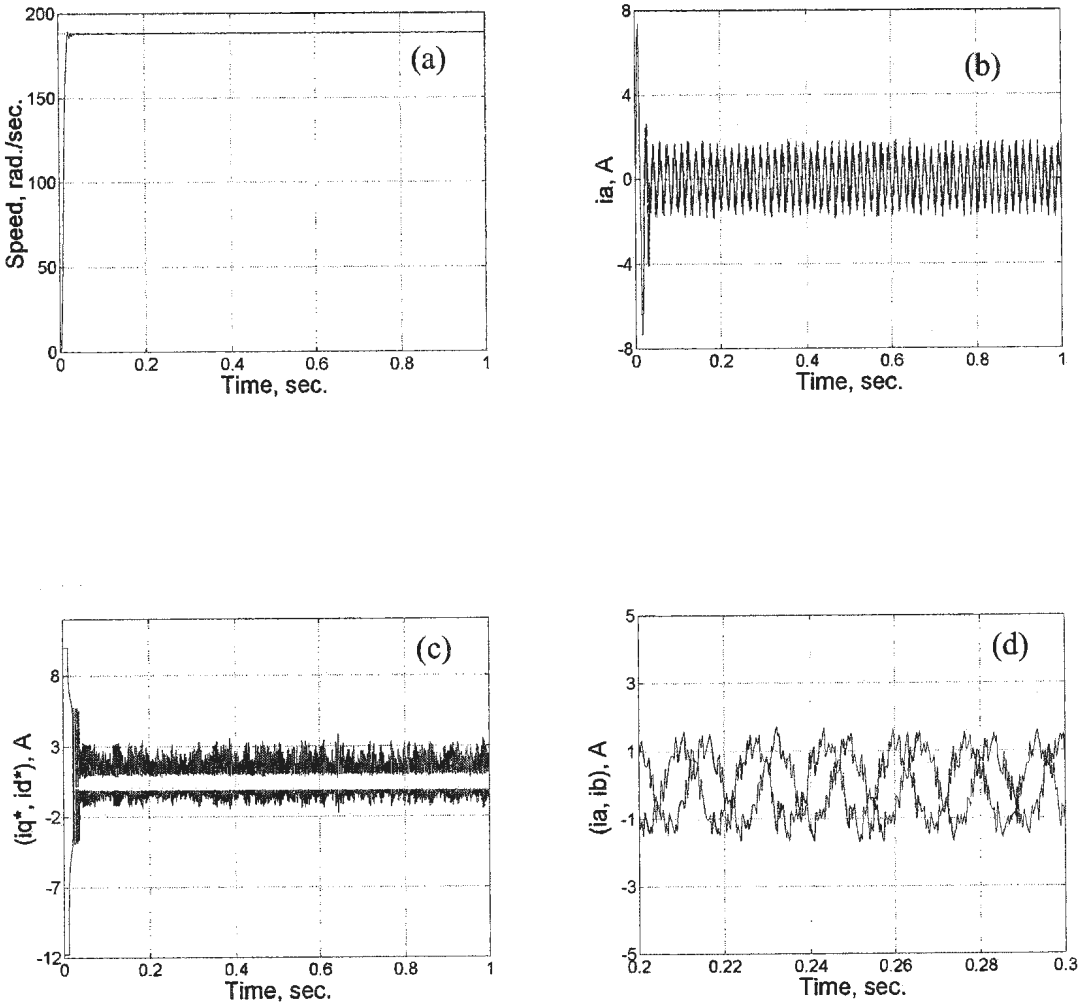

Fig. 4.7. Simulated responses of the simplified FLC based/MTPA IPMSM drive: a) speed, (b) steady-state actual phase current, (c) q-axis and d-axis command currents and (d) steady-state actual phase currents i_a and i_b at half load and rated speed conditions.

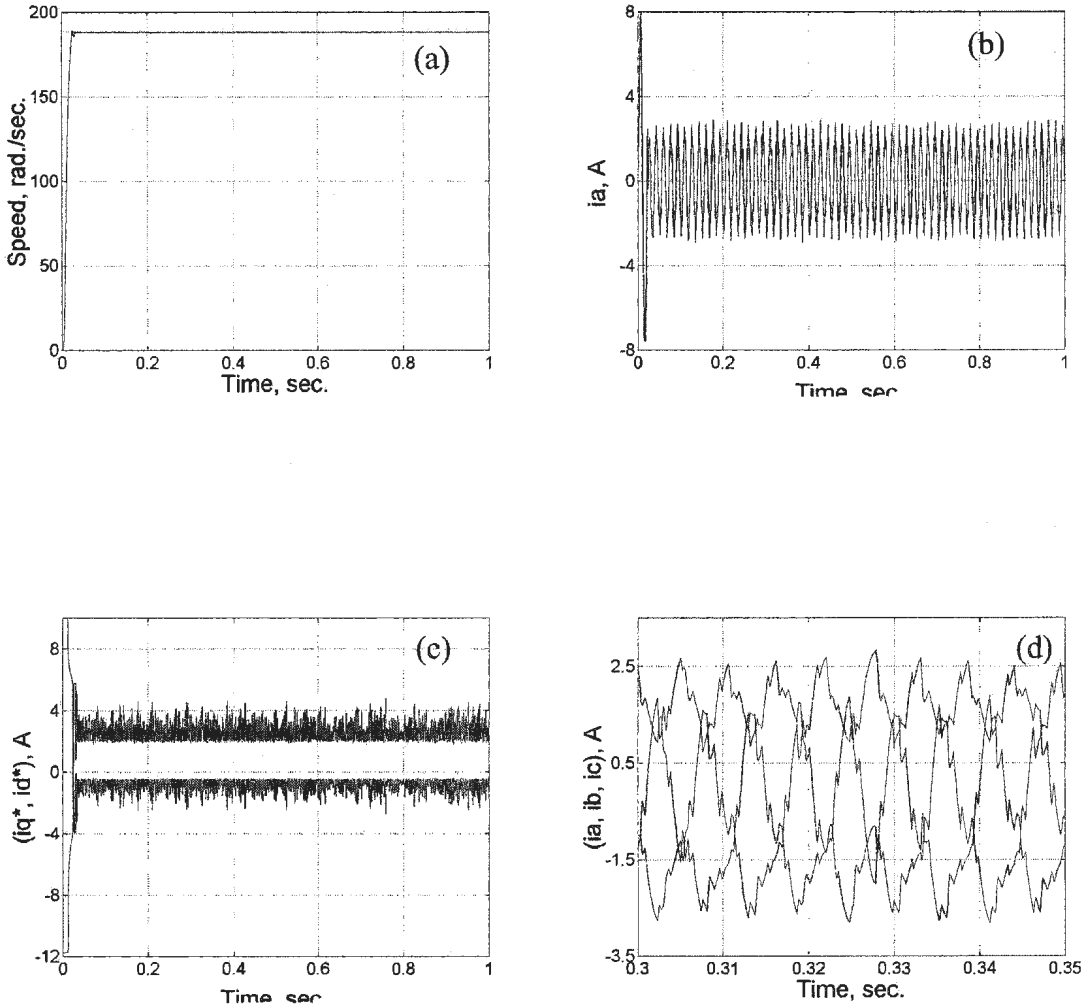

Fig. 4.8. Simulated responses of the simplified FLC based/MTPA IPMSM drive: a) speed, (b) steady-state actual phase current, (c) q-axis and d-axis command currents and (d) steady-state actual phase currents i_a, i_b and i_c at full load and rated speed conditions.

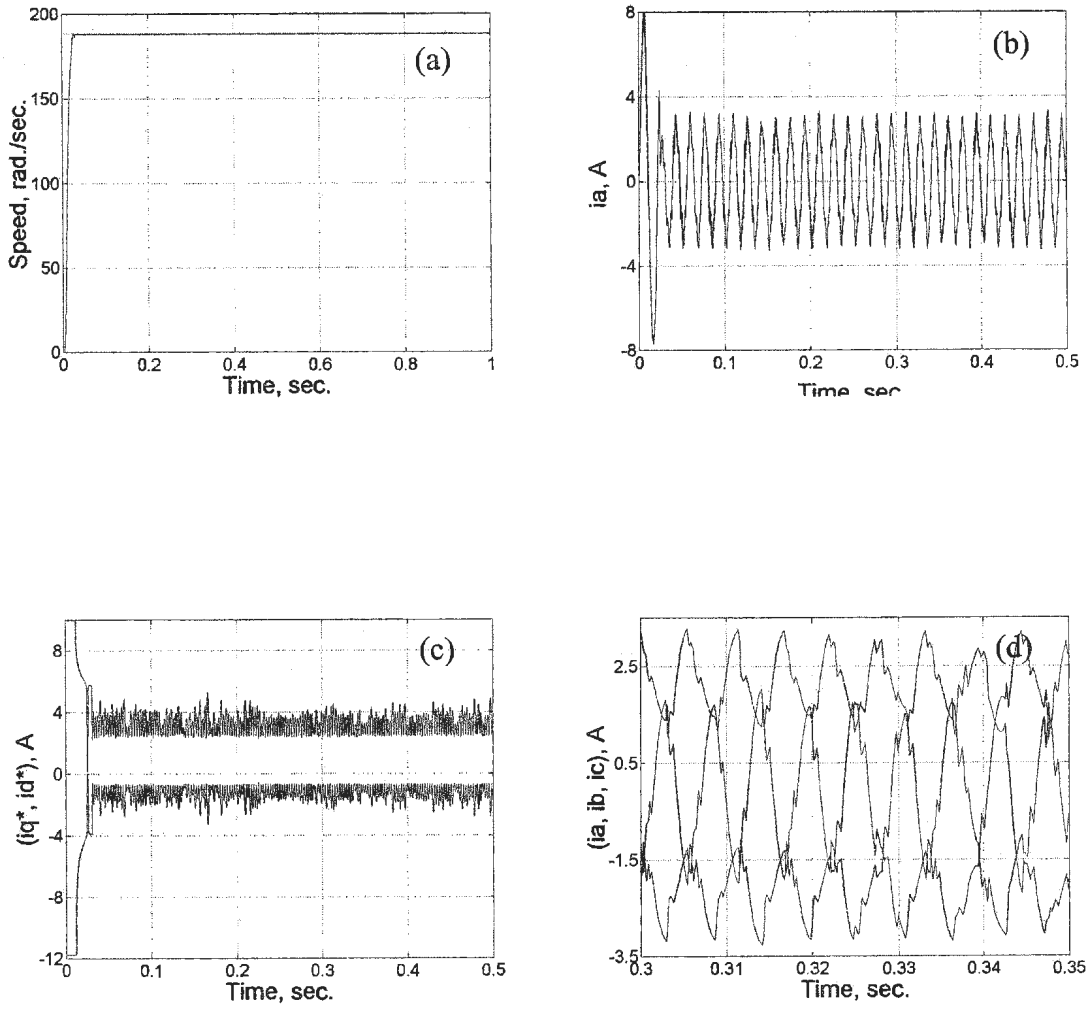

Fig. 4.9. Simulated responses of the simplified FLC based/MTPA IPMSM drive: a) speed, (b) steady-state actual phase current, (c) q-axis and d-axis command currents and (d) steady-state actual phase currents i_a, i_b and i_c at full load + 25% and rated speed conditions.

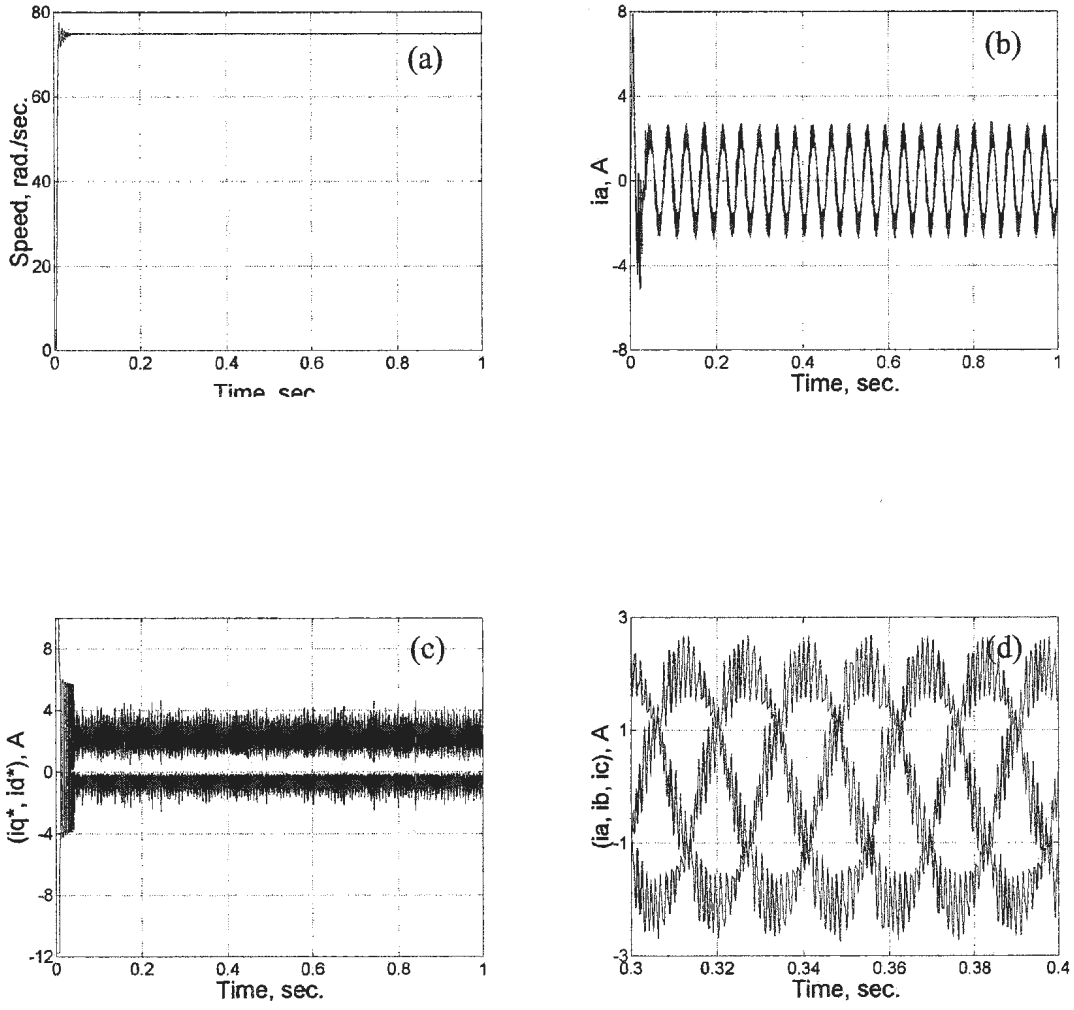

Fig. 4.10. Simulated responses of the simplified FLC based/MTPA IPMSM drive: a) speed, (b) steady-state actual phase current, (c) q-axis and d-axis command currents and (d) steady-state actual phase currents i_a, i_b and i_c at full load and low speed (75 rad./sec.) conditions.

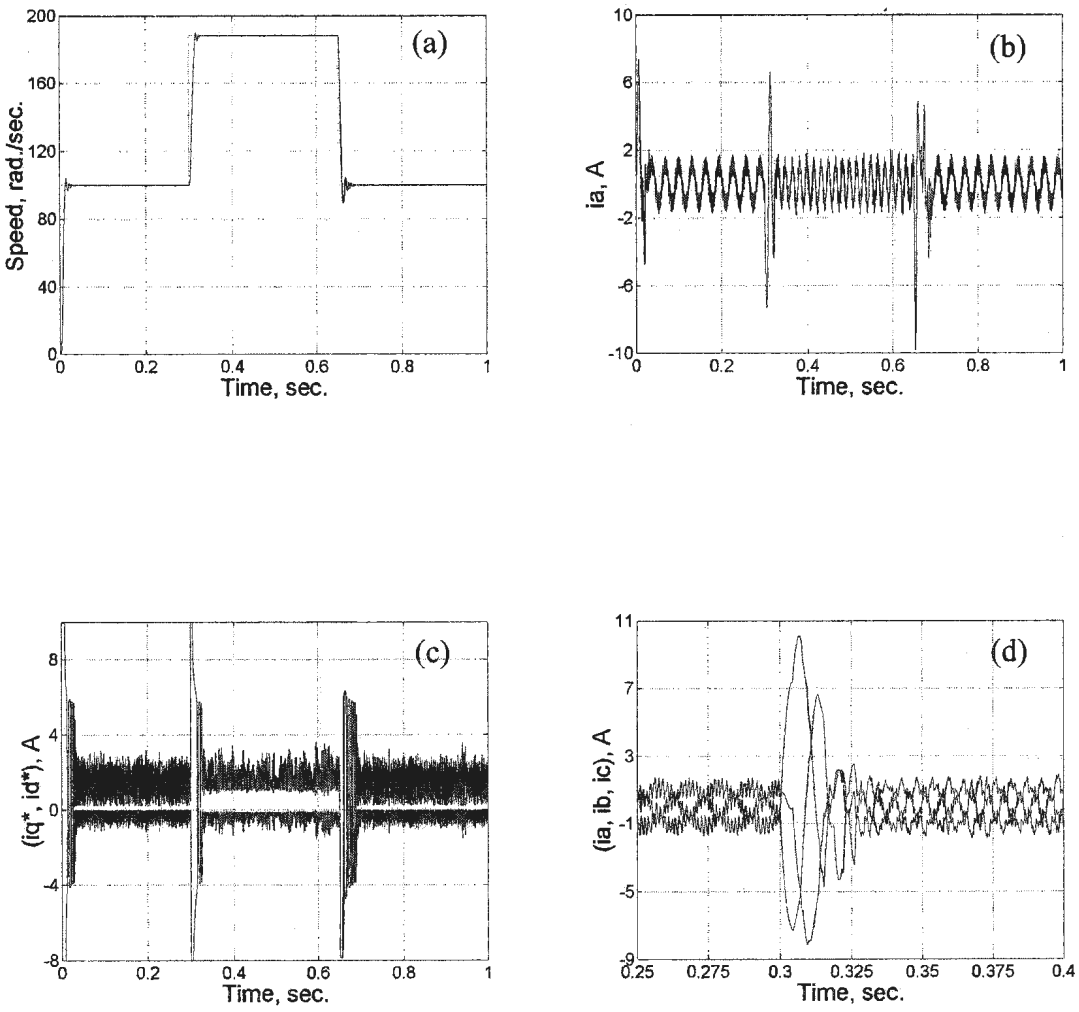

Fig. 4.11. Simulated responses of the simplified FLC based/MTPA IPMSM drive: a) speed, (b) steady-state actual phase current, (c) q-axis and d-axis command currents and (d) steady-state actual phase currents i_a, i_b and i_c for a step change of speed at half load conditions.

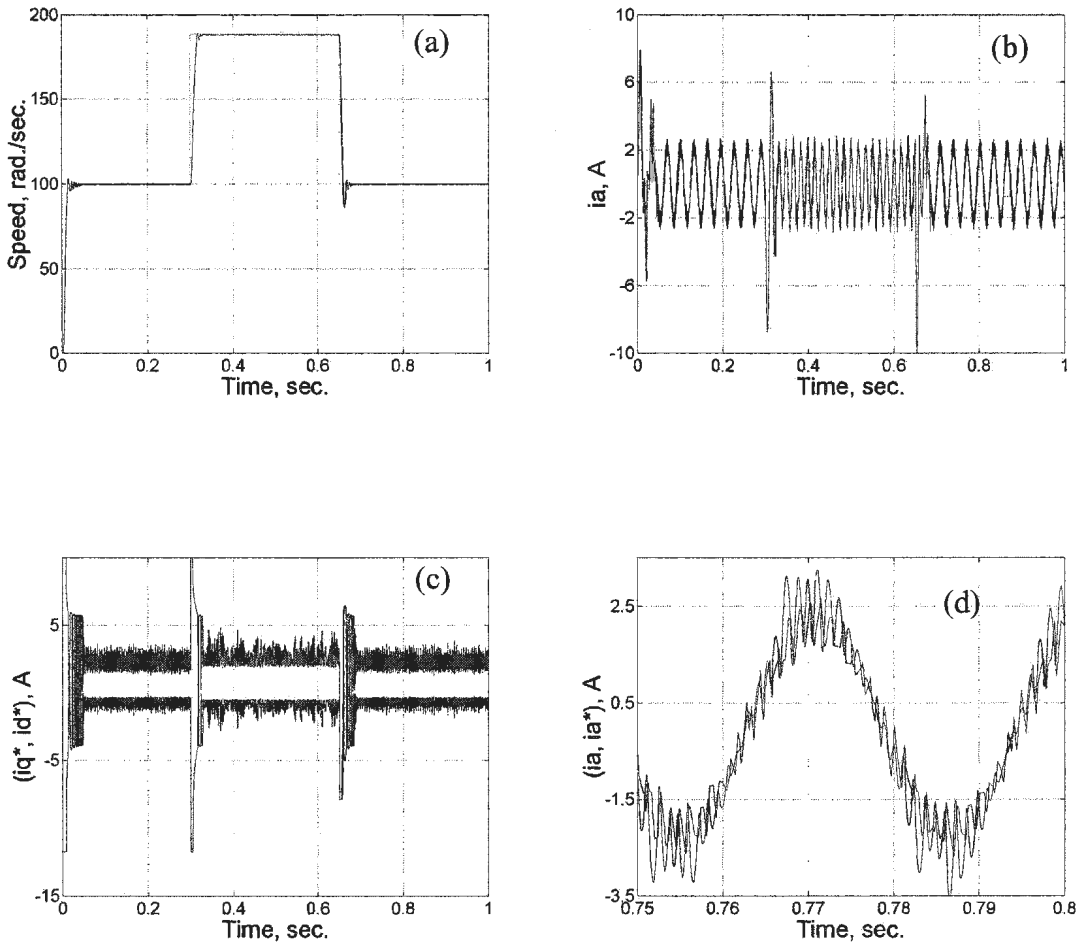

Fig. 4.12. Simulated responses of the simplified FLC based/MTPA IPMSM drive: a) speed, (b) steady-state actual phase current, (c) q-axis and d-axis command currents and (d) steady-state actual and command phase currents i_a and i_a^* for a step change of speed at full load conditions.

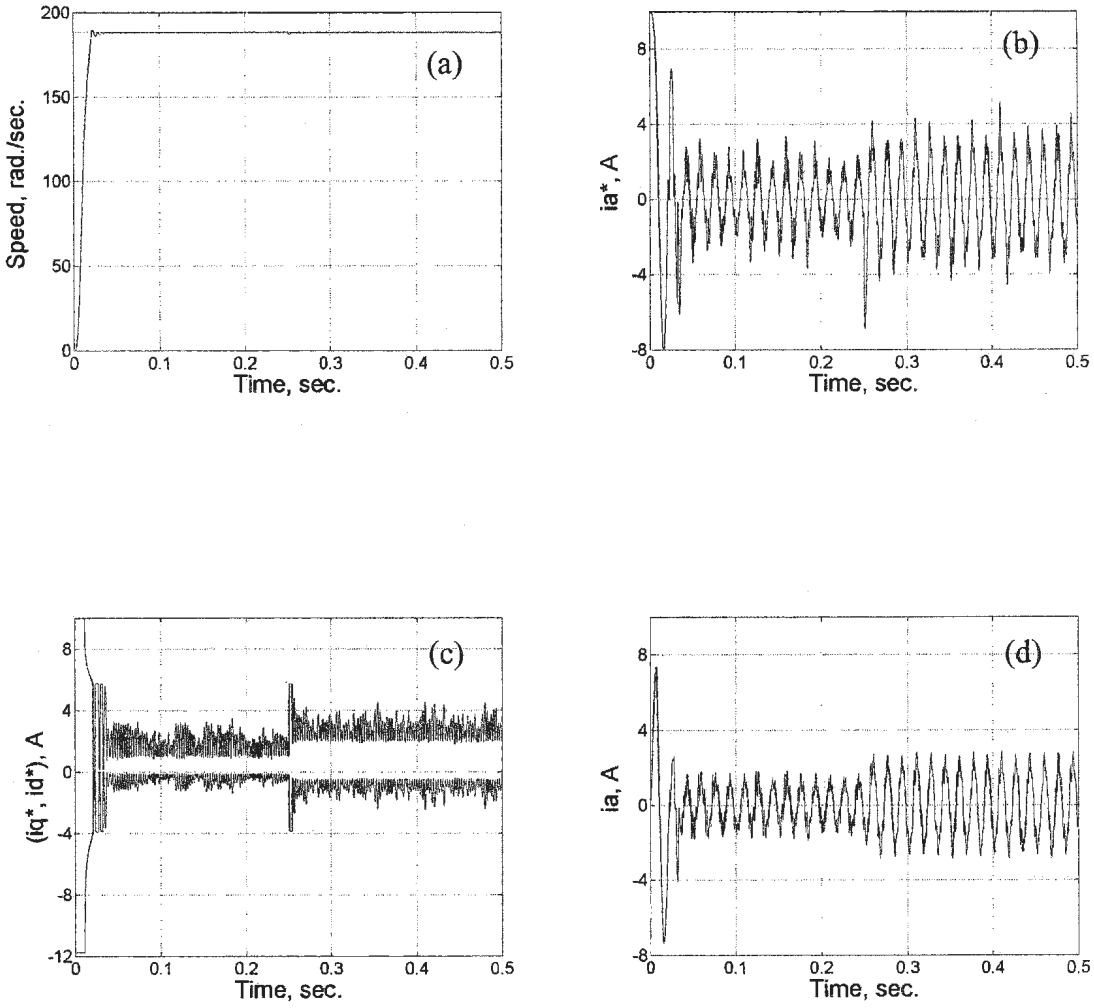

Fig. 4.13. Simulated responses of the simplified FLC based/MTPA IPMSM drive: a) speed, (b) command phase current, (c) q-axis and d-axis command currents and (d) steady-state actual phase current i_a for a sudden change of load (from half load to full load) at rated speed.

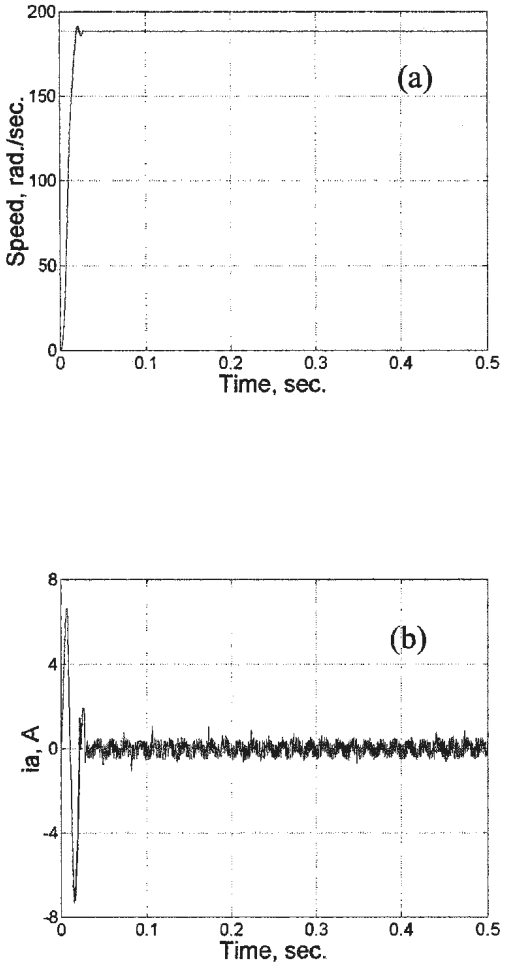

Fig. 4.14. Simulated responses of the simplified FLC based/MTPA IPMSM drive: a) speed, (b) steady-state actual phase current i_a for a sudden change of stator resistance (R to 2R) at no load and rated speed.

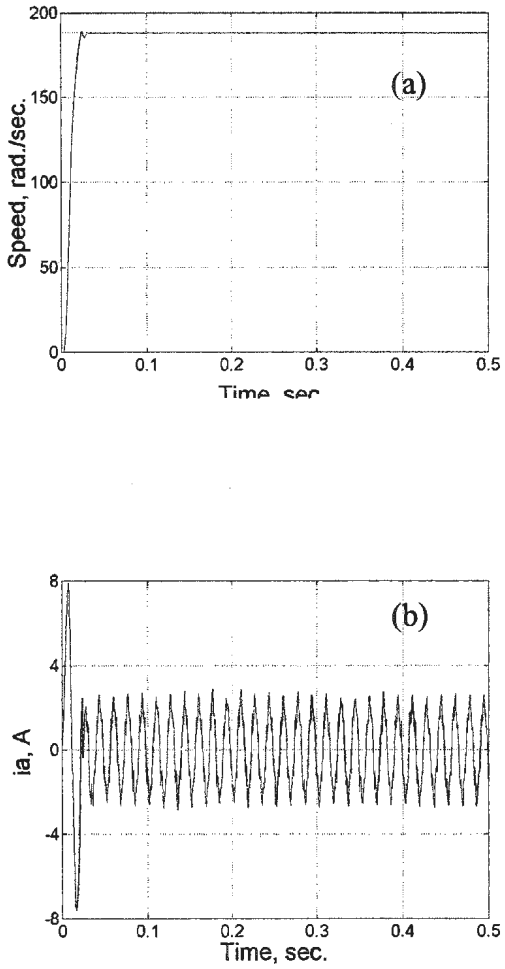

Fig. 4.15. Simulated responses of the simplified FLC based/MTPA IPMSM drive: a) speed, (b) steady-state actual phase current i_a for a sudden change of stator resistance (R to 2R) at full load and rated speed.

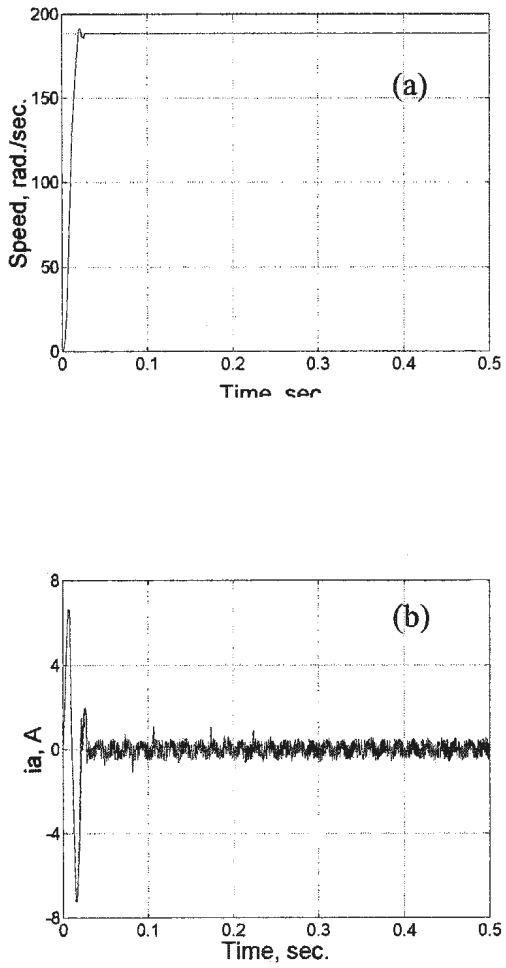

Fig. 4.16. Simulated responses of the simplified FLC based/MTPA IPMSM drive: a) speed, (b) steady-state actual phase current i_a for a sudden change of rotor inertia (J to 2J) at no load and rated speed.

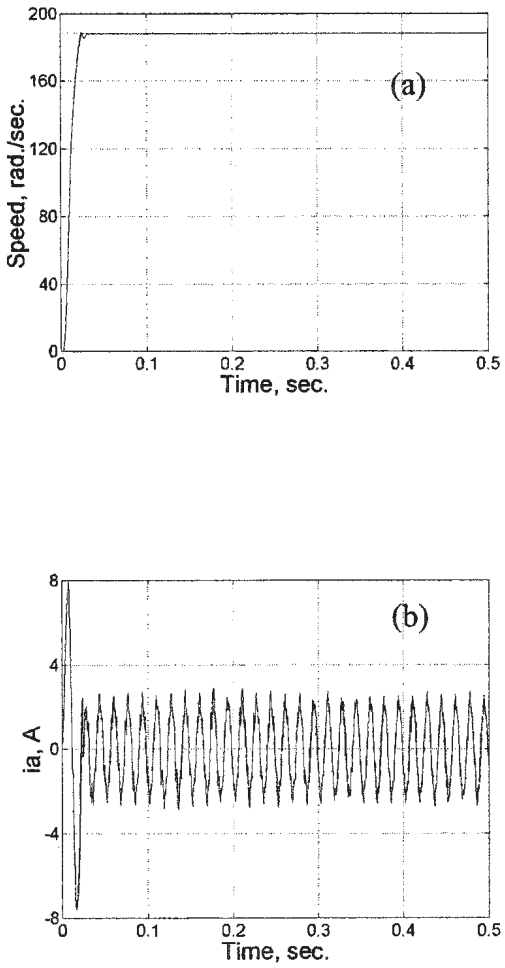

Fig. 4.17. Simulated responses of the simplified FLC based/MTPA IPMSM drive: a) speed, (b) steady-state actual phase current i_a for a sudden change of rotor inertia (J to 2J) at full load and rated speed.

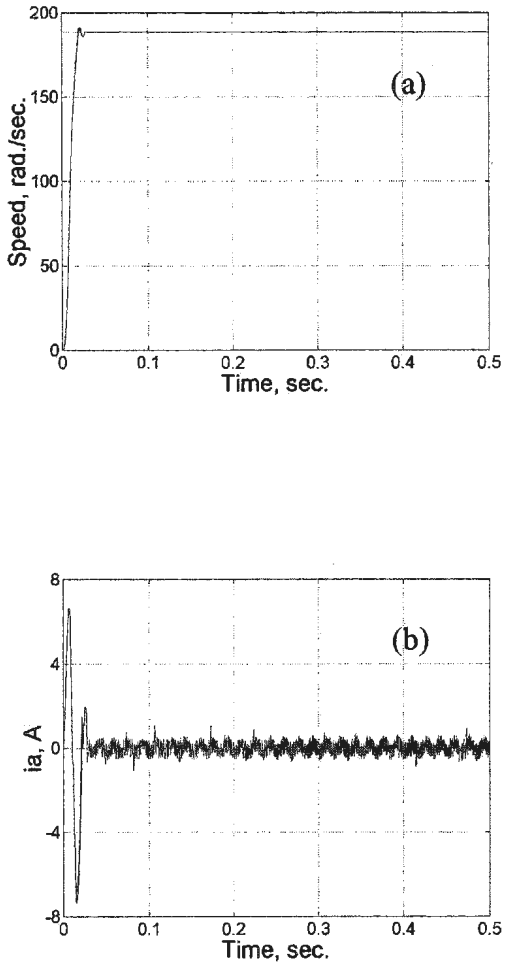

Fig. 4.18. Simulated responses of the simplified FLC based/MTPA IPMSM drive: a) speed, (b) steady-state actual phase current i_a for a sudden 50% decrease of L_q at no load and rated speed.

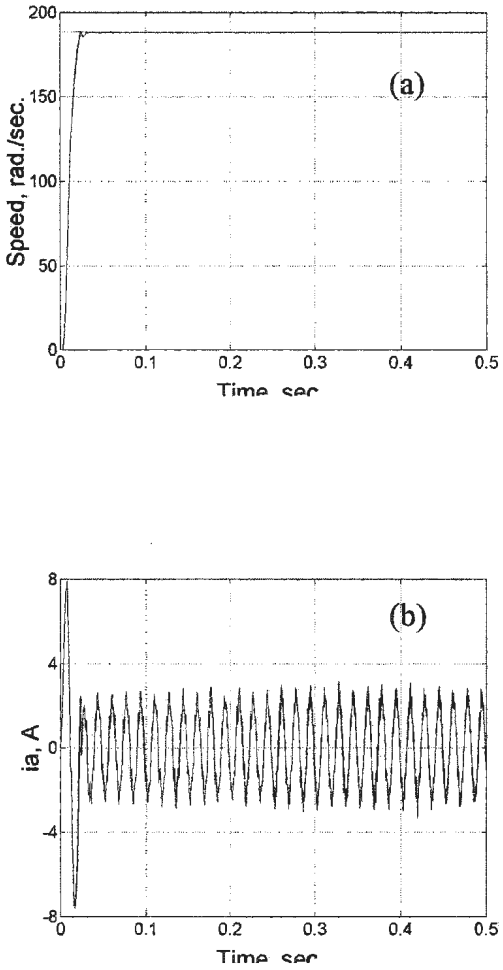

Fig. 4.19. Simulated responses of the simplified FLC based/MTPA IPMSM drive: a) speed, (b) steady-state actual phase current i_a for a sudden 50% decrease of L_q at full load and rated speed.

4.4 Concluding Remarks

The simulation results show encouraging performances of the proposed drive. The simplified FLC can accommodate different operating conditions such as load change, parameter variations and step change of command speed. Therefore, the simplified FLC with MTPA can be a good substitute for the conventional fixed gain PI or PID controllers or for more complex FLC schemes.

Generally, as the number of fuzzy rules increase better performance can be attained, but by use of the maximum torque per ampere with Taylor series approximation scheme, and the prudent simplification of the fuzzy algorithm, high performance can be obtained along with a reduction of computational burden. The simulation results confirm the robustness of the simplified FLC/MTPA controller in an IPMSM drive.

In order to validate the efficacy of the proposed drive, the laboratory implementation of the complete vector control scheme of the drive has been carried out in real-time as an integrated part of the proposed work. In addition, the non-simplified FLC with $i_d = 0$ drive has been implemented in the lab also.

Chapter 5

Experimental Implementation of the Simplified FLC Based MTPA Vector Control of the IPMSM

5.1 General Introduction

The implementation of a fuzzy controlled drive often presents difficulties in that the high computational burden imposed necessitates both high-level hardware and software. Because of this, the real-time implementation of the FLC for motor drives has presented a challenge to control engineers. This work overcomes such problems by utilizing a simplified FLC along with an approximated MTPA scheme.

The experimental implementation of the complete simplified FLC/MTPA IPMSM drive is presented in this chapter. This is the first time that the maximum torque per ampere mode of operation has been implemented with a fuzzy logic controller for the IPMSM in real-time.

The drive has been realized by use of a PC interfaced with a current controlled voltage source inverter through a dSPACE DS1102 digital-signal-processor (DSP) controller board. This chapter presents the detailed implementation of both hardware and software programming. In order to validate the efficacy of the drive, various experimental results under different dynamic operating conditions are presented and discussed.

5.2 Experimental Setup

5.2.1 Hardware Implementation

The hardware schematic for real-time implementation of the proposed IPMSM drive is shown in Fig. 5.1. The DSP board was installed in a personal computer (PC) with uninterrupted communication capabilities through dual-port memory. The DS1102 board is based on a Texas Instrument (TI) TMS320C31 32-bit floating point digital signal processor. The DSP has been supplemented by a set of on-board peripherals used in digital control systems, such as analog to digital (A/D), digital to analog (D/A) converters and incremental encoder interfaces. The DS1102 board has one 4 channel (2 12-bit and 2 16-bit) A/D and one 4 channel (12-bit each) D/A converter and two 16-bit incremental encoders. The DS1102 is also equipped with a TI-TMS320P14 16 bit micro controller DSP that acts as a slave processor and provides the necessary digital input/output (I/O) ports and powerful timer functions such as input capture, output capture and PWM waveform generation.

In this work, the slave processor was used only for digital I/O configuration. The actual motor currents were measured by Hall effect sensors, which have good frequency response, and were fed to the DSP board through the A/D converter. As the motor neutral was not grounded, only two phase currents were fed back and the

other phase current calculated from them. The rotor position angle was measured by an absolute incremental encoder mounted on the rotor shaft via a flexible coupler, and fed to the DSP board through an encoder interface. The encoder generates 4096 pulses per revolution, which are fed to the incremental encoder interface of the board. By using a 4-fold pulse multiplication the output of the encoder is increased to 4x4096 pulses per revolution in order to get a better resolution. A 24-bit position counter is used to count the encoder pulses. The counter is reset once per revolution by the index pulse generated from the encoder. The motor speed was computed from the measured rotor position angles using numerical differentiation.

In order to implement the vector control algorithm, the fixed-band hysteresis controller was used as the current controller. The command currents are generated from the speed controller. The hysteresis current controller compares the command currents with the corresponding actual motor currents and generates the logic signals, which act as firing pulses for the inverter switches. Thus, these six PWM logic signals are the output of the DSP board and were fed to a base drive circuit for the insulated gate bipolar transistor (IGBT) or bipolar junction transistor (JCT) inverter power module. The base drive circuit was used to provide isolation between the high power supply and the low power logic circuits and also to improve the voltage level so that it is sufficient to drive the inverter. The dc power supply for the inverter was obtained by rectifying the ac power through a variac.

In order to provide loading, the laboratory IPMSM was coupled to a dynamometer using a belt. The dynamometer serves as a simple mechanical load on the motor. A digital storage oscilloscope was used to capture the desired signals coming out through the D/A port of the DSP board.

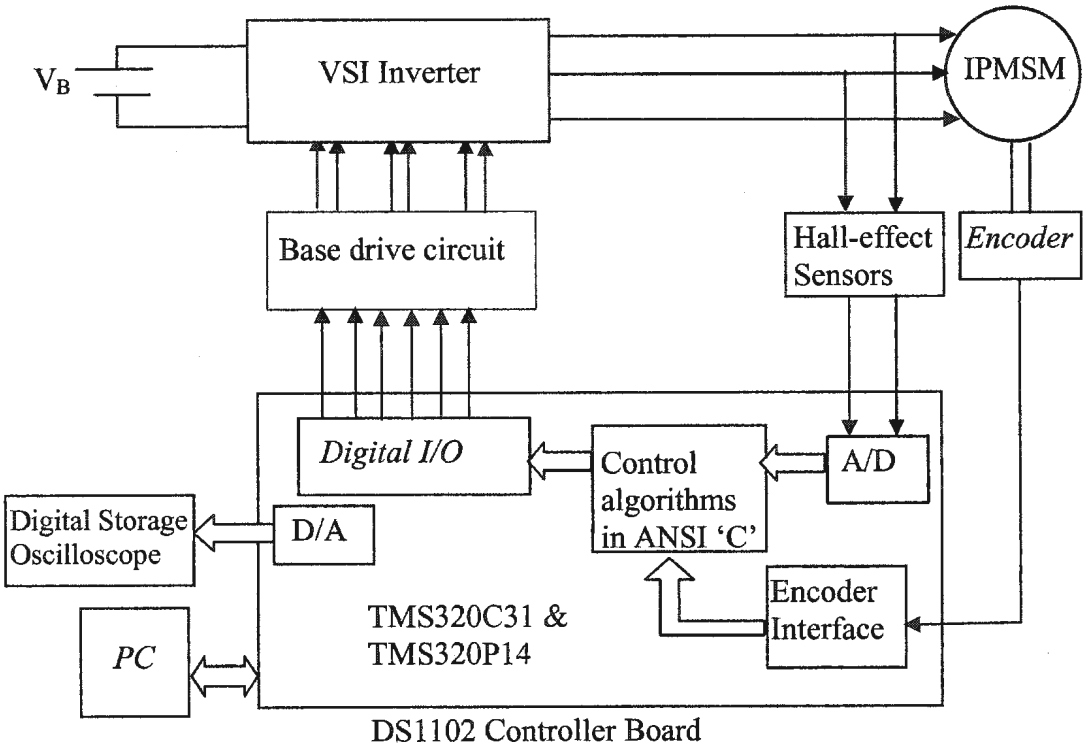

Fig. 5.1. Hardware schematic for experimental implementation of the IPMSM drive.

5.2.2 Software Implementation

Software was developed for the simplified FLC, approximated MTPA method and the fixed-band hysteresis current controller for the IPMSM drive in the ANSI 'C' programming language. Because of the reduced computational burden of the simplified FLC scheme the sampling frequency used was 10 kHz, which is

adequate for successful real-time implementation of the drive. The detailed software implementation is described below.

Step 1: All the peripherals of the DSP board are initialized in order to access the on-board peripherals. Macro functions supplied with the DS1102 controller board achieve this task. The macro function *init()* initializes the D/A converter subsystem of the DS1102 for output. This command also resets the interrupt request bits and calibrates the 16-bit A/D converters. The functions *timer*0() and *timer*1() are used to initialize the DS1102-TMS320C31's on-chip timers to generate timer interrupts at a predefined sampling rate as given in Table I. This is essential for real-time implementation. The detailed initialization and the I/O functions for the A/D converters and 16 bit I/O ports can be obtained from the reference manual of the DS1102 [71].

Table I: Peripheral initialization

```
void main()
{
 init(); /*init DAC mode, calibrate ADCs */
 init_slave_DSP_digital_i_o();
      /* initialize i/o ports for output*/
 *error=NO_ERROR;
     /* initialize overload error flag */
 dp_mem[0].f=0.0;
    /* init 1st dp-mem loc for float */
 dp_mem[1].f=0.0;
    /* init 2nd dp_mem loc for float */
 ds1102_inc_clear_counter(1);
    /* clear incr. encoder counter */
 start_isr_t0(TS);
    /* initialize sampling clock timer  */
 while(*error==NO_ERROR);
     /* background process  */
}
```

Step 2: After initializing all the required variables, an interrupt service routine (isr) is used to read the actual motor currents and rotor position angles at 100 μsec intervals (corresponding to the 10 kHz sampling frequency) following the steps shown in Table II. In this table, the constants K_a and K_b are used to get the actual motor currents through A/D channels 3 and 4. These constants depend on the type of Hall-effect sensors used. The incremental gain (INCG) is used to get the actual rotor position depending on the incremental encoder. In this work, the constants K_a, K_b and INCG have been determined to be 11.49, 10.93 and 3216.99049, respectively. The rotor speed is calculated by differentiating the present and past samples of rotor position. The command torque is generated by the simplified fuzzy logic based speed controller from the error between the command and present sample of actual speed. The components of the simplified FLC are fuzzification, fuzzy inference engine (rule base) and defuzzification. The implementations of these components in real-time using ANSI 'C' language are presented below.

Table II: Interrupt service routine to read the motor currents and rotor position.

```
void  isr_t0()
 {
      .
                .

   ds1102_ad_start();
   i_a = Ka*ds1102_ad(3);
   i_b = Kb*ds1102_ad(4);
   i_c = -(i_a+i_b);
   θr = INCG*ds1102_inc(1 or 2);
      .
      .
      .
 }
```

Step 3 (Fuzzification): The normalized values of the inputs $\Delta\omega_r$ and Δe are passed to the fuzzification stage which uses pre-selected membership functions to convert the crisp values of $\Delta\omega_m$ (cvalue) to its corresponding fuzzy value fvalue. In this work, the trapezoidal and triangular membership functions as developed in chapter 2 are used to reduce the computational burden in real-time.

In order for fuzzification, a routine (Fuzzy) for a singleton fuzzifier is written in 'C' language as shown in Table III. In this table, the term NS is the number of fuzzy sets, cvalue is the crisp value, fvalue is the fuzzy value for a particular input, i denotes the i-th fuzzy set of a particular input, b_l is the bottom low value, t_l is the top low value, t_h is the top high value, b_h is the bottom high value and cent is the centroid of a trapezoidal membership function.

Table III: 'C' code for fuzzification.

```
for(i=0; i<NS; i++)
 {
 fvalue[i] = 0;
   if ((cvalue >= b_l[i]) && (cvalue < t_l[i]))
      fvalue[i] = (cvalue - b_l[i])/(t_l[i] - b_l[i]);
      else
        {
        if ((cvalue >= t_l[i]) && (cvalue <= t_h[i]))
           fvalue[i] = 1;
           else
              {
              if ((cvalue > t_h[i]) && (cvalue <= b_h[i]))
                 fvalue[i] = (cvalue - b_h[i])/(t_h[i] - b_h[i]);
              }
        }
 }
 if (cvalue < cent[0])
    fvalue[0] = 1;
      else
        {
        if (cvalue > cent[NS-1])
           fvalue[NS-1] = 1;
        }
```

Step 4 (Fuzzy inference engine - rule base): The fuzzy inference engine is composed of a set of conditional ("if-then") statement control rules that obtain the results of all applicable rules. In the case of the simplified FLC, it computes the fuzzy value of the output based on a single fuzzy input. This is a highly simplified form of fuzzy rule inference as there are no AND or OR statements. The routine for the fuzzy inference engine (FuzzyEngine) is written in 'C' language as given in Table IV. In this table, NS1 (=5) and NS2 (=5) are the number of fuzzy sets for $\Delta\omega_m$, and i_{qn}^*, respectively.

Table IV: 'C' code for rule evaluation.

```
for (i=0; i<NS2; i++)
                fvalue2[i] = 0.0;
    for (j=0; j<NS1; j++)
     {
     minval = fvalue[j];
     fvalue2[j] = minval;
     }
```

Step 5 (Defuzzification): The input for the defuzzification process is a fuzzy set and the output is a single number, which is non-fuzzy (i.e., a crisp value). In order to reduce the computational burden for on-line implementation the following mathematical form is obtained using the center of gravity method [72],

$$i = \frac{\sum_{j=1}^{NS} A_j * \mu_{C_j}(i) * Cent_j}{\sum_{j=1}^{NS} A_j} \qquad (5.1)$$

where A_j is the area , $Cent_j$ is the centroid of the jth output set C_j, NS is the number of output fuzzy sets, $\mu_{C_j}(i)$ is the fuzzy value which scales the output set C_j.

According to the above mathematical formula, a new routine for defuzzification has also been written in 'C' language as given in Table V.

Table V: 'C' code for center of area defuzzification.

```
temp1 = 0;
cvalue2 = 0.0;
 for (i=0; i<NS3; i++)
   {
    temp2 = fvalue2[i]*areas_2[i];
    cvalue2 += temp2*cent_2[i];
    temp1 += temp2;
   }
 cvalue2 /= temp1;

TEC = KI * cvalue2;
```

where areas_2[i] is the area, cent_2[i] is the centroid of the ith fuzzy set of the output.

After finishing the FLC calculations the command currents i_a^*, i_b^* and i_c^* are generated from the command torque T_e^* and the rotor position angle θ_r using the inverse Park's transformation. These command phase currents are compared with the actual motor currents in the hysteresis current controller, which provides the

necessary driving pulses for the inverter switches. The hysteresis current controller algorithm is also written in 'C' language. The digital I/O ports are configured as output ports for the six PWM logic pulses, which are fed to the base-drive circuit of Inverpower 3-phase voltage source inverter module No. P111. For the sake of simplicity, the steps 1-5 are summarized in the flow chart of Fig. 5.2.

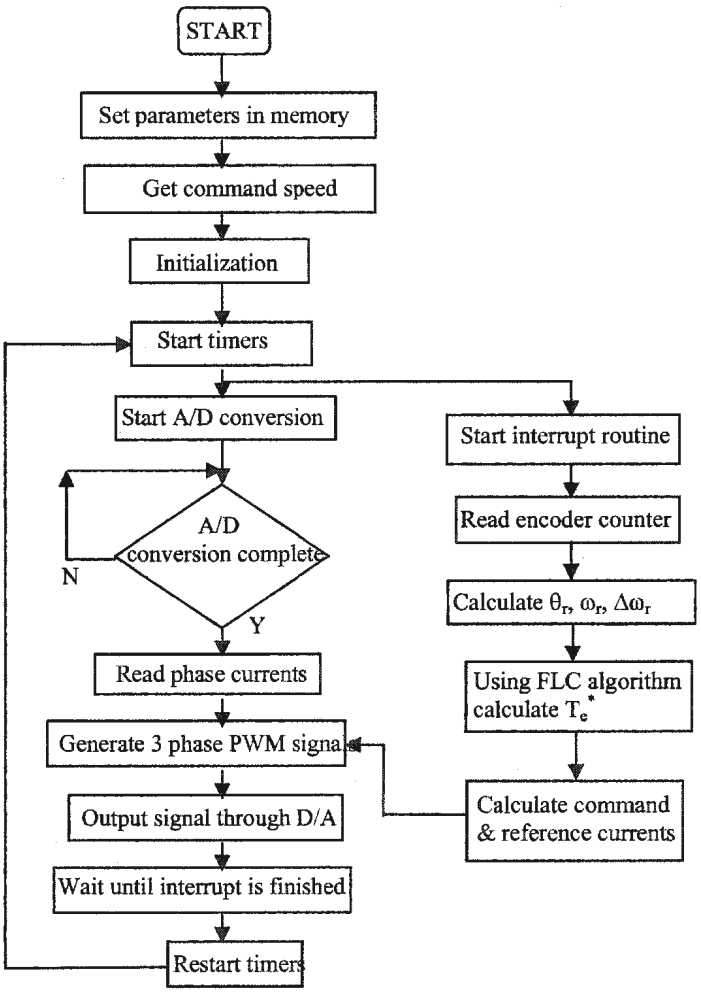

Fig. 5.2. Flow chart of the software for real-time implementation of the FLC based IPMSM drive.

Finally, the program is compiled by the TI C compiler and downloaded to the DSP board using dSPACE loader program down1102.

5.3 Experimental Results and Discussion

Please note that in the following experimental results, unless otherwise noted, the time scale for speed responses is 0.5 seconds per horizontal division, for a full-graph time span of 5 seconds. The time scale for simulated tests was either 1.0 or 0.5 seconds for full-graph time span. This difference is due to the operational nature of the manually operated experimental setup. The results reveal that the experimental startup responses are not as rapid as the simulation results would indicate. This is because the experimental setup dictates that voltage be applied to the inverter manually in a ramp-like fashion and not instantaneously as is the case with simulation.

The speed response and corresponding actual 'a' phase current for the simplified FLC based/MTPA IPMSM drive are shown in Figs. 5.3 (a) and (b), respectively, for no load and rated speed (188.5 rad./sec.) conditions. The results show that the drive achieves the command speed very promptly, with no observable overshoot or oscillation, and follows command speed accurately. Steady-state error appears to be zero. Phase current is within the rated values of the machine.

Figures 5.4 (a) and (b) show the speed response and actual phase current, respectively, for the simplified FLC based/MTPA IPMSM drive at rated load and rated speed conditions. Again the drive follows the command speed without detectable steady-state error, and achieves this quickly with no observable overshoot or oscillation. Again, phase current is within the rated values of the machine, but has increased slightly from the lightly loaded case.

Figures 5.5 (a)-(c) show the speed response, q- and d-axis command currents and actual phase current, respectively, for the simplified FLC based/MTPA IPMSM drive at light load and low speed (90 rad./sec.) conditions. Here, it can be seen that the drive follows the command speed promptly, without overshoot and no visible steady-state error. As in the simulated case, i_d^* appears to be a scaled opposite of i_q^*. The phase current remains within rated values of the machine. These results verify that the FLC based/MTPA IPMSM drive can quickly achieve, and precisely follow, command speed under various loading conditions.

The responses of the simplified FLC based/MTPA IPMSM drive to sudden changes in command speed at light load conditions are shown in Figs. 5.6 (a) to (c). It is demonstrated that the drive can follow the command speed quickly and accurately during a step increase (90 rad./sec.→188.5 rad./sec.) and decrease (188.5 rad./sec.→125 rad./sec.) of speed under light load conditions and also under rated load conditions (80 rad./sec.→165 rad./sec. and 165 rad./sec.→80 rad./sec.). There are no detectable over- or undershoots or steady-state errors. Figure 5.6 (c) illustrates the increase in phase current frequency with increased motor speed. A software program (Dspeed.c), included in Appendix D, was used to achieve the real-time step change of command speed.

The ability of the drive to accommodate sudden changes in load was also examined experimentally. Figures 5.7 (a)-(c) show the speed response, q- and d-axis command currents and actual phase current at steady-state after loading, respectively, for the simplified FLC based/MTPA IPMSM drive for a sudden increase of load (from no load to rated load) at rated speed. It can be seen that the drive is virtually insensitive to such a load disturbance. Also, i_d^* appears to be a

scaled opposite of i_q^* and the phase current remains within rated machine parameters.

Figures 5.8 (a) and (b) show the speed response and actual phase current, at steady-state after loading, for the simplified FLC based/MTPA IPMSM drive for a sudden increase of load (from no load to rated load) at low speed (90 rad./sec.). Once again, the drive remains detectably insensitive to the load disturbance. These results indicate that the drive can accommodate sudden increases in load, at varying speeds, without disturbance of rotor speed and while remaining within the rated phase currents of the machine.

Therefore, the efficacy and robustness of the simplified FLC based/MTPA IPMSM are verified.

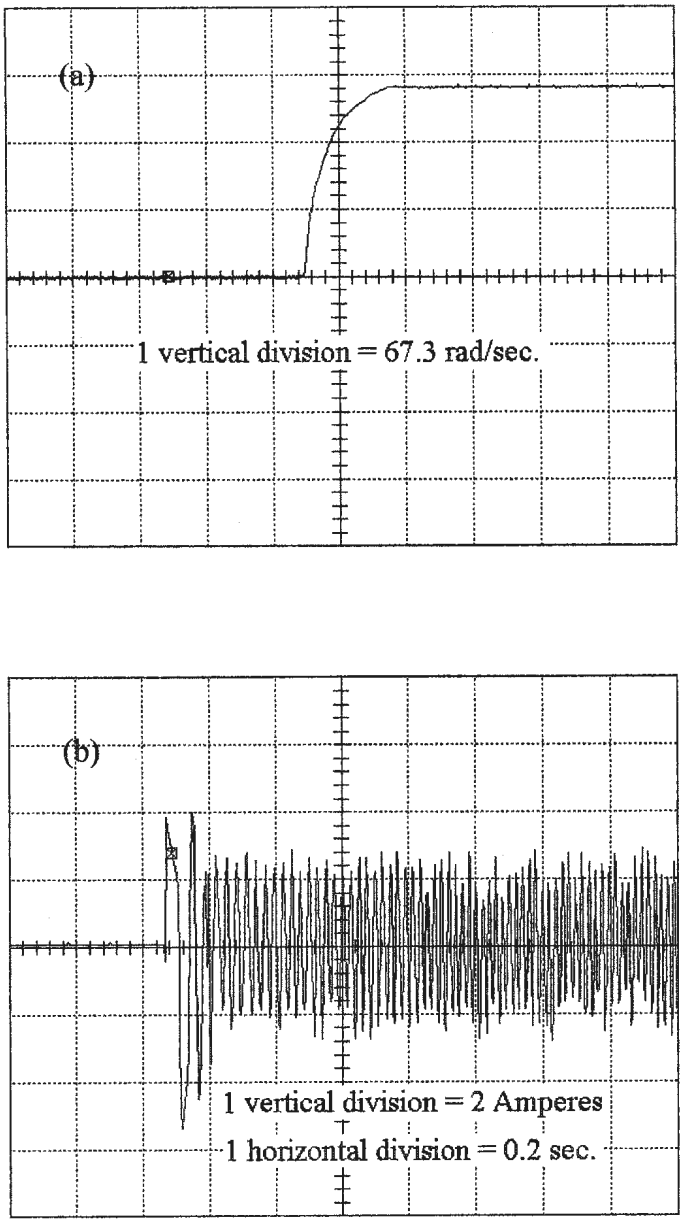

Fig. 5.3. Experimental responses of the simplified FLC based/MTPA IPMSM drive: a) speed and (b) actual phase current at light load and rated speed conditions.

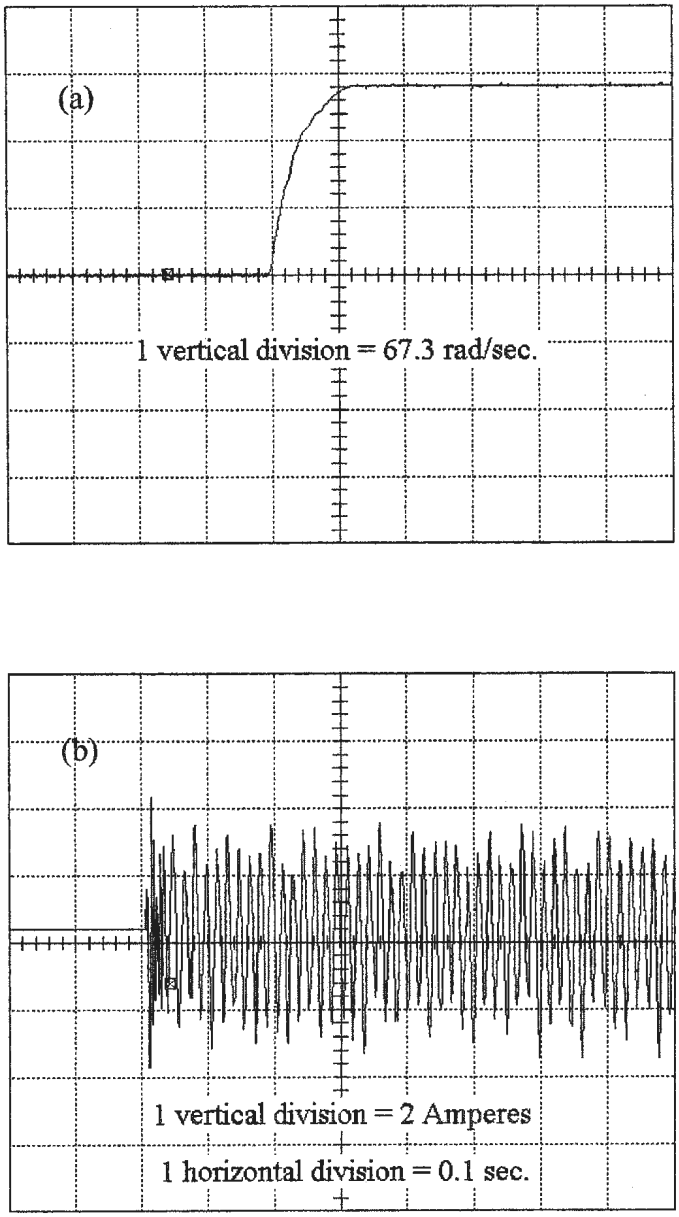

Fig. 5.4. Experimental responses of the simplified FLC based/MTPA IPMSM drive: a) speed and (b) actual phase current at rated load and rated speed conditions.

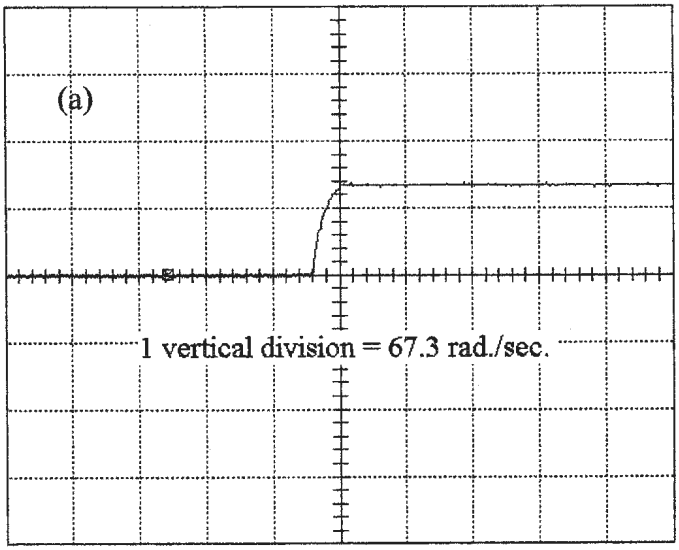

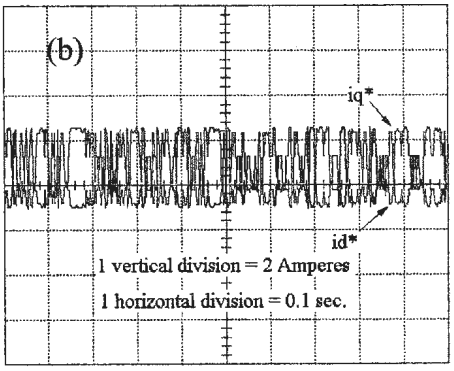

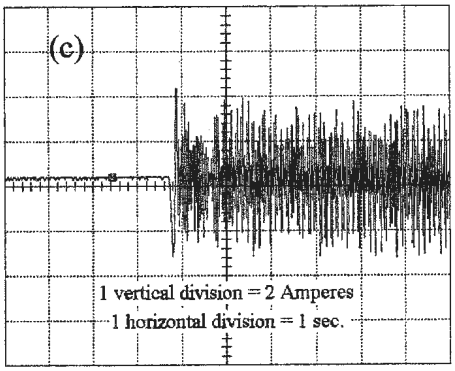

Fig. 5.5. Experimental responses of the simplified FLC based/MTPA IPMSM drive: a) speed, (b) q- and d-axis command currents at steady-state and c) actual phase current at light load and low speed (90 rad./sec.) conditions.

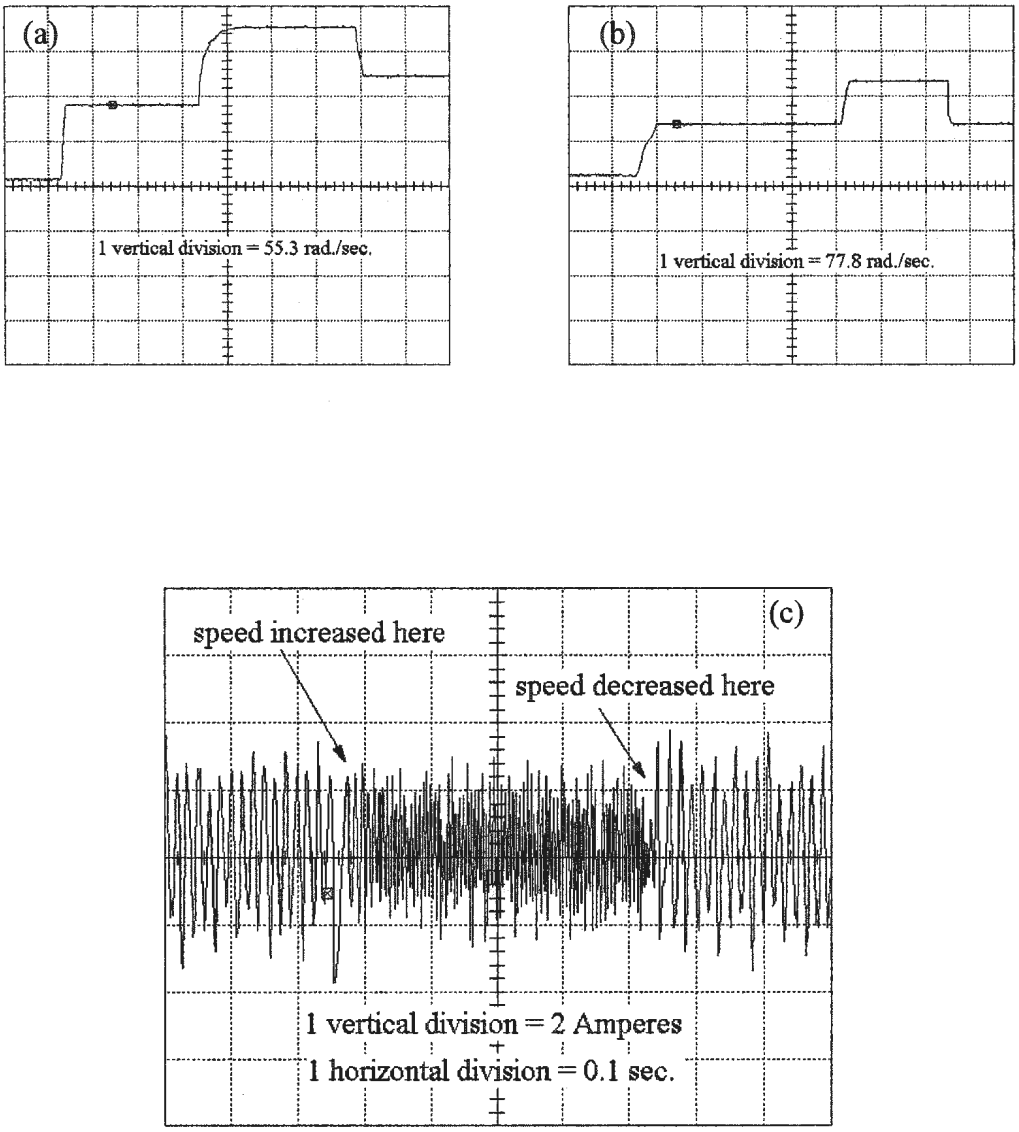

Fig. 5.6. Experimental responses of the simplified FLC based/MTPA IPMSM drive for sudden changes in command speed: a) speed at light load, (b) speed at rated load (note scale difference) and c) actual phase current at light load conditions.

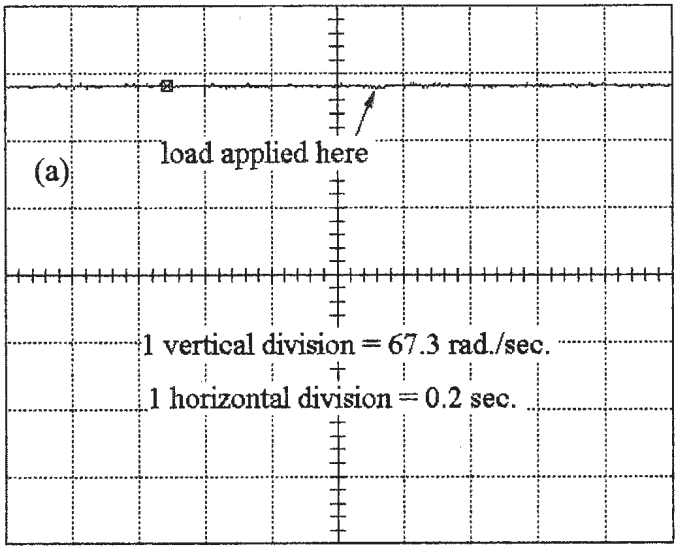

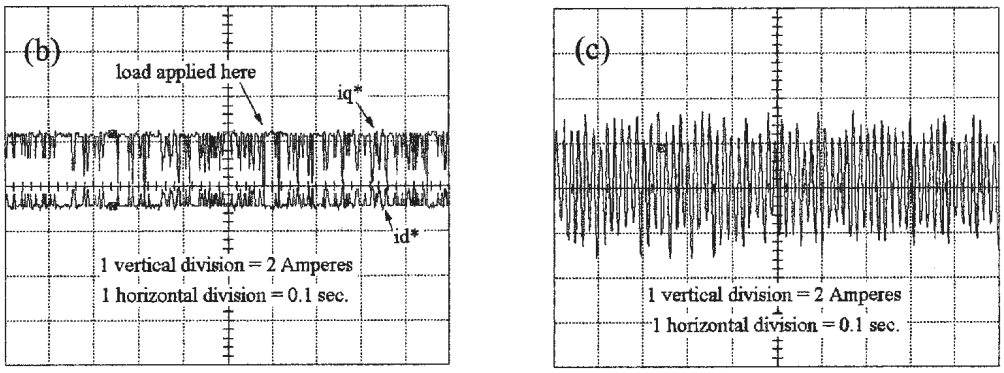

Fig. 5.7. Experimental responses of the simplified FLC based/MTPA IPMSM drive for a sudden increase of load at rated speed: a) speed, (b) q- and d-axis command currents and c) actual phase current at steady-state after loading.

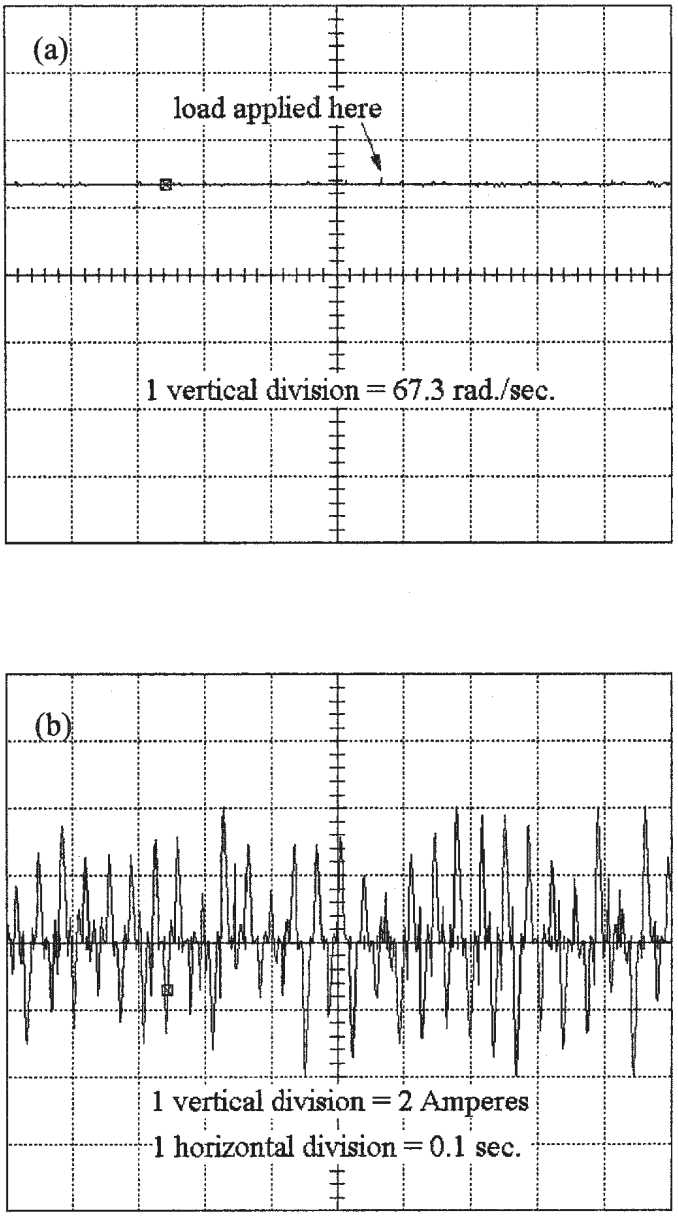

Fig. 5.8. Experimental responses of the simplified FLC based/MTPA IPMSM drive for a sudden increase of load at low speed (90 rad./sec.): a) speed, (b) actual phase current at steady-state after loading.

5.4 Concluding Remarks

The detailed DSP based real-time implementation procedure for the simplified FLC with approximated maximum torque per ampere mode operation for the IPMSM drive has been presented in this paper. The complete drive has been implemented, through both hardware and software, using a digital signal processor board on a laboratory 1 hp interior permanent magnet motor.

The performance of the proposed IPMSM drive has been investigated experimentally at different dynamic operating conditions such as sudden changes of command speed and under varying loads. The drive is found to be robust for use in high performance industrial drive applications. The experimental results have validated the simulation results presented in chapter 4.

Chapter 6

Conclusions

6.1 General

The literature review of chapter 1 has established that, when coupled with an appropriate controller, the interior permanent magnet synchronous motor (IPMSM) can be a favourable choice for use in variable speed high performance electric motor drives. Speed controllers for the IPMSM, however, typically require knowledge of machine parameters, which, in the case of the IPMSM, are not constant under dynamic operating conditions. This makes the design of such controllers cumbersome and imprecise. Fixed gain controllers suffer from overshoot, undershoot, steady-state error and even instability in their applications for high performance IPMSM drives. Conventional adaptive controllers require complex, and usually expensive, hardware and software for their implementation.

The simplified FLC controller coupled with maximum torque per ampere operation can overcome these problems by providing an adaptive speed controller which can accommodate parameter variations, system uncertainties and non-linearities as well as load disturbances while requiring a minimum of computing

power and complexity of hardware. This is done through the proposed vector control scheme of the IPMSM.

Chapter 2 has detailed the analysis and modeling of the pulse-width modulated (PWM) voltage source inverter (VSI) fed IPMSM drive. Included in this chapter is a new method for incorporating the maximum torque per ampere (MTPA) mode of operation in real-time for the IPMSM.

The development of the fuzzy logic controller for the IPMSM drive, including the concepts of fuzzy logic, linguistic variables, fuzzy sets, membership functions, fuzzification, fuzzy rule evaluation, and defuzzification, have been included in the chapter 3. Also, a simplified FLC based speed controller has been presented.

Chapter 4 presents the comparative simulation results of both a conventional FLC based IPMSM drive with $i_d^* = 0$ and the proposed simplified FLC based drive with $i_d \neq 0$ incorporating the MTPA mode of operation. It is to be noted that the latter mode of operation is most suitable for practical IPM motor drive systems. Extensive simulations have verified that the proposed drive can outperform the conventional FLC based controller with regards to speed response, current minimization and robustness, with reduced computational burden and need for high-end hardware.

In chapter 5 the real-time implementation of the new simplified FLC with MTPA in the IPMSM drive has been presented. Experimental investigation of the proposed drive under varying dynamic operating conditions has verified that the drive can achieve and follow command speed promptly without over- or undershoot and virtually zero steady-state error for a variety of operating conditions. The robustness of the controller has been verified.

6.2 Major Contributions of this Work

- The practical, real-time implementation of the maximum torque per ampere mode of operation of the IPMSM has been developed.

- A new FLC based controller has been developed for the IPMSM for operation in the MTPA mode. This controller has been purposefully simplified so as to reduce computational burden while maintaining high performance standards.

- The proposed FLC drive with $i_d \neq 0$ has been simulated along with a conventional FLC drive with $i_d^* = 0$ for comparison purposes. These comparative simulations have illustrated the ability of the proposed controller to handle ever-changing motor dynamics as well as non-linear load disturbances.

- The proposed simplified FLC/MTPA has been implemented in real-time through a laboratory 1 hp IPMSM using a digital signal processor controller board. The efficacy and robustness of the drive has been verified by experimental investigation of the performance of the drive under various dynamic operating conditions such as sudden changes in command speed and loading.

6.3 Future Direction of Research

It has been established that the FLC is insensitive to changes in motor parameters. However, in the development of the maximum torque per ampere mode of operation the q- and d-axis reactances, L_q and L_d have been assumed to be constant. Of course, this assumption does not hold true under changing operating conditions. Although any negative impact appears to be not very significant for typical uses, it should be further investigated in the context of high performance adjustable speed drive requirements. In the future, some form of adaptive technique, such as artificial neural networks or further FLC and neuro-fuzzy implementations, should be used to accommodate these changes in reactance parameters.

6.4 Conclusions

- The maximum torque per ampere technique using Taylor series approximation can be used in the high performance IPMSM drive for operating speeds under rated conditions. This allows the motor to develop maximum mechanical torque with minimum values of stator currents.

- The proposed drive can be used effectively for accurate, precise and robust speed control of the IPMSM under different dynamic operating conditions such as, command speed change, load change, system uncertainties and parameter variations.

- The proposed drive provides an adaptive, intelligent control technique for the IPMSM with minimal complexity, computational burden and hardware requirement.

- The efficacy of the new control system has been established both theoretically and experimentally.

References

[1] P. C. Sen, "Electric Motor Drives and Control – Past, Present and Future", *IEEE Trans. on Industrial Electronics*, vol. 37, no. 6, Dec. 1990, pp. 562-575.

[2] M. A. Rahman, "Modern Electric Motors in Electronic World", *IEEE/IECON'93 Conference Record*, (Hawaii), pp. 644-648.

[3] G. R. Slemon, *Electric Machines and Drives*, Addison-Wesley Publishing Company, 1992.

[4] B. K. Bose, *Power Electronics and AC Drives*, Englewood Cliffs, NJ: Prentice Hall, 1986.

[5] P. C. Sen, *Principles of Electric Machines and Power Electronics*, New York: Wiley, 1988.

[6] M. H. Rashid, *Power Electronics-Circuits, Devices and Applications*, Englewood Cliffs, NJ: Prentice Hall, 1996.

[7] F. Blaschke, "The Principle of Field Orientation as Applied to the New Transvector Closed-Loop Control System for Rotating Field Machines", *Siemens Review*, Vol. 34, May 1972, pp. 217-220.

[8] M. A. Rahman, "Permanent Magnet Synchronous Motors - A Review of the State of Design Art", *Proceedings of International Conference On Electric Machines, Athens*, 1980, pp. 312-319.

[9] K. Hasse, "On the Dynamic Behaviour of Induction Machines Driven by Variable Frequency and Variable Voltage Sources", *ETZ A, Bd. 89,* H.4, pp. 77-81, 1968.

[10] M. A. Rahman, T. S. Radwan, A. M. Osheiba and A. E. Lashine, "Analysis of Current Controllers for Voltage Source Inverters", *IEEE Trans. Ind. Electronics*, vol. 44, Aug. 1997, pp. 477-485.

[11] H. Le-Huy, K. Silmani and P. Viarouge, "Analysis and Implementation of a Real-Time Predictive Current Controller for Permanent Magnet Synchronous Servo Drives", *IEEE Trans. on IEEE Trans. on Industrial Electronics*, vol. 41, no. 1, Feb. 1994, pp. 110-117.

[12] H. Le-Huy and L. A. Dessaint, "An Adaptive Current Control Scheme for PWM Synchronous Motor Drive: Analysis and Simulation", *IEEE Trans. on Power Electronics*, vol. 4, no. 4, Oct. 1989, pp. 486-495.

[13] A. Tripathi and P. C. Sen, "Comparative Analysis of Fixed and Sinusoidal Band Hysteresis Current Controllers for Voltage Source Inverters", *IEEE Trans. on Ind. Electronics*, vol. 39, Feb. 1992, pp. 63-73.

[14] D. M. Brod and D. W. Novotny, "Current Control of VSI-PWM Inverters", *IEEE Transactions on Industry Applications*, Vol. IA-21, No. 4, May/June 1985, pp. 562-570.

[15] J. Holtz and S. Stadtfeld, "A Predictive Controller for the Stator Current Vector of the ac Machines fed from Switching Voltage Source", *Proc. Int. Power Engineering Conf.*, Tokyo, Japan, Apr. 1983, pp. 1665-1675.

[16] A. B. Plunkett, "A Current Controlled PWM Transistor Inverter Drive", *Conf. Rec. IEEE-IAS Annu. Meeting*, Oct. 1979, pp. 951-957.

[17] M. N. Uddin, T. S. Radwan, G. H. George and M. A. Rahman, "Performance of Current Controllers for VSI-Fed IPMSM Drive", *IEEE Transactions on Industry Applications*, Vol. 36, No. 6, Nov./Dec. 2000, pp. 1531-1538.

[18] B. K. Bose and P. M. Szczesny, "A Microcomputer-Based Control and Simulation of an Advanced IPM Synchronous Machine Drive System for Electric Vehicle Propulsion", *IEEE Trans. on Industrial Electronics*, vol. 3, no. 4, Nov. 1988, pp. 547-559.

[19] A. V. Gummaste and G. R. Slemon, "Steady State Analysis of a Permanent Magnet Synchronous Motor Drive with Voltage Source Inverter", *IEEE Trans. on Industrial Applications*, vol. IA-17, no. 2, March/April 1981, pp.143-151.

[20] G. R. Slemon and A. V. Gummaste, "Steady State Analysis of a Permanent Magnet Synchronous Motor Drive with Current Source Inverter", *IEEE Trans. on Industrial Applications*, vol. IA-19, no. 2, March/April 1983, pp. 190-197.

[21] T. H. Liu, C. M. Young and C. H. Liu, "Microprocessor Based Controller Design and Simulation of Permanent Magnet Synchronous Motor Drive", *IEEE Trans. on Industrial Electronics*, vol. 35, no. 4, Nov. 1988, pp. 516-523.

[22] P. Pillay and R. Krishnan, "Modeling of permanent magnet motor drives", *IEEE Trans. on Industrial Electronics*, vol. 35, no. 4, Nov. 1988, pp. 537-541.

[23] P. Pillay and R. Krishnan, "Modeling, Simulation and Analysis of Permanent Magnet Motor Drives, Part I: The Permanent-Magnet Synchronous Motor Drive", *IEEE Trans. on Industry Applications*, vol. 25, no. 2, March/April 1989, pp. 265-273.

[24] P. Pillay and R. Krishnan, "Modeling, Simulation and Analysis of a High Performance Vector Controlled Permanent Magnet Synchronous Motor Drive", *IEEE/IAS Annual Meeting Conference Record*, 1987, pp 253-261.

[25] P. Pillay and R. Krishnan, "Control Characteristics and Speed Controller Design for High Performance Permanent Magnet Synchronous Motor Drive", *IEEE Trans. on Power Electronics*, vol. 5, no. 2, April 1990, pp.151-159.

[26] M. A. Rahman, M. Vilathgamuwa, M. N. Uddin & K .J. Tseng, " Non-linear control of interior permanent magnet synchronous motor drive", *IEEE Trans. on Industry Applications*, Vol.39, Mar/April 2003, pp.408-416.

[27] P. Pillay, C. R. Allen and R. Budhabhathi, "DSP-Based Vector Control and Current Controllers for Permanent Magnet Synchronous Motor Drive", *IEEE/IAS Annual Meeting Conference Record*, Seattle, Washington, 1990, pp. 539-544.

[28] B. K. Bose, "A High Performance Inverter Fed Drive System of an Interior Permanent Magnet Synchronous Machine", *IEEE Trans. on Industry Applications*, vol. IA-24, no. 6, 1988, pp. 987-997.

[29] H. Le-Huy and L. A. Dessaint, "An Adaptive Current Control Scheme for PWM Synchronous Motor Drive: Analysis and Simulation", *IEEE Trans. on Power Electronics*, vol. 4, no. 4, Oct. 1989, pp. 486-495.

[30] H. Le-Huy, K. Silmani and P. Viarouge, "Analysis and Implementation of a Real-Time Predictive Current Controller for Permanent Magnet Synchronous Servo Drives", *IEEE Trans. on IEEE Trans. on Industrial Electronics*, vol. 41, no. 1, Feb. 1994, pp. 110-117.

[31] B. K. Bose and P. M. Szczesny, "A Microcomputer-Based Control and Simulation of an Advanced IPM Synchronous Machine Drive System for

Electric Vehicle Propulsion", *IEEE Trans. on Industrial Electronics*, vol. 3, no. 4, Nov. 1988, pp. 547-559.

[32] T. M. Jahns, G. B. Kilman and T. W. Neumann, "Interior Permanent Magnet Synchronous Motors for Adjustable Speed Drives", *IEEE Trans. on Industry Applications*, vol. IA-22, no. 4, July/August 1986, pp. 738-747.

[33] T. M. Jahns, "Flux-Weakening Regime Operation of an Interior Permanent Magnet Synchronous Motor Drive", *IEEE Trans. on Industry Applications*, vol. IA-23, no. 4, 1987, pp. 681-689.

[34] S. Morimoto, Y. Takeda and T. Hirasha, "Current Phase Control Methods for Permanent Magnet Synchronous Motors", *IEEE Trans. on Power Electronics*, vol. 5, no. 2, April 1990, pp. 133-139.

[35] S. Morimoto, Y. Takeda, T. Hirasa and K. Taniguchi, "Expansion of Operating Limits for Permanent Magnet Motor by Current Vector Control Considering the Inverter Capacity", *IEEE Trans. on Industry Applications*, vol. 26, no. 5, Sept./Oct. 1990, pp.866-871.

[36] S. Morimoto, Y. Takeda, K. Hatanaka, Y. Tong, and T. Hirasa, "Design and Control System of Permanent Magnet Synchronous Motor for High Torque and High Efficiency Operation", *IEEE/IAS Annual Meeting Conference Record*, 1991, pp. 463-468.

[37] S. Morimoto, K. Hatanaka, Y. Tong, Y. Takeda and T. Hirasa, "Servo Drive System and Control Characteristics of salient Pole Permanent Magnet Syn-

chronous Motor", *IEEE Trans. on Industry Applications*, vol. 29, no. 2, March/April 1993, pp. 338-343.

[38] S. Morimoto, Y. Takeda, and T. Hirasa, "Flux Weakening Control Method for Surface Permanent Magnet Synchronous Motors", *IPEC Conference. Record, Tokyo, Japan,* 1990, pp. 942-950.

[39] S. Morimoto, M. Sanda and Y. Takeda, "Effects and Compensation of Magnetic Saturation in Flux-Weakening Controlled Permanent Magnet Synchronous Motor Drives", *IEEE Trans. on Industry Applications*, vol. 30, no. 6, Nov./Dec. 1994, pp. 1632-1637.

[40] M. F. Rahman, L. Zhang and K. W. Lim, "A Direct Torque Controlled Interior Permanent magnet Synchronous Motor Drive Incorporating Field Weakening", *IEEE/IAS Annual Meeting Conference Record*, 1997, pp. 67-74.

[41] S. Vaez, V. I. John and M. A. Rahman, "An On-Line Loss Minimization Controller for Interior Permanent Magnet Motor Drives", *IEEE Trans. on Energy Conversion*, Paper No. PE-I345-EC-0-07-1998.

[42] T. S. Radwan, M. A. Rahman, A. M. Osheiba and A. E. Lashine, "Performance of a Hybrid Current-Controlled VSI Permanent Magnet Synchronous Motor Drive", *IEEE/PESC Conference Record*, 1996, pp.951-957.

[43] M.A. Hoque, Casey Butt and M.A.Rahman, "A Novel Approach for MTPA Speed Control of IPMSM Drive", *Proc. 2nd IEEE International Confer-*

ence of Electrical & Computer Engineering, Dhaka, Dec. 26-27, 2002, pp. 336-339.

[44] R. Krishnan, "Control and Operation of PM Synchronous Motor Drives in the Field Weakening Region", *IEEE/IECON'93 Conference Record, Hawaii*, 1993, pp. 745-750.

[45] S. R. Macminn and T. M. Jahns, "Control Techniques for Improved High–Speed Performance of Interior PM Synchronous Motor Drives", *IEEE Trans. on Industry Applications*, vol. 27, no. 5, Sep./Oct. 1991, pp. 997-1004.

[46] R. Dhanuadi and N. Mohan, "Analysis of Current-Regulated Voltage Source Inverters for Permanent Magnet Synchronous Motor Drives in Normal and Extended Speed Range", *IEEE Trans. on Energy Conversion*, vol. 5, no. 1, March 1990, pp. 137-147.

[47] A. Kumamoto and Y. Hirame, "A Flux-Weakening Method for a Buried Permanent Magnet Motor with Consideration of Parameter Detunning on System Performance", *IPEC Conference Record, Tokyo, Japan*, 1990, pp. 950-955.

[48] I. Choy, T. Yoon, K. Kim, and M. Park, "Microprocessor-Based Permanent Magnet Synchronous Motor Drives using MRAC", *IPEC Conference Record, Tokyo, Japan*, 1990, pp. 481-488.

[49] E.Cerruto, A. Raciti and A. Testa, "A Robust Adaptive Controller for PM Motor Drives in Robotic Applications", IEEE Trans. on Power Electronics, vol. 10, no. 1, Jan. 1995, pp. 62-70.

[50] Y. Sozer and D. A. Torrey, "Adaptive Flux Weakening Control of Permanent Magnet Synchronous Motors", *IEEE/IAS Annual Meeting Conference Record*, 1998, pp. 475-482.

[51] C. Namudri and P. C. Sen, "A Servo-Control System using a Self-Controlled Synchronous Motor (SCSM) with Sliding Mode Controller", *IEEE/IAS Annual Meeting Conference Record*, 1987, pp. 283-295.

[52] A. Consoli and Antonio, "A DSP Based Sliding Mode Field Oriented Control of an Interior Permanent Magnet Synchronous Motor Drive", *IPEC Conference Record*, Tokyo, Japan, 1990, pp. 263-303.

[53] M. Ghirby and H. Le-Huy, "Optimal Control and Variable Structure Combination using Permanent Magnet Synchronous Motor", *IEEE/IAS Annual Meeting Conference Record*, 1994, pp. 408-415.

[54] R. B. Sepe and J. H. Lang, "Real Time Adaptive Control of the Permanent Magnet Synchronous Motor", *IEEE/IAS Annual Meeting Conference Record*, 1990, pp. 545-552.

[55] M. A. El-Sarkawi, A. A. El-Samahy and M. L. El-Syed, "High Performance Drive of dc Brushless Motors Using Neural Network", *IEEE Trans. on Energy Conversion*, vol. 9, no. 2, June 1994, pp. 317-322.

[56] C. Shiguo, D. G. Holmes and W. A. Brown, "Digital Control of a Servo System using Neural Network", *IEEE/IAS Annual Meeting Conference Record*, 1995, pp. 129-133.

[57] M. A. Rahman and M. A. Hoque, "On-Line Adaptive Artificial Neural Network Based Vector Control of Permanent Magnet Synchronous Motors", *IEEE Trans. on Energy Conversion*, vol. 13, no. 4, 1998, pp. 311-318.

[58] Y. Yi, D. M. Vilathgamuwa and M. A. Rahman, "A New Artificial Neural Network Controller for an Interior Permanent Magnet Motor Drive", *IEEE/IAS Annual Meeting*, Chicago, 2001, pp. 1115-1120.

[59] M. A. Rahman , M. A. Hoque, C. B. Butt, M. N. Uddin and M. A. Abido, "Testing of Genetic-PI Based Controller for IPMSM Drive", *IEEE Conference on Industrial Technology, Bangkok, Thailand*, Dec. 2002, CD-ROM.

[60] K. Inoue, Y. Takakado and M. Nakaoka, "Auto Tuning Technology for Fuzzy Algorithms Based DC Brushless Servo Systems", *IEEE/PESC Conference Record*, 1993, pp. 446-450.

[61] K. Erenay, I. Ciprut, L. Tezduyar, Y. Istefanopulos, "Application of Fuzzy Algorithms to the Speed Control of Washing Machines with Brushless DC Motors", *Proceedings of International Conference on Electric Machines, Istanbul, Turkey*, 1998, pp. 1231-1236.

[62] Z. Koviac, S. Bogdan and P. Crnosija, "Fuzzy Rule-Based Model Reference Adaptive Control of Permanent Magnet Synchronous Motor", *IEEE/IECON Conference Record*, 1993, pp. 207-212.

[63] M. N. Uddin and M. A. Rahman, "Fuzzy Logic Based Speed Control of an IPM Synchronous Motor Drive", *Journal of Advanced Computational Intelligence,* vol. 4, no. 2, 2000, paper #JACI-CCECE-S-05.

[64] M. A. Rahman and Ping Zhou, "Field Circuit Analysis of Brushless Permanent Magnet Synchronous Motors", *IEEE Trans. on Ind. Elect.*, vol.43, No.2, April 1996, pp. 256-267.

[65] P. C. Krause, *Analysis of Electric Machinery*, McGraw-Hill Inc., 1986.

[66] T. Sebastian, G. R. Slemon and M. A. Rahman, "Modelling of Permanent Magnet Synchronous Motors", *IEEE Trans. on Magnetics*, vol. MAG-22, no. 5, 1986, pp. 129-134.

[67] S. Morimoto, M. Sanda and Y. Taketa, "Wide-Speed Operation of Interior Permanent Magnet Synchronous Motors with High-Performance Current Regulator", *IEEE Trans. on Ind. Applicat.,*Vol. 30, July/Aug, 1994, pp.920-926

[68] L. A. Zadeh, "Outline of a New Approach to the Analysis of Complex System and Decision Processes", *IEEE Trans. on Syst, Man and Cybern.*, vol. SMC-3, 1973, pp. 28-44.

[69] *Fuzzy Logic Toolbox User Guide*, The Math Works Inc., 1997.

[70] M. A. Rahman and M. A. Hoque, "On-Line Self-Tuning ANN Based Speed Control of a PM DC Motor", *IEEE/ASME Trans. on Mechatronics*, vol. 2, No. 3, Sept. 1997, pp. 169-178.

[71] *DS1102 Program Loader User's Guide*, dSPACE, Paderborn, Germany, Ver. 2, 1996

[72] H. T. Nguyen, M. Sugeno, R. Tong and R. R. Yager, *Theoretical Aspects of Fuzzy Control*, John Wiley & Sons, Inc., 1995.

[73] S. M. Zeid, *Master of Engineering Thesis*, Faculty of Engineering and Applied Science, Memorial University of Newfoundland, Dec. 1998.

[74] M. A. Hoque, *Doctor of Philosophy Thesis*, Faculty of Engineering and Applied Science, Memorial University of Newfoundland, Aug. 1996.

[75] T. S. Radwan, *Doctor of Philosophy Thesis*, Faculty of Engineering and Applied Science, Memorial University of Newfoundland, Aug. 1996.

[76] M. N. Uddin, *Doctor of Philosophy Thesis*, Faculty of Engineering and Applied Science, Memorial University of Newfoundland, Aug. 2000.

APPENDIX A

IPMSM Parameters

Number of phase = 3

Number of poles = 4

Rated current = 3 A

Rated frequency = 60 Hz

Rated power = 1 hp

Rated input line to line voltage = 208 V

q-axis inductance L_q = 0.07957 H

d-axis inductance L_d = 0.04244 H

Stator resistance per phase r_s = 1.93 Ω

Inertia constant J_m = 0.003 Kg.m^2

Rotor damping constant B_m = 0.0008 (N-m)/rad./sec.

Permanent magnet flux linkage ψ_m = 0.314 volts/rad./sec.

Magnet type = Samarium Cobalt

APPENDIX B

Simulink Model of IPMSM Drive

In modelling the system in SIMULINK it is necessary to work from the principle equations governing the IPMSM drive system rather than base the individual components of the model strictly on the schematic of the vector control scheme. This is because working in the d-q reference frame necessitates the use of transformation operations that are not implemented physically in real-world systems. Fig. B.1 presents the SIMULINK schematic of the complete current-controlled VSI-fed IPMSM drive system that was developed in this work.

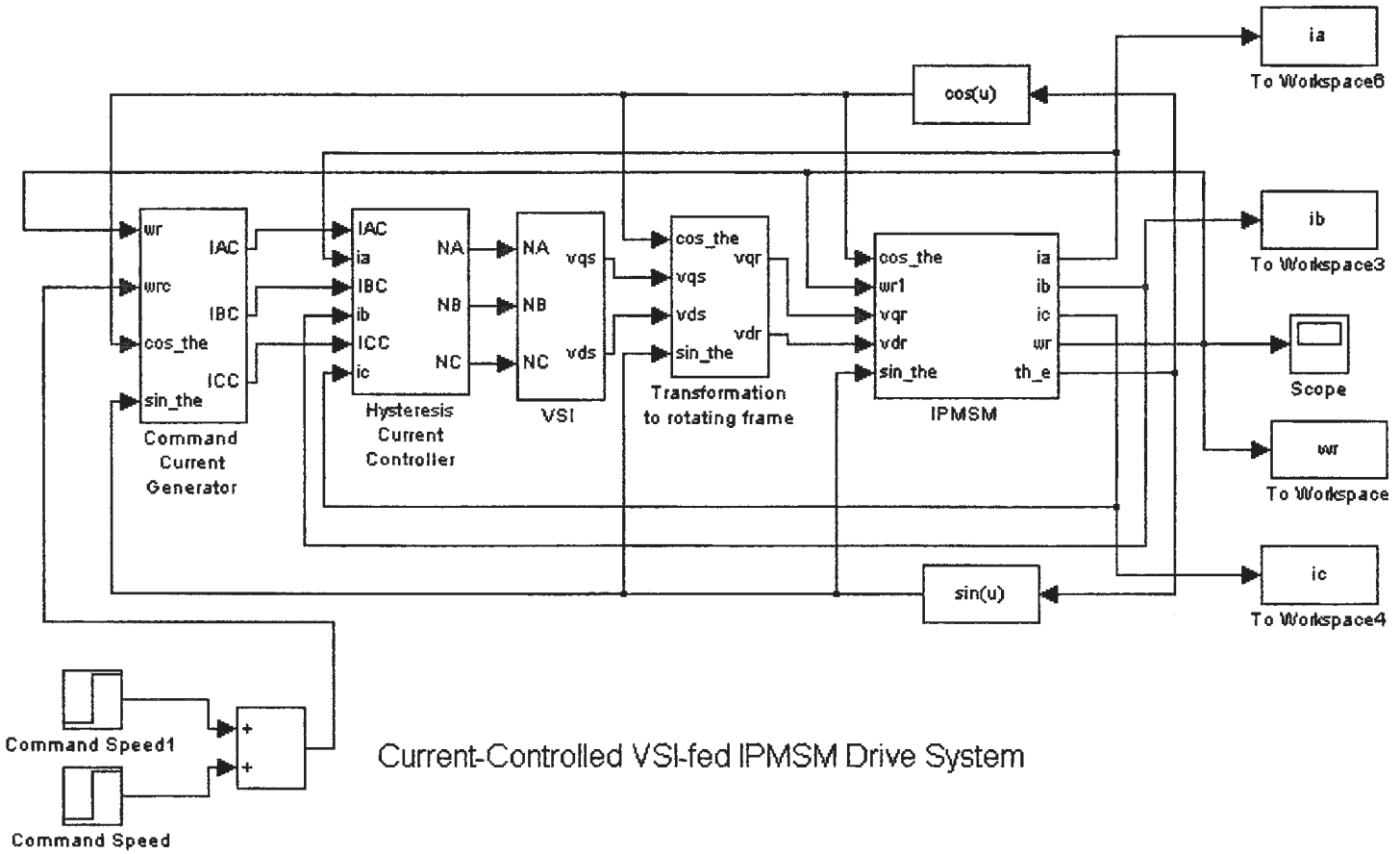

Figure B.1. Simulink model of the proposed drive.

The following subsections will present the purpose and design of each of the component blocks of the model in detail. Only the simplified FLC/MTPA scheme will be addressed.

B.1 Command Current Generator

The Command Current Generator block generates the command currents necessary to maintain the desired rotor speed of the motor. To do this, rotor speed and rotor angular position are necessary inputs. The schematic of the Command Current Generator block is shown in Figs. B.2a and B.2b.

The command torque necessary to achieve the desired rotor speed is calculated from the difference between the command speed and the actual speed of the rotor by the FLC. This command torque is then used to obtain i_q^{r*} by means of Eqn. 2.40. i_q^{r*} is then used to attain i_d^{r*} by Eqn. 2.39. Then, using the appropriate transformations, i_a, i_b, and i_c are found. This block is shown in Figs. B.2a and B.2b.

B.2 Current Controller

The next block in the model represents the controller for the voltage source inverter. The current controller takes as input the three phase command currents from the Command Current Generator and outputs the logic variables NA, NB and NC used to control the VSI. A fixed band hysteresis controller, as shown in Fig. B.3, is employed.

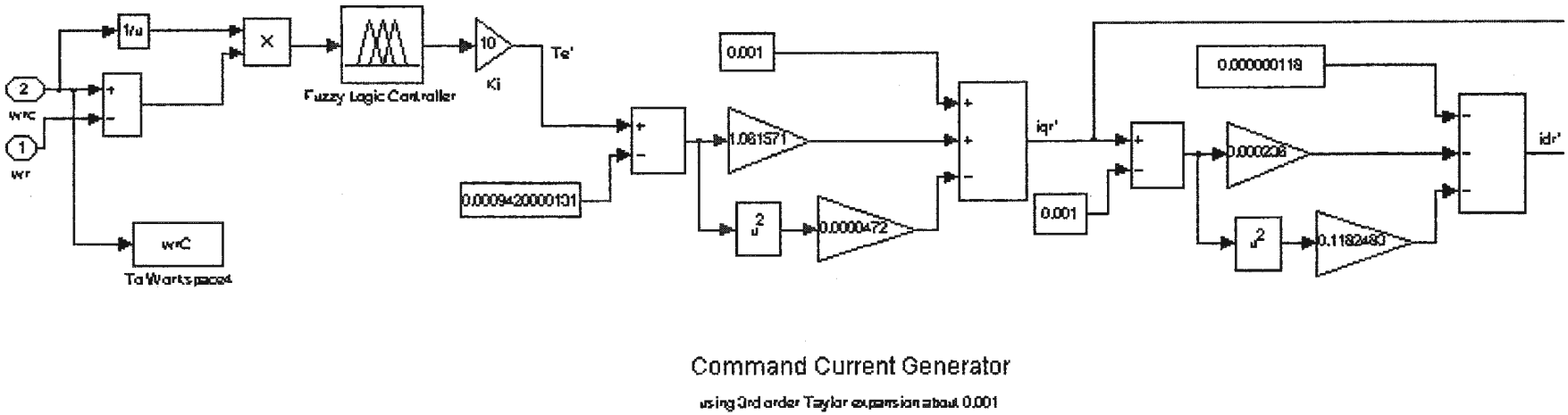

Figure B.2a. Command current generator block.

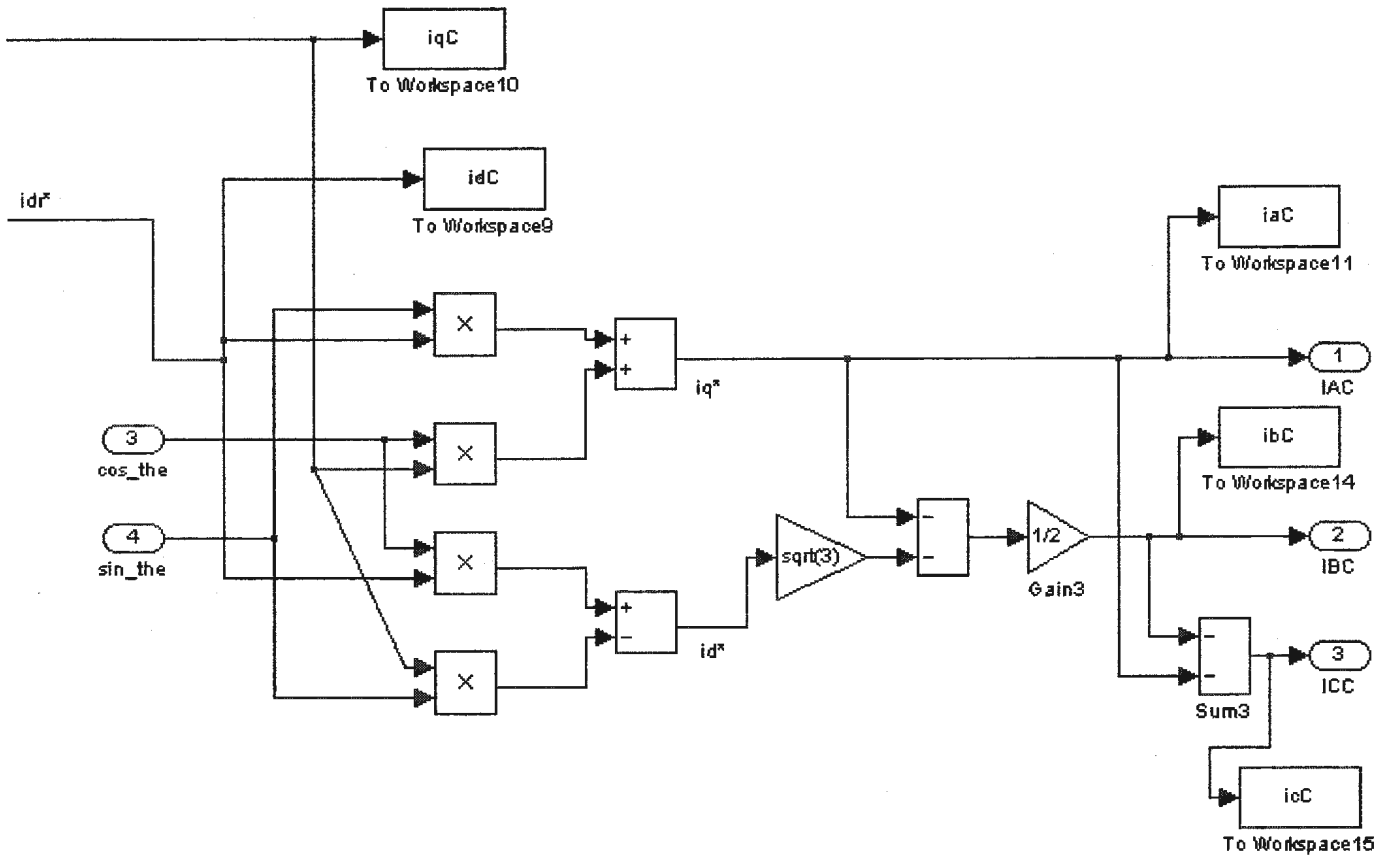

Figure B.2b. Command current generator block (continued).

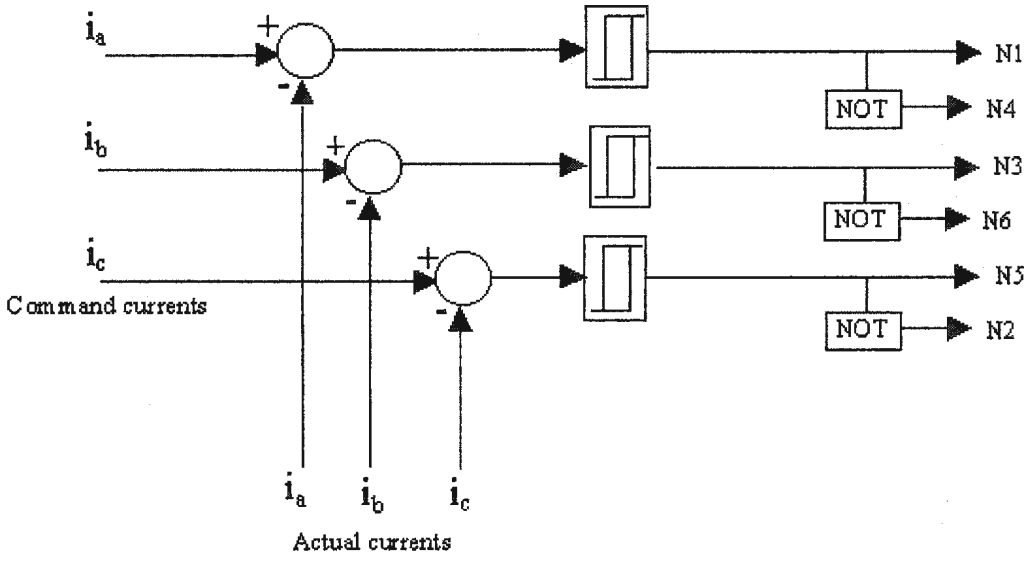

Fig. B.3. Hysteresis current controller.

B.3 Voltage Source Inverter

The next block in the model represents the voltage source inverter and is designed according to the following equations,

$$\begin{bmatrix} v_a \\ v_b \\ v_c \end{bmatrix} = \frac{1}{3}\begin{bmatrix} 2 & -1 & -1 \\ -1 & 2 & -1 \\ -1 & -1 & 2 \end{bmatrix}\begin{bmatrix} NA \\ NB \\ NC \end{bmatrix} V_B \qquad \text{(B.1)}$$

and Eqn. 2.11. Outputs are the v_q^* and v_d^* command voltages. This block is shown in Fig. B.4.

B.4 Transformation to Rotating Frame

The IPMSM model equations require i_q^{r*} and i_d^{r*} to give the outputs ω_r and θ_r. Therefore, v_q^* and v_d^*, as obtained from the VSI, must be transformed to the rotating d-q frame in order to give v_q^{r*} and v_d^{r*}. This is done, as shown in Fig. B.5, using Eqn. 2.12.

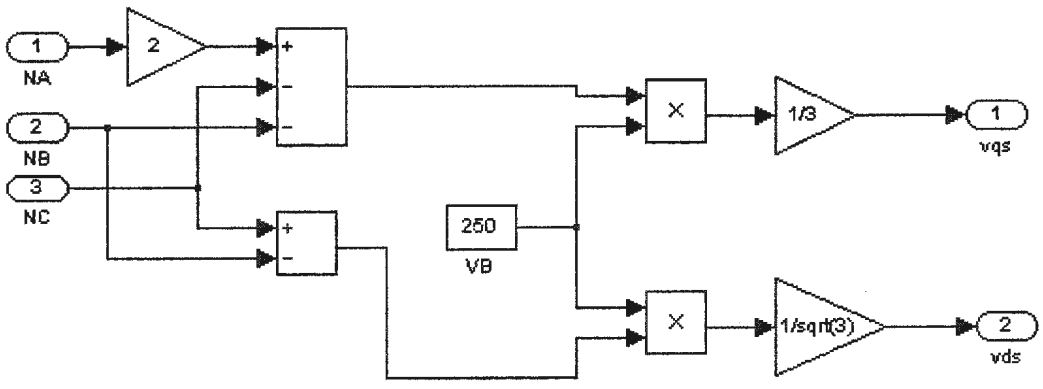

Fig. B.4. Voltage source inverter block.

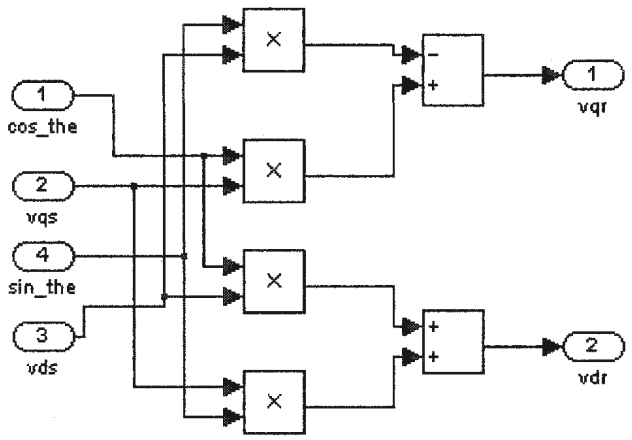

Fig. B.5. Transformation to rotating reference frame block.

B.5 IPMSM

This block (Fig. B.6) represents the actual motor. Inputs are v_q^{r*}, v_d^{r*} and ω_r. In addition, v_q^{r*} and v_d^{r*} must be converted to i_q^{r*} and i_d^{r*} for use in the equations governing the motor dynamics, and this conversion requires the input of $\cos\theta_r$ and $\sin\theta_r$.

Because several functions are performed in this block, it is further composed of three sub-blocks which each perform specific tasks.

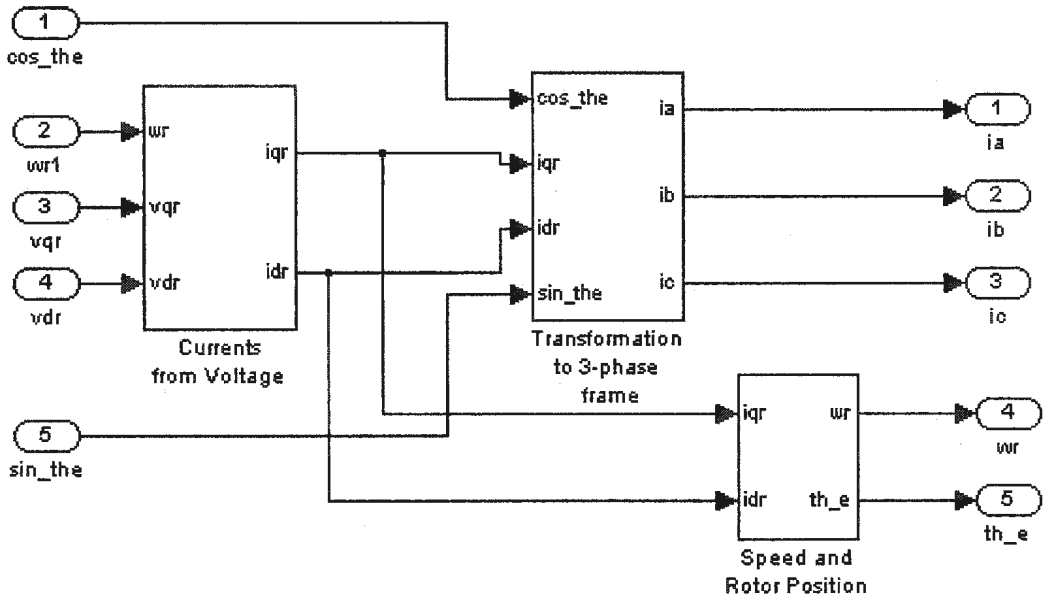

Fig. B.6. IPMSM block.

The first sub-block (Fig. B.7) calculates the actual motor i_q^r and i_d^r from v_q^{r*}, v_d^{r*} and ω_r. This is done via the IPMSM equations, Eqns. 2.26 and 2.27.

The second sub-block (Fig. B.8) converts i_q^r and i_d^r to i_a, i_b, and i_c via Eqns. 2.13 and 2.10.

The third sub-block calculates the motor's rotor speed and position via Eqns. 2.24 and 2.28. This sub-block is shown in Fig. B.9.

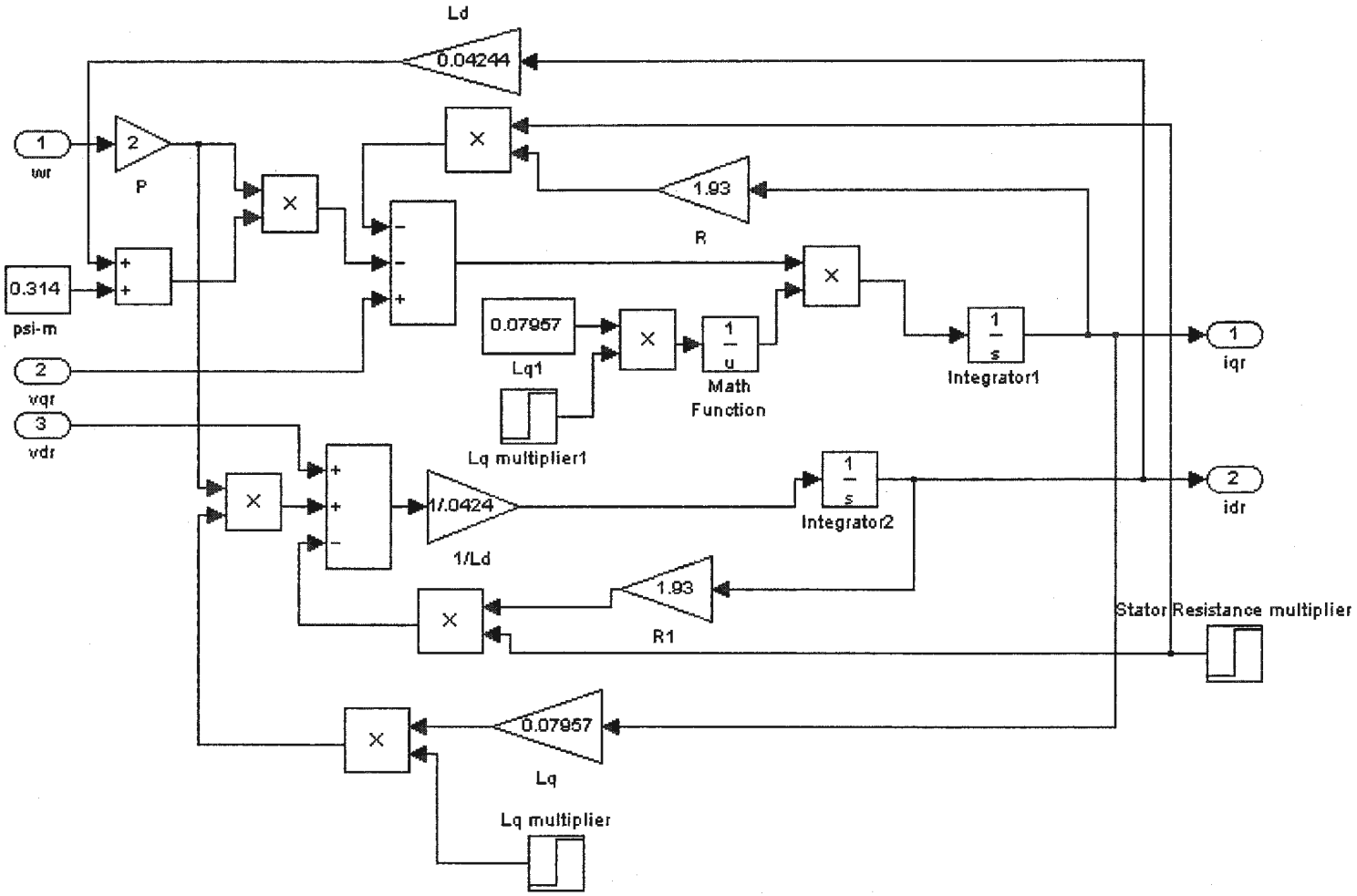

Fig. B.7. Calculation of q- and d-axis currents from q- and d-axis command voltages.

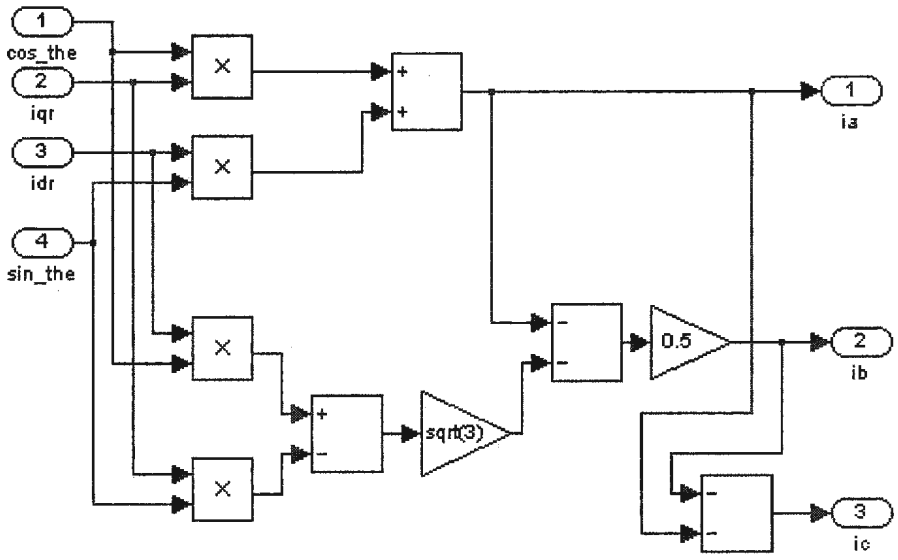

Transformation to 3-phase Frame

Fig. B.8. Calculation stator currents from q- and d-axis currents.

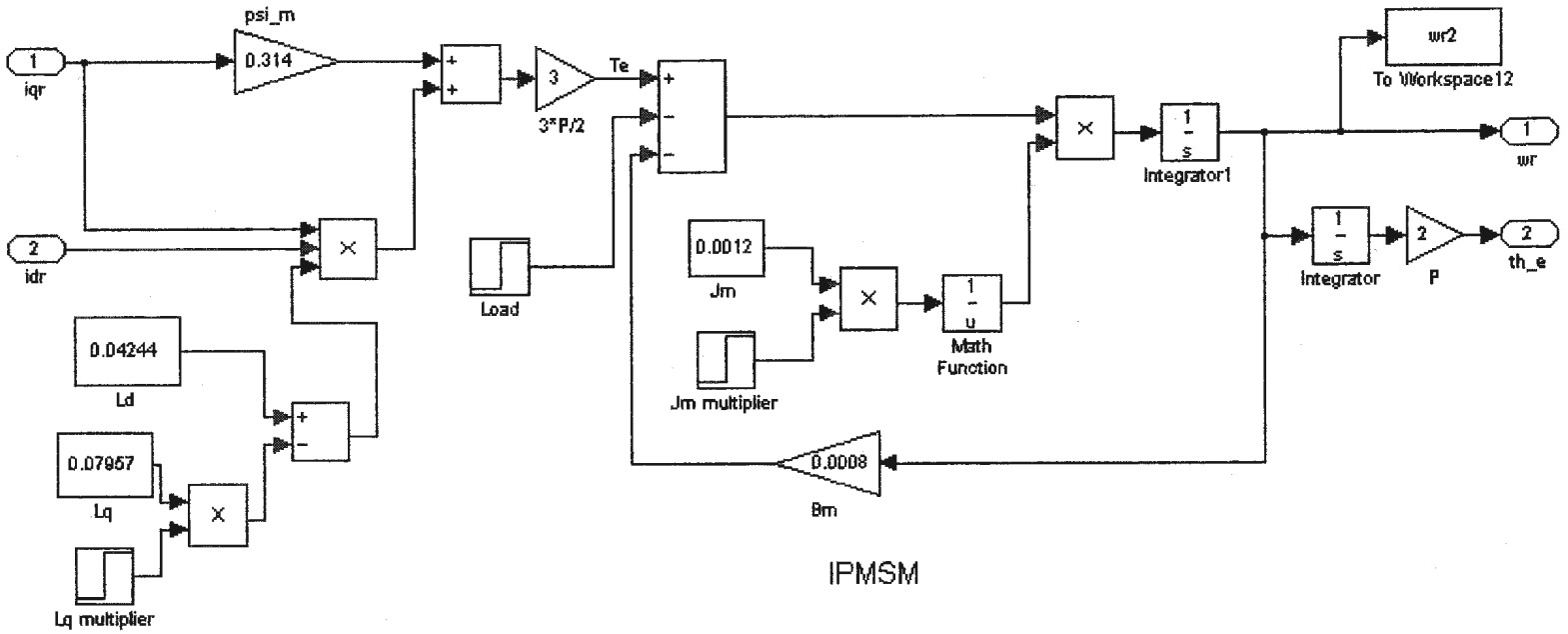

Fig. B.9. Motor speed and position sub-block.

APPENDIX C

IGBT Inverter

The insulated gate bipolar transistor (IGBT) has the advantages of both the bipolar junction transistor (BJT) and metal-oxide-semiconductor field-effect transistor (MOSFET). Because the IGBT has a high input impedance, like a MOSFET, the gate draws a very small leakage current. So, even though it has low conduction losses like a BJT, it doesn't suffer from second breakdown problems as do BJTs.

The IGBT is a voltage-controlled device, like a power MOSFET, however, its performance is closer to that of a BJT than a MOSFET. The IGBT has lower switching and conduction losses than the MOSFET while sharing many of its appealing features such as ease of gate drive, high peak current capability and ruggedness. IGBT maximum switching frequencies are higher than BJTs but slower than power MOSFETs. An IGBT is a three terminal device consisting of a gate, collector and emitter terminal. Current and voltage ratings of an IGBT can be up to 400 A, 1200 V with a switching frequency of up to 20 kHz.

The schematic of the IGBT inverter module with its snubber circuit is shown in Fig. C.1. Although the IGBT is capable of handling both soft and hard switching a snubber circuit has been used to limit the rate of change of voltage across the inverter legs because of unpredictable transient behavior of the IPMSM.

R = 25 Ω, 50 W

C = 450 μF, 450 V (dc)

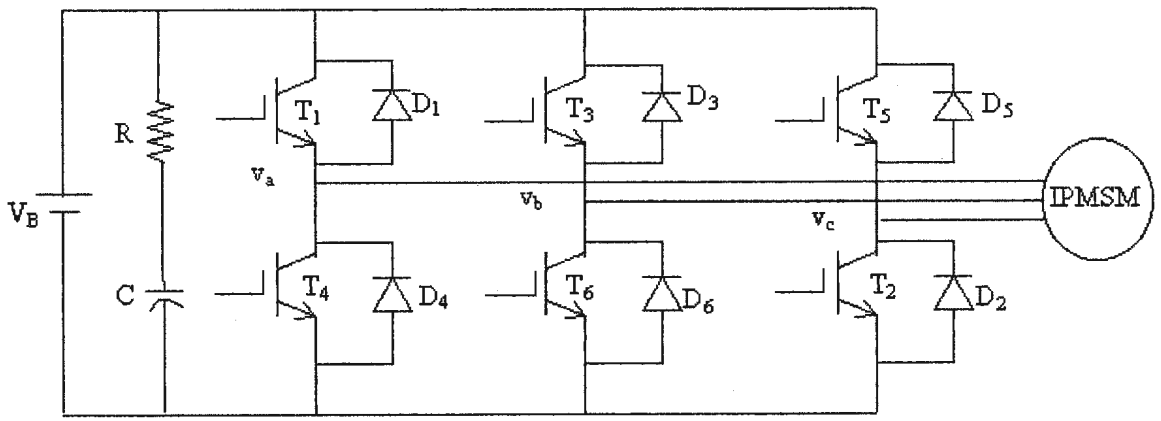

Fig. C.1. Basic circuit of an IGBT inverter module.

C.1 Base Drive Circuits

The main function of the base drive circuit is to generate six pulses having proper voltage levels for the six IGBTs of the VSI. In order to operate the IGBTs as switches, the gate voltages must be such that the IGBTs are into the saturation mode for low on-state voltages. The outputs of the digital I/O subsystem of the DSP board are six pulses having magnitudes of 5 V. This is not sufficient voltage to be used as gate signals to drive the IGBTs and amplification is required. In addition, isolation is needed between the logic circuits and the IGBTs because logic signals should be applied between the gates and the emitters of the IGBTs. This means that for the transistors of the upper legs (T1, T3 and T5), the ground of the logic pulses will not be common. Therefore, a base drive circuit is needed to provide isolation and appropriate voltages to the gates of the IGBTs in the inverter.

The base drive circuit, which was in the Power Research Laboratory of M.U.N., is shown in Fig. C.2a and C.2b. The SN7407N chip has been used as a level shifter that shifts the voltage level from +5V to +15V. The HP2531 chip is an optocoupler, which has been used to provide isolation between the logic circuit and the power circuit of the inverter. The IR2130 chip is the main driver, which provides six driving pulses for the six switches of the inverter. In order to provide +20V isolated power to the optocoupler and the driver an isolated power supply has been built, which is shown in Fig. C.2b.

Resistance and capacitor values:

$R_{18\text{-}23} = 22\ \Omega$, $R_{12\text{-}17} = 680\ \Omega$, $R_{5\text{-}10} = 3.3\ \Omega$, $R_{11} = 3.3\ k\Omega$

$C_{3\text{-}5} = 10\ \mu F$, $C_{6\text{-}11} = 180\ pF$, $C_{12} = 100\ \mu F$, $C_{13} = 47\ \mu F$

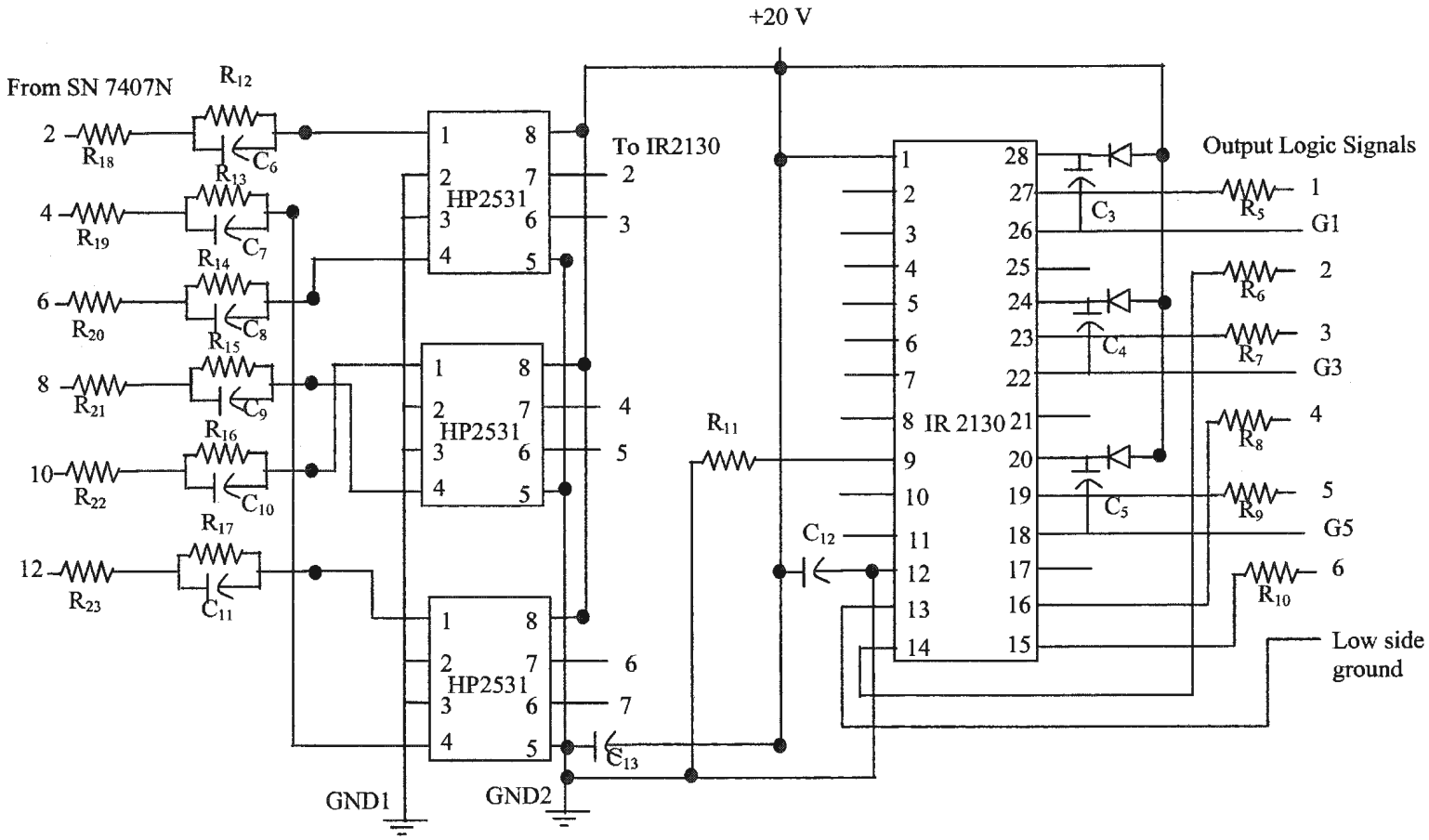

Fig. C.2a. Base drive circuits for the VSI.

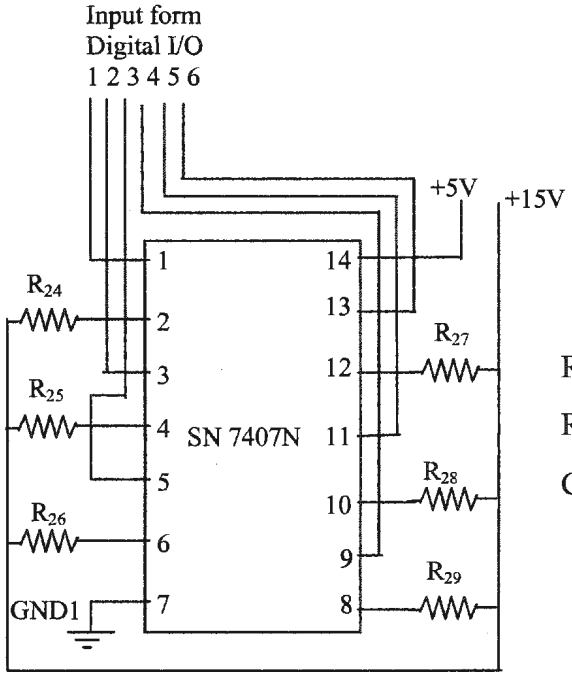

Resistance and capacitor values:

$R_{24\text{-}29} = 1.5\ k\ \Omega$, $R_1 = 1.1\ k$, $R_4 = 3.3\ k\ \Omega$

$C_1 = 2200\ \mu F$, $C_2 = 10\ \mu F$

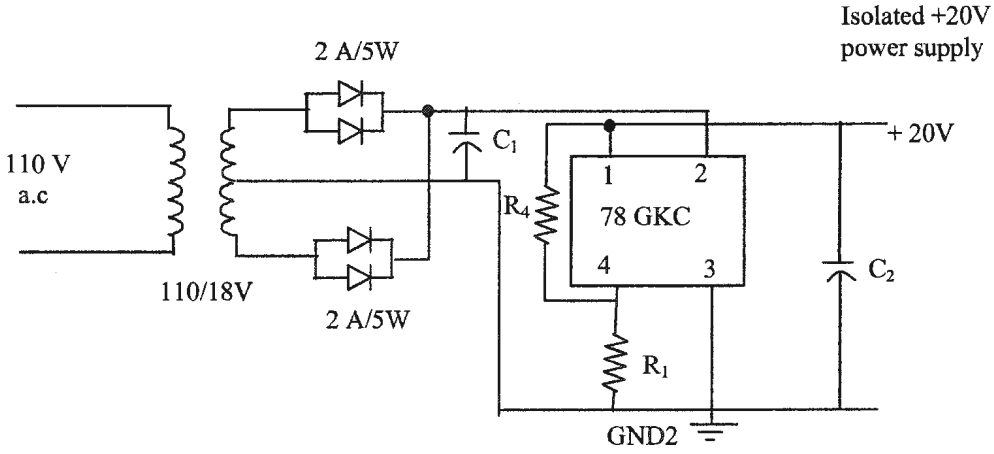

Fig. C.2b. Base drive circuits for the VSI (continued).

APPENDIX D

Dspeed.c

```
/* dspeed.c ************************************************************
*                                                                      *
* Instruction to compile with Borland C:                               *
*  bus version:                                                        *
*     bcc /ml dspeed.c bcdclib.lib                                     *
************************************************************************/

#include <stdlib.h>
#include <stdio.h>

#include <clib.h>          /* Host-DSP interface library include file */

#define DP_MEM_OFFS    0       /* use first dual-port memory address */

unsigned int board_index;
float speed,delta_speed;
void close_and_exit (int error_code)
{
  DSP_unregister_host_app();
  exit(error_code);
}


void write_dual_port_memory (UInt32 address, UInt32 value)
{
  int error;
  error = DSP_lock_board(board_index);
  if(error != DSP_NO_ERROR)
  {
        printf("Error: can't lock board  error = %d.\n\n",error);
        close_and_exit(5);
  }
  error = DSP_write_dual_port_memory(board_index, address, value);
  DSP_unlock_board(board_index);
```

```
  if(error != DSP_NO_ERROR)
  {
        printf("Error %d writing the DSP board's dual-port memory !\n\n",
            error);
        close_and_exit(5);
  }
}


void main (int argc, char *argv[])
{
  int error;

  printf("\n dspeed ``change speed reference from key board..."\n\n");

  if(argc != 2)
  {
        printf("Usage: dspeed board\n\n");
        exit(1);
  }

  error = DSP_register_host_app("dspeed");
  if(error != DSP_NO_ERROR){
        switch(error){
          case DSP_DEVICE_DRIVER_NOT_FOUND:
            printf("\nDevice Driver not installed.\n");
            break;
          case DSP_VXD_NOT_LOADED:
            printf("\nVirtual device driver not installed.\n");
            break;
          case DSP_NO_FREE_HOST_APP_IDX:
            printf("\nNo free host application index.");
            break;
#ifdef NET
          case DSP_NET_ERROR:
            printf("\nNetwork error.");
            break;
#endif
          default:
            printf("\nDSP_register_host_app: error code %d\n",error);
            break;
        }
        exit(1);
  }

  error = DSP_board_index(argv[1],&board_index);
  if(error != DSP_NO_ERROR)
  {
        printf("\nBoard %s not registered, error = %d.\n",
            argv[1],error);
        close_and_exit(2);
  }
```

```
  /* initialize output signal with 0.0 */
  write_dual_port_memory(DP_MEM_OFFS,
                                        DSP_cvt_ieee_to_ti((Float32) 0.0));

  /* set output signal to speed */
  do{
  printf("\n please enter the delta_speed in rpm...\n");
  scanf("%f", &delta_speed);
  speed=delta_speed*0.104719755;
  write_dual_port_memory(DP_MEM_OFFS,
                                      DSP_cvt_ieee_to_ti((Float32) speed));
  } while (delta_speed!=0.0);
  printf("Press RETURN to abort ...\n");
  rewind(stdin);
  getchar();

  /* reset output signal to 0.0 */
  write_dual_port_memory(DP_MEM_OFFS,
                                DSP_cvt_ieee_to_ti((Float32) 0.0));

  close_and_exit(0);
}
```